UCLouvain

École polytechnique de Louvain

Functional neuroimagery for the assessment of patients suffering from addiction

Author: **Maxime Boyens**
Supervisors: **Benoît Macq, Laurence Dricot**
Readers: **Mélissa Salavrakos, Ron Kupers**
Academic year 2022–2023
Master [120] in Biomedical Engineering

Acknowledgements

First of all, I would like to thank Professor Benoît Macq for giving me the opportunity to work on this captivating research topic.

I would also express my sincere gratitude to Professor Laurence Dricot and Doctor Mélissa Salavrakos for their time, support and encouragement, and for trusting me with this project. Knowing their heartfelt investment in this topic makes me appreciate the opportunity even more.

A heartfelt appreciation goes to Manon Dausort, Nicolas Delinte and Colin Vandenbulcke, whose help and suggestions for structuring and reading my thesis were very valuable and much appreciated.

Lastly, I would like to express my profound gratitude to all the people who have supported and encouraged me throughout my studies and this thesis. Sincere thoughts go to my family, friends and loved ones.

Abstract

Alcohol use disorders (AUD) have widespread consequences for individuals' health and well-being. This thesis uses the powerful tool of functional magnetic resonance imaging (fMRI) to explore the effects of alcohol abstinence on brain function in individuals with AUD. Through fMRI, alterations in neural activity related to alcohol stimuli are examined. The study involves 73 participants in three scanning sessions, providing insights into changes during abstinence. The thesis encompasses a theoretical background on fMRI and AUD, experimental setup, data processing, and analysis. The analysis reveals alterations in brain activation for addiction, emotional processing, memory, cognitive control, and reward systems. Additionally, ANOVA analysis highlights specific brain regions, including the putamen, caudate, and hippocampus, which may contribute to relapse risk. The study highlights the potential for neuroplasticity and recovery and emphasizes the need for further research in this area. More generally, it contributes to understanding brain changes during alcohol abstinence and to the development of targeted treatments.

Contents

List of Figures

List of Tables

Acronyms

ACC Anterior Cingulate.

ANOVA Analysis Of Variance.

ATP Adenosine Triphosphate.

AUD Alcohol Use Disorder.

BA Brodmann Area.

BV BrainVoyager.

DA Dopamine.

DALY disability-adjusted life years.

DLS Dorsolateral Striatum.

DMS Dorsomedial Striatum.

DS Dorsal Striatum.

EPI Echo Planar Imaging.

FA Fine-tuning Alignment.

FFX Fixed Effects.

FID Free Induction Decay.

FMR Functional Magnetic Resonance.

fMRI Functional Magnetic Resonance Imaging.

GLM General Linear Model.

Hb Hemoglobin.

IA Initial Alignment.

MDM Multi-subject design matrix.

MR Magnetic Resonance.

NAc Nucleus Accumbens.

PFC Prefrontal Cortex.

PRT Protocol.

RBC Red Blood Cells.

RF Radio-frequency.

RFX Random-Effects.

SDM Single-subject design matrix.

TE Time of Echo.

TR Time of Repetition.

VMR Volume Magnetic Resonance Imaging.

VS Ventral Striatum.

VTA Ventral Tegmental Area.

VTC Volume Time Course.

Introduction

This thesis focuses on the use of functional magnetic resonance imaging (fMRI) to better understand alcohol use disorders (AUD), and more especially the effects of alcohol abstinence on brain function in people suffering from it. AUD is characterized by a reduced ability to control or stop alcohol consumption, which poses major public health problems. Worldwide, alcohol abuse is responsible for around 5.3% of deaths, estimated at 3 million a year. [1]

The impact of alcohol consumption extends beyond physical and mental health as it also affects social behaviours and individual well-being. Therefore, it is imperative to fully understand the mechanisms linked to this mental condition, presenting a vast field for exploration. In this context, fMRI has emerged as a valuable tool for observing and quantifying alterations in brain function. By measuring blood oxygenation levels, fMRI provides insights into the neural activity associated with specific tasks or resting-state conditions. Consequently, this modality enables researchers to study the effects of alcohol abstinence on brain function.

In the study presented here, a total of 73 participants were recruited to undergo three scanning sessions, providing a longitudinal perspective on the changes in brain function during the abstinence period. The multi-session design allows us to examine the temporal changes and potential recovery of brain activity following alcohol cessation. By comparing the fMRI data across the scanning sessions, the study aims at elucidating the impact of alcohol abstinence on various brain regions and functional networks. This study also proposes results with control participants, enabling the comparison between two groups presenting different dependence levels.

To analyze the acquired fMRI data, task-based protocols were employed. Task-based fMRI involves participants performing specific cognitive or motor tasks while their brain activity is monitored, revealing the neural substrates involved in these processes. In this case, the task consisted in watching figures displayed on a computer screen. These images were alcoholic beverages, non-alcoholic beverages or food. This variety of stimuli allowed us to directly spot alcohol-related activation while withdrawing general activation due to stimulus exposition.

This thesis is structured in four chapters, followed by a conclusion. The first chapter presents a comprehensive theoretical background and literature review on fMRI and AUD, setting the stage for the subsequent analysis. This part covers

initially the principles of magnetic resonance imaging and then focuses precisely on fMRI. Concerning AUD, it explores the concept of alcohol dependence and the association between alcoholics and alcohol-associated stimuli.

The second chapter describes the experimental setup and procedures employed in the study. It includes a detailed description of the experiment itself. After that, it will develop the treatment of data from raw data to the analyzable form of it, passing through important steps such as preprocessing and standardization. Finally, the analysis methodology and the use of Python scripting will be discussed.

In the third chapter, the fMRI data collected during the three scanning sessions were analyzed to investigate changes in brain activation patterns during alcohol abstinence. Several regions known to be involved in addiction, emotion, memory, cognitive control, and reward systems were examined. Notably, specific brain regions showed significant differences in activation, suggesting potential neuroplasticity and recovery. The findings provide valuable insights into the behaviour of the alcoholic brain during periods of abstinence.

In the final chapter, the results of the fMRI analysis were discussed, offering interpretations and insights into the observed changes in brain activation. The findings were related to the existing literature, contributing to our understanding of functional changes during alcohol abstinence. Additionally, the impact of abstinence on the relapse factor was explored, revealing potential associations between certain brain regions and the risk of relapse.

Finally, the study concludes by suggesting some ideas for further work and summarizing the key findings, shedding light on the impact of short-term abstinence in the treatment of AUD.

By leveraging the capabilities of fMRI and employing a multi-session design, this study aims to provide valuable insights into the effects of alcohol abstinence on brain function in individuals with AUD. Through the meticulous analysis of the acquired fMRI data, it strives to enhance our understanding of the neural changes associated with abstinence, potentially guiding future therapeutic interventions and improving the treatment outcomes for individuals affected by AUD.

Chapter 1

Theoretical background

1.1 Magnetic resonance imaging

Before diving into the main topic, it is essential to have a solid understanding of the methods used in this thesis. That's why we first explore magnetic resonance imaging (MRI) and its functional application, functional magnetic resonance imaging (fMRI).

1.1.1 Magnetic concepts behind MRI

As fMRI is one of the many modalities of Magnetic Resonance Imaging (MRI), the general aspects of this imaging technique will first be discussed.

In order to understand the effects of a magnetic field on tissues, it is helpful to view them as clusters of atoms, with a notable presence of hydrogen atoms. A model can be used in which certain nuclei, behave like small magnets by spinning around their own axes. Normally, these tiny magnets are randomly distributed in space and cancel each other out, resulting in a net magnetic vector of zero (as shown in Fig.1.1). However, when a strong external magnetic field ($\overrightarrow{B_0}$) is applied to the patient, nuclei can adopt one of two possible orientations: parallel or anti-parallel to the external field (as shown in Figure 1B). Parallel alignment corresponds to a lower energy state and therefore to the preferred orientation compared to anti-parallel alignment. The difference in energy between the two states is small. The population disparity between the two states generates a net magnetization vector ($\overrightarrow{M_z}$) which aligns with the external magnet.[2]

The individual nucleus does not align perfectly with the magnetic field but rotates around the direction of the external field (as depicted in Figure 2A). This movement is called the precession. The rate of this rotation is called the precessional frequency (or Larmor frequency) and can be calculated using the Larmor equation:$F = \gamma B_0/2\pi$ where F represents the precessional frequency, B_0 is the strength of the magnetic field, and γ is the gyromagnetic ratio specific to each nucleus. [2]

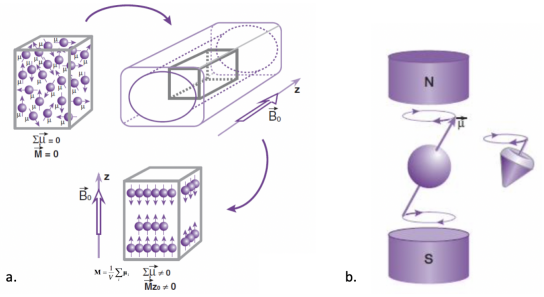

Figure 1.1: Alignment and precession of protons. *On* ***a.*** *we can see a block representing the tissue as a grouping of protons (hydrogen atoms). Once this block is placed in an external magnetic field* $\overrightarrow{B_0}$*, protons align in either parallel or anti-parallel direction to this external field (as depicted on the lower part of* ***a.****). On* ***b.*** *we can observe the precession of a proton around an axis determined by the magnetic field induced by a "north-south" magnet. Retrieved from [3].*

Unfortunately, direct measurement of the equilibrium macroscopic magnetization vector along the principal axis (Oz) is not possible as it is infinitely small compared to $\overrightarrow{B_0}$. To measure it, a second magnetic field (or radiofrequency wave) in another direction than $\overrightarrow{B_0}$ is used to tilt the magnetization into the orthogonal plane (xOy). This radiofrequency, better known as RF-pulse, corresponding thus to a new magnetic field B_1, is applied in the xOy plane along Ox. For energy to be transferred to the system which is at equilibrium, the rotational frequency of the rotating magnetic field must be synchronized with the specific Larmor frequency of the protons in the given field. To do this, radio-frequency (RF) energy pulses are applied at the exact Larmor frequency.[3]

As aforementioned, the purpose of these RF pulses is to tilt the resulting magnetization of our nuclei and thus our macroscopic magnetization vector. This tilt depends on the magnitude of our RF-pulse (B_1) and its duration (T_{RF}), and can be determined by the following equation: $\Theta = \gamma \int_{T_{RF}} B_1(t)dt \Leftrightarrow \Theta = \gamma T_{RF} B_1$. [4]

After the RF frequency transmitter is switched off, the system will try to reach the former equilibrium state. This means that the magnetization decays over time, which is represented by a decreasing magnitude of $\overrightarrow{M_z}$ in the transverse plane. Consequently, the induced signal in the receiver coil will decrease in time. This decreasing signal is called free induction decay (FID). The time required for the signal to return to equilibrium is called the relaxation time.

Two relaxation processes exist: longitudinal relaxation and transverse relaxation. Both processes are independent. The first one corresponds to the spin-lattice relaxation and is more often called the T_1 relaxation. This T_1 relaxation relates to the process of realignment to the external magnetic field, with $\overrightarrow{M_z} \rightarrow \overrightarrow{M_0}$. T_1 relaxation time is defined as the time required for the system to recover to 63% of its equilibrium value after it has been exposed to a 90° RF pulse. Various human tissues have

different T_1 values. [2, 4, 5] The equation depicting this spin-lattice relaxation over time is the following: $M_z(t) = M_0 + [M_z(0) - M_0]e^{-\frac{t}{T_1}}$.

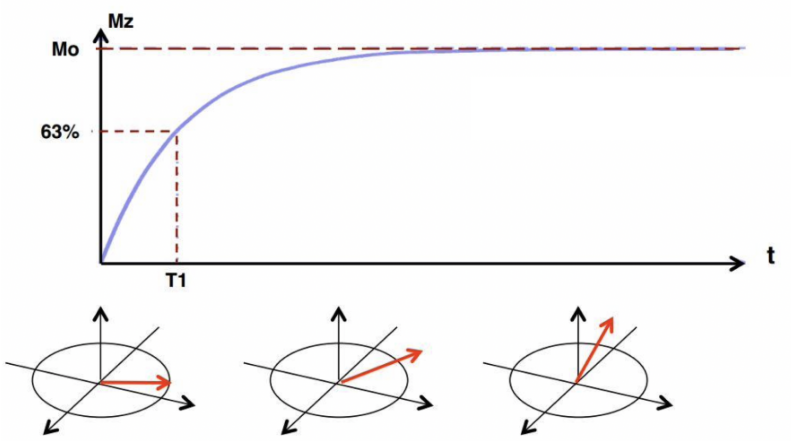

Figure 1.2: T1 relaxation. *On the upper part of the figure is a plot of the evolution of $\overrightarrow{M_z}$ overtime after an RF pulse. The time when $\overrightarrow{M_z}$ has recovered 63% of its equilibrium value M_0 is corresponding to T_1. On the lower part is a representation of this vector $\overrightarrow{M_z}$ in a 3D space. Retrieved from [3].*

The second process of relaxation, the transverse relaxation, depends on the spins precessing around $\overrightarrow{B_0}$. This is the spin-spin relaxation and is more often called T_2 relaxation. Initially, after the excitation by the RF pulse, the spins precess completely in phase. However, as time passes, the observed signal starts to decrease because the spins begin to dephase. It is the variation in the molecular field which will determine the T_2 relaxation time. Indeed, due to diverse molecular environments, small local magnetic fields are added to or subtracted from the primary magnetic field. These small perturbations in the magnetic field will thus induce that spins undergo precession at slightly dissimilar (higher or lower) angular speeds than ω_0. As a result, the spins do not stay in phase and the magnetization in the (xOy) plane will cancel out ($M_{xy} \to 0$). The T2 relaxation time is the time it takes for dephasing to decay the signal to 37% of its original value. The T2 time from various tissues is different, but the T2 time is always shorter than the T1 time.[2, 4, 5] The equation depicting this spin-spin relaxation over time is the following: $M_{xy}(t) = M_{xy}(0)e^{-\frac{t}{T_2}}$

In addition to these two relaxation processes comes a third one, likely to the T_2, which is called T_2^*. This last type of relaxation is due to inhomogeneities of the magnetic field $\overrightarrow{B_0}$. It represents the spin's dephasing due to this constant heterogeneity and is given by: $\frac{1}{T_2^*} = \frac{1}{T_2} + \gamma\Delta B_0$ where γ represents the gyromagnetic ratio and ΔB_0 the locally varying field strength difference.[3, 4]

On the 1.4 is shown the impact of this dephasing due to inhomogeneities on the free induction decay (FID)

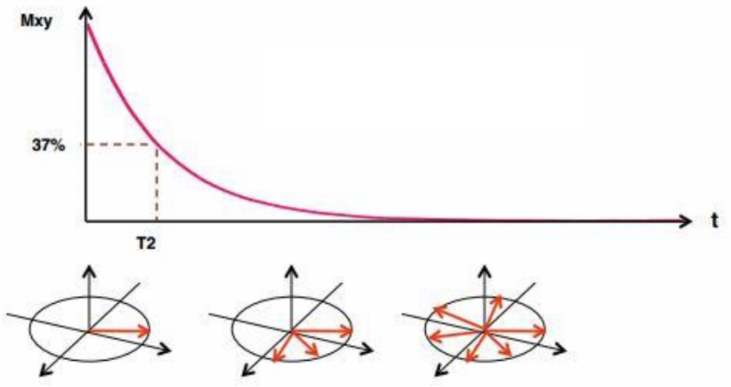

Figure 1.3: T2 relaxation. *On the upper part of the figure is a plot of the evolution of $\overrightarrow{M_{xy}}$ overtime after an RF pulse. The time when $\overrightarrow{M_{xy}}$ returns to 37% of its maximum value is corresponding to T_2. On the lower part is a representation of the vectors composing $\overrightarrow{M_{xy}}$ in a 3D space. Retrieved from [3].*

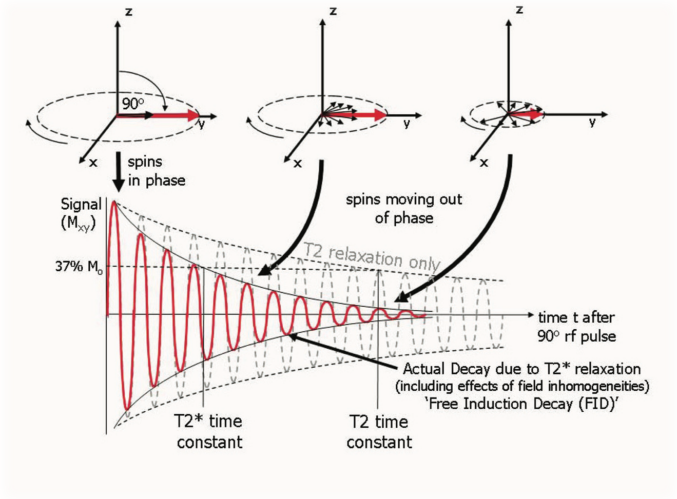

Figure 1.4: T_2^* Relaxation. *On the upper part of this figure are shown, similarly to Fig.1.3, the black vectors composing $\overrightarrow{M_{xy}}$ in a 3D space, dephasing with time. Still on this part, there is in red the sum of all aforementioned vectors, corresponding thus to $\overrightarrow{M_{xy}}$. On the lower part is represented in red the signal as it normally is, with its envelope being the FID. There is also the signal as it would be if the T_2^* effect was neglected, which corresponds to T_2 relaxation. Retrieved from [6].*

Mathematically, the FID is the envelope of the time-depending function of the transverse magnetization M_{xy}. This magnetization follows a decreasing exponential and is a result of the combination of the T_2 and T_2^*.

1.1.2 Imaging sequences

Now that the magnetic aspects of the MRI are better understood, it is time to focus on how these processes are turned into usable signals.

As explained earlier, the measurement of magnetization changes primarily focuses on what happens in the transverse plane (M_{xy}) following RF pulses, rather than the main axis (M_z). The signal we detect, called free induction decay (FID), reflects both T_2 and T_2^* relaxations. However, in the context of MRI, the choice of the relaxation to weight (e.g. T_1, T_2 or T_2^*) depends on the experiment. Therefore, it is thus important to find a way of withdrawing the effect of T_2^* relaxation in the FID.

Another reason why the original FID is not used directly for medical imaging is due to the timing of our measurements. There is indeed a certain time needed to perform the spatial encoding (which will be discussed later), and even with ultra-fast MR scanners, it is not possible to do this before the FID decreases.[2]

For these reasons, researchers employ a technique called "spin-echo" imaging sequences, which offer several advantages in MRI. This technique not only allows the creation of multiple images with different contrast properties, emphasizing the T_1 or T_2 relaxation characteristics of the tissues, but it also enables us to gain acquisition time.

Spin-echo imaging involves the application of two RF pulses. The first RF pulse is typically a 90° pulse. It is used to rotate the spins of the protons from $\overrightarrow{B_0}$ to the transverse plane. As a result, the protons start to precess around the magnetic field direction, while gradually losing phase coherence due to T_2 and T_2^* relaxations.

However, a second RF pulse, known as a 180° pulse, is applied after the initial pulse. This 180° pulse flips the spins by an additional 180°, effectively reversing the dephasing process. As a consequence, the spins start to rephase.

The rephasing of spins leads to the formation of an echo signal, which occurs when the amplitude of the measured signal reaches its maximum. The time at which this echo signal is at its peak is referred to as the time of echo (TE). By manipulating the timing of the RF pulses and the TE, we can control the contrast and acquire images with specific T_1 or T_2 weightings.

One of the significant advantages of spin-echo imaging is its ability to enhance acquisition time efficiency. The rephasing of spins allows us to take advantage of the echo signal, which provides valuable information about tissue properties. By utilizing this echo signal, we can extract image data more effectively, reducing the time required for acquisition compared to other imaging sequences.[2, 6, 5]

There are two main parameters in these sequences. The first parameter has already been explained and is the echo time (TE). The second one is the time separating two consecutive 90° RF-pulses which is called the time of repetition (TR).

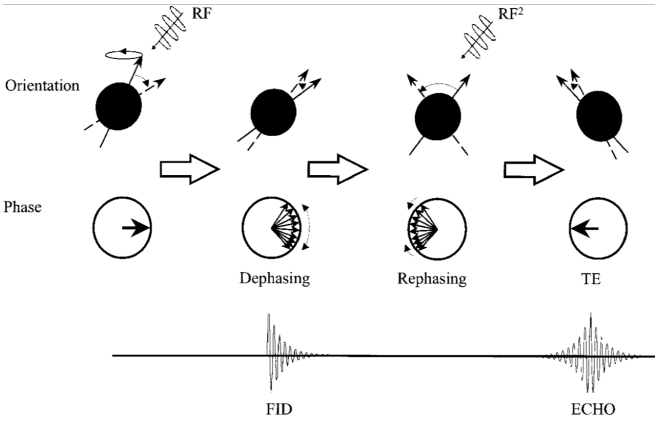

Figure 1.5: Spin echo. *Here are depicted (row-wise description) a global view of the spin's orientation, a view of the magnetization vectors in the transverse plane and the measurable signal. Once the RF pulse is applied, the spins come together in phase before naturally dephasing. During this dephasing, a second RF pulse is applied, realigning the spins at 180° compared to their orientation after the first RF pulse. Retrieved from [2].*

This second parameter also has high importance in the image measured by our MRI. Because the measurements are made in the transverse plane and because the 90° pulse aims to orient the proton spins from $\overrightarrow{B_0}$ axis to this transverse plane, it is important to have an important amount of protons rotating around $\overrightarrow{B_0}$ before applying this first 90° RF-pulse. And the more time we have between two 90° pulses (high TR), the more the system has time to regain its equilibrium condition which is to process around $\overrightarrow{B_0}$ while in this strong magnetic field.

1.1.3 Contrasts

Thanks to these two main parameters depicted here above, MRI has the potential to visualize the difference in T_1 and T_2 of different tissues. In fact, three different contrasts are obtainable while playing with these parameters: T_1, T_2 and "Proton-density" contrast.

The first contrast to be explained is the T_1. For obtaining this, both short TR and TE should be used. As explained earlier, the scale of TR determines the amount of spin-lattice relaxation one allows. We have also seen earlier (cf. Fig. 1.2) that the T_1 relaxation curve becomes more "right-angled" as T_1 decreases. Therefore, a short TR is required to compare the curvature of spin-lattice relaxation among different tissues. If a long TR were used, the magnetization vector M_z would always return to its original value (M_0), regardless of the tissue's T1. A short TE is used to avoid any bias linked to the T_2.

Logically the second contrast, T_2, is the opposite. Here both long TR and long

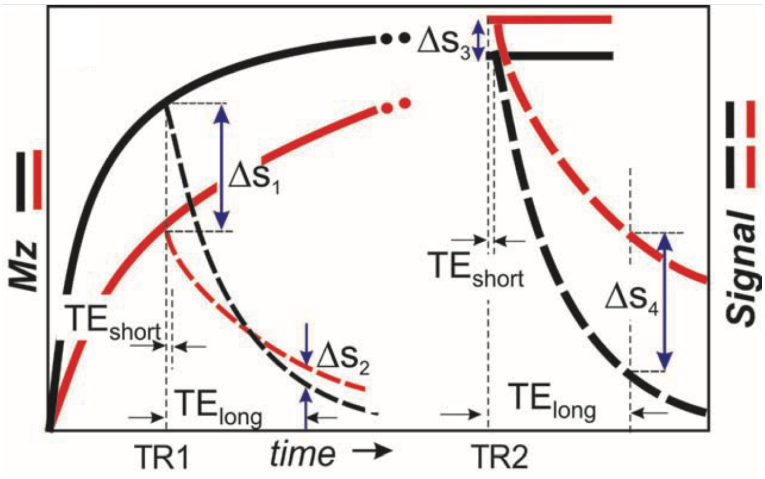

***Figure 1.6: Contrasts and magnetizations in function of TE and TR**, retrieved from [5]. The red line represents a tissue with high T_1 and T_2 relaxation times, while the other line, in black, has both short T_1 and T_2 constants. The first observation is that we have all possible combinations of parameters depicted here, where the short TR (here TR1) case is detailed on the left of the figure and the long TR (here TR2) is shown on the right. In each of these cases, we can see the difference between using either a short or a long TE. The contrasts are represented here by ΔS_n as they all present possible combinations of TE and TR, inducing different MRI weighting techniques except ΔS_2, which is there to show the inefficiency of combining short TR with long TE. Indeed, this ΔS_2 represents well the bias which can be obtained while combining these parameters, as the tissue represented by the red line has higher T_1 and T_2 than the other tissue (in black). The other possible weighting with a short TR is thus the one with a short TE, commonly called T_1 weighting. It is here represented by ΔS_1. The right side of the figure lets us thus the two remaining contrasts: proton density and T_2 weighting. The first one is represented here by ΔS_3 and is the combination of a short TE with a long TR. The last one is corresponding to ΔS_4 and is obtained when combining both long TE and TR.*

TE are employed. Indeed, the higher the TR, the smaller the impact of T_1 will be as explained above. The objective here is to maximize the difference between two tissues with different T_2 values. Therefore a long TE is used because tissues with high T_2 will dephase way slower than the other ones (cf. Fig. 1.3), allowing for really noticing the difference after a long echo time.

The last contrast is not aiming at highlighting a T_1 or T_2 characteristic of the tissue. As explicitly mentioned in its name, the purpose of this contrast is to show the differences in the proton density of the tissues. This contrast is realized by combining a long TR with a short TE. By using a long TR, a high M_z value is obtained a very high M_z value, making thus the highest number of protons available rotate around $\overrightarrow{B_0}$. Since the objective is to measure a substantial number of protons, a short TE is employed to minimize the influence of T2 relaxation on the measure-

ments.[5, 3, 4]

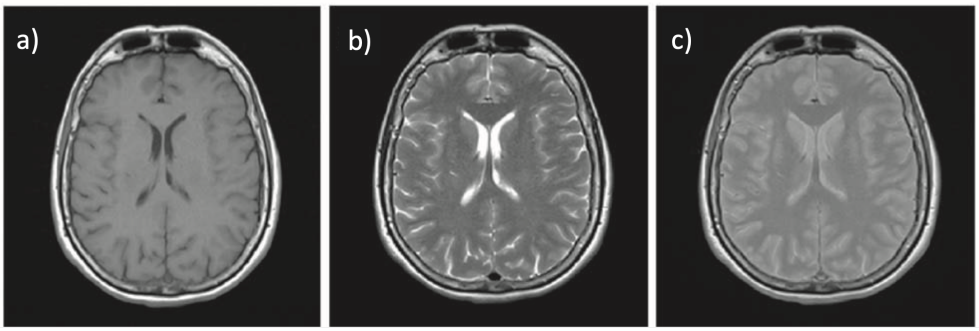

***Figure 1.7: Examples of the different contrasts on a same brain**, retrieved from [5]. The three thirds of the figure represent T1-weighted (a), T2-weighted (b), and proton density-weighted (c) images which result from combinations of varying TR and TE values.*

1.1.4 Spatial encoding

Now that the magnetic fundamentals behind MRI have been explained, it is time to understand how these magnetic behaviours are interpreted to generate an image. MRI differs significantly from other medical imaging techniques in this regard. Unlike CT, ultrasound, or X-ray imaging, where receiver coils can be collimated to limit the signal to a specific location, MRI relies on a different approach. As the MR signal is coming from the entire object, this imaging technique needs a method for defining the position of every proton in the object. This is called "spatial encoding".

This spatial encoding is divided into three steps: slice selection, frequency encoding, and phase encoding.

The first step involves adding a magnetic gradient in a specific direction. This gradient is typically ranging from 10 mT/m to 25 mT/m when added to a 1.5T magnetic field. It induces thus a small variation relative to the original magnetic field ($\approx 1\%$). This gradient aims at selecting a narrow range of frequencies in order to stimulate a thin slice of hydrogen protons within the body. By inducing a variation in the Larmor frequency, protons respond differently to RF pulses based on their position along the gradient axis, enabling the detection of the desired slice. This is what produces our slice detection. It's worth noting that by altering the gradient direction for slice encoding, slices in other directions can be acquired. Considering these slices as xy planes, the initial gradient direction is denoted as $\overrightarrow{z}$. The gradient will therefore be referred to as Gz, as seen in Fig.1.8.

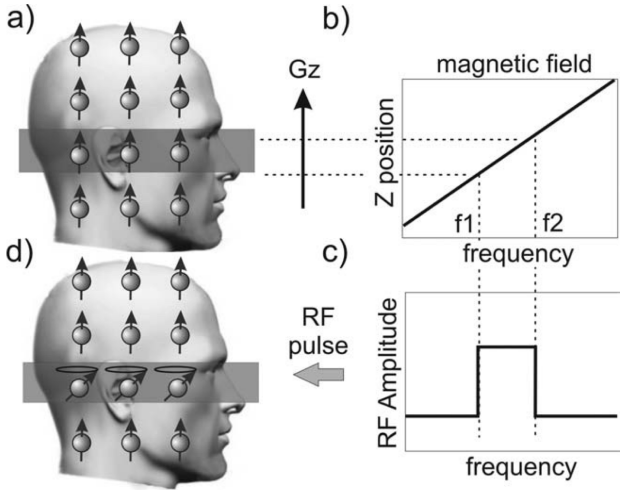

***Figure 1.8: Slice selection**, retrieved from [5]. The aim of slice selection is to generate transverse magnetization in the shaded section (a). This involves applying a gradient Gz, creating a position-dependent frequency. The range of frequencies from f1 to f2 in (b) corresponds to the extent of the slice. For generating a transverse magnetization in this shaded location (d), we will apply a brief RF magnetic field with frequencies spanning f1 to f2 (c) to the tissue.*

The two last processes will be defined simultaneously because they are both responsible for encoding the two-dimensional image of each slice (obtained thanks to the slice selection discussed above). Indeed, frequency and phase encoding are used to obtain information for the individual points within a slice, which are called pixels in 2D imaging, or voxels in 3D imaging. All these voxel's information will then be stored in a grid which will be explained later.

Concerning phase encoding, a short temporary change in the magnetic field is applied between the RF excitation pulse and the readout of the signal. This change causes a shift in the phase of the precessing spins. The magnitude of the phase shift depends upon the duration of this gradient switch. By repeating this process with varying durations of the temporary gradient, signals with different phase encodings are obtained. This phase encoding gradient allows for the division of the slice into "rows" on our grid previously mentioned. When considering the slice as an XY plane, this gradient varies along the Y axis and is therefore referred to as Gy (see Fig.1.9).

The next step involves frequency encoding, which is used to differentiate pixels within the same phase encoding. During signal readout, a magnetic gradient is applied. This causes a specific shift in the resonance frequency, similar to the effect of the slice-encoding gradient. This shift allows the differentiation of voxels within the same phase. When we refer back to our grid, this frequency encoding gradient represents the information stored in the "columns". The variation of this gradient follows the X axis, perpendicular to the phase encoding gradient, and it is denoted as Gx (see Fig.1.10).

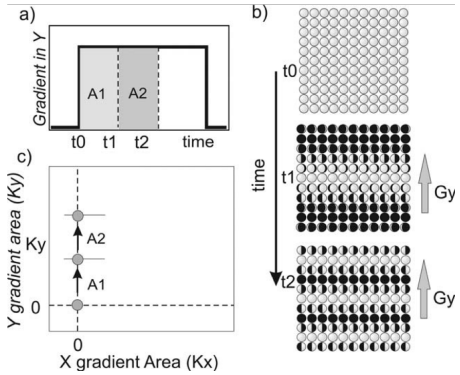

***Figure 1.9: Phase encoding**, retrieved from [5]. During the application of a Gy gradient, the slice (here represented as a square array of spheres) undergoes precession (b) for different durations (a). The resulting k-space encoding can be characterized by plotting the gradient area against time (c), which provides information about the rows of this space (Ky).*

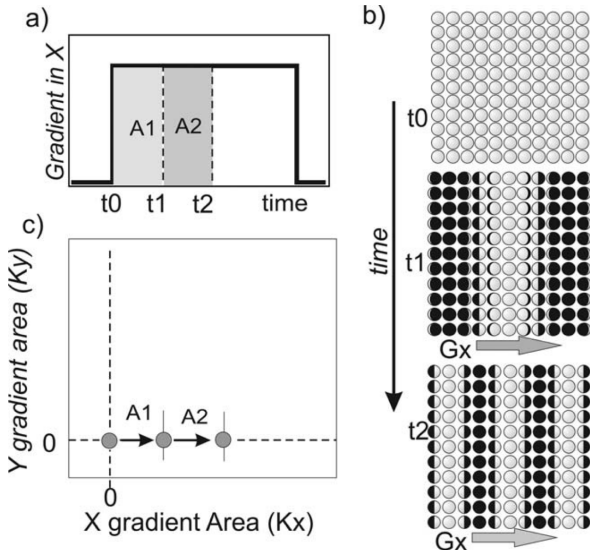

***Figure 1.10: Frequency encoding**, retrieved from [5]. During the application of a Gx gradient, the slice undergoes precession (b) for different durations (a). The resulting k-space encoding can be characterized by plotting the gradient area against time (c), which provides information about the columns of this space (Kx).*

Combining phase and frequency information allows thus the creation of our grid (see Fig. 1.11). This raw data grid consists of a regrouping of all the slice information, but in a different space than the original one, called the k-space or Fourier space. In this space, with columns and rows respectively defined by frequency and phase encoding, each pixel has a defined combination of phase and frequency. This "k-space" data represent thus functions with given amplitudes as a function of time and can be transformed using a Fast Fourier Transform. The Fourier transform

produces a curve representing an amplitude as a function of the frequency, with the amplitude of each frequency representing the intensity of each pixel of the row. Applying the Fourier transform in both the frequency and phase encoding directions allows for the acquisition of the desired image.

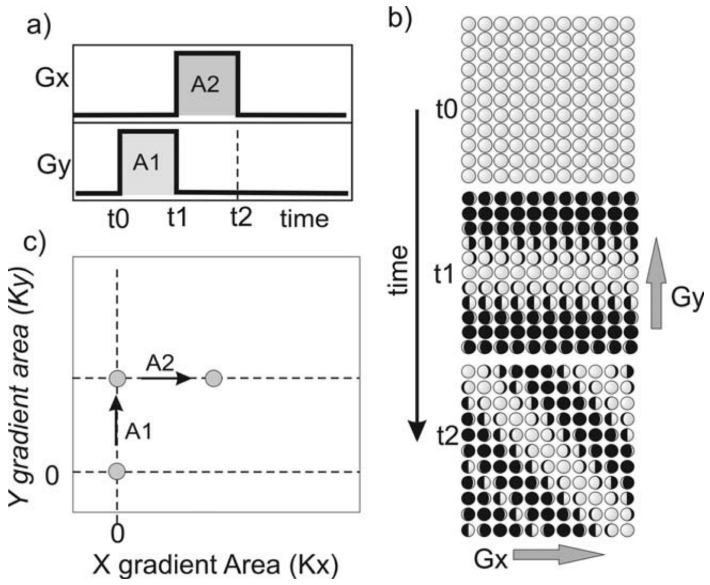

Figure 1.11: Combination of phase and frequency encodings*, retrieved from [5]. We can see here the combination of a phase encoding gradient (Gy) followed by a frequency encoding gradient (Gx).*

1.2 Functional magnetic resonance imaging

Now that MRI has been properly defined, we can dive into the understanding of a precise type of MRI which is Functional Magnetic Resonance Imaging, or fMRI.

1.2.1 Definition of fMRI

Functional MRI is thus a modality of MRI which allows the measurement of brain activity and connectivity, hence its name. By contrast, structural MRI is an imaging technique able to show anatomical properties and help in the analysis of different tissues or particular anatomical structures.

FMRI consists in identifying changes in brain metabolism during a certain experiment. These changes can of course be provoked by using a task cognitive state changes, e.g. moving an arm or reacting to visual stimuli. Another measurement can be made when not asking the patient anything, letting him in his thoughts. This second type of experiment is called a resting-state experiment.

What has been stated here above is also suitable for other functional imaging techniques, such as positron emission tomography or electroencephalography, but fMRI uses the blood as an indicator. More precisely, it uses the Blood Oxygen Level Dependent (BOLD) contrast.

1.2.2 Haemodynamic response

For understanding the BOLD contrast, it is first important to understand brain metabolism and how it is affected by a task.

Brain metabolism refers to the biochemical processes occuring within the brain to support its functioning and energy needs. It involves the conversion and utilization of nutrients, such as glucose and oxygen, to produce energy and essential molecules required for neuronal activity.

Like in the rest of the human body, glucose is the primary energy source for the brain. To generate energy, it undergoes glycolysis to produce adenosine triphosphate (ATP), the cell's energy molecule. Besides sugar, oxygen is also essential in this process. Indeed, oxygen allows for oxidative phosphorylation, a process which occurs within the mitochondria to produce additional ATP. Together, glycolysis and oxidative phosphorylation provide the energy required for various cellular activities in the brain.

When a subject is performing a task, there are neuronal signals. Thanks to the previous paragraph, it is now understood that these signals consume adenosine triphosphate (ATP). As this molecule (ATP) is produced by glycolytic oxygenation of glucose, there is an increase in O_2 need. For satisfying this need for oxygen, there is an increase in local cerebral blood flow (CBF). This rapid delivery of blood due to neuronal activity is called haemodynamic response and it follows a particular function (Haemodynamic Response Function) as depicted in Fig. 1.12. More generally, one will describe the coupling between neuronal activity and blood flow as neurovascular coupling. [7, 8]

These changes in blood flow will also induce perturbations in oxygen concentration in defined zones and the BOLD contrast allows us to observe these oxygen perturbations.

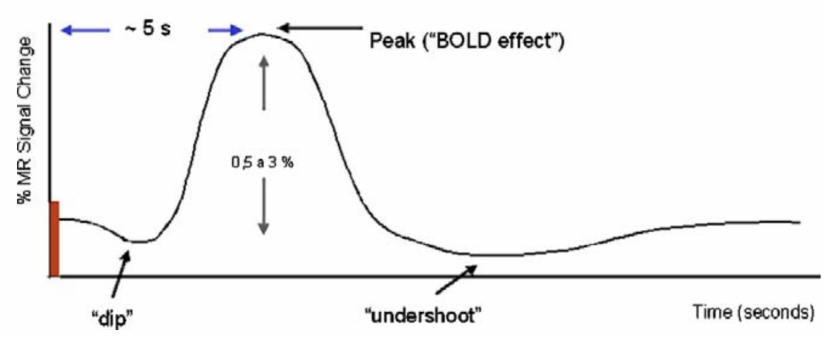

***Figure 1.12: Haemodynamic response function in function of time**, retrieved from [9]. The initial "dip" is happening before the high increase in CBF. During this phase, there is oxygen consumption which is not adequately compensated by blood flow. This is followed by a peak, which is the point where the BOLD contrast is measured. During the peak, there is a substantial influx of oxygenated blood, resulting in an imbalance between oxygenated and deoxygenated blood. This peak can be transformed into a plateau depending on the stimulus. Afterwards, an "undershoot" occurs. an "undershoot" phase occurs, where In this case, the oxygenated blood is depleted and transformed into deoxygenated blood. Finally, a recovery phase takes place, during which the system returns to its initial conditions.*

1.2.3 BOLD contrast

BOLD contrast is the contrast used in almost all fMRI experiments. As mentioned above, it is highly correlated to the haemodynamic response. Indeed, as BOLD stands for Blood Oxygen Level Dependent, it is easy to understand that it is linked to the proportion and amount of oxygenated blood in a certain region of interest.

Actually, this contrast is a result of changes in the magnetic properties of the blood depending on its oxygenation level. The properties of the blood are due to the magnetic behaviour of the hemoglobin (Hb).

Hb is a protein contained in the red blood cells (RBC) which transports oxygen in humans and many other animals. The process allowing Hb to capture oxygen is known as oxygen binding and is due to its structure. Each hemoglobin molecule contains four iron-containing heme groups, and each heme group can bind to one oxygen molecule. When they are not bound to oxygen, each heme group present an unpaired electron.

Because of its structure, Hb alone, without any O_2 thus, has 4 unpaired electrons and is therefore highly paramagnetic. However, once it gains an O_2 and becomes an oxygenated HbO_2, it becomes diamagnetic and magnetically indistinguishable from other brain tissues. With this big difference in terms of magnetic behaviour between these two states of hemoglobin, the paramagnetism of the deoxygenated Hb is used

to detect the changes in blood supply and oxygen level.

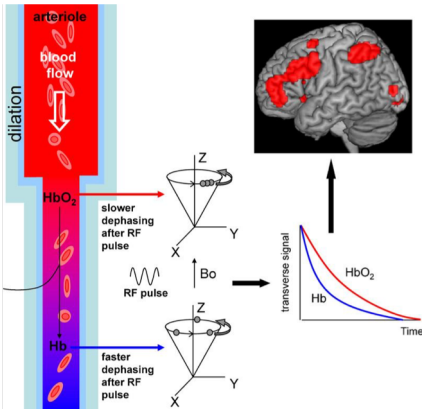

Figure 1.13: Magnetization of Hemoglobin depending on its oxygen state. *In this figure, blue represents deoxyhemoglobin while red stands for oxyhemoglobin. We see on the left that blood comes with Hb charged in oxygen and leave without oxygen. In the middle part is shown the dephasing rate of different states of hemoglobin. These rates are depicted again on the right part where it is clearly stated that $Hb0_2$ is the slowest to dephase, adopting thus a diamagnetic behaviour. Retrieved from [10].*

As depicted in Fig. 1.13, the dephasing of the protons in HbO_2 is much slower than in deoxygenated Hb. The rate of this dephasing corresponds to the combination of T_2 and T_2^* relaxations, where T_2 is a parameter determined by the anatomical location affected by the RF-pulses and T_2^* is due to the heterogeneity of the magnetic field $\overrightarrow{B_0}$.

What happens during the haemodynamic response is thus the following. In the presence of locally deoxygenated blood, an influx of oxygenated blood occurs due to neurovascular coupling, which displaces the deoxygenated blood. This displacement results in a longer spin-spin relaxation time in activated brain regions, as oxygenated blood has lower susceptibility. As a result, a small increase in signal is observed in the activated brain tissue, which is represented by the overshoot and positive BOLD response in the second part of the curve shown in Fig. 1.12.

For choosing our contrast in fMRI, it is important to choose the right weighting. At magnetic field strengths of 1.5T and 3T, the dominant contrast in MRI is T_2^* weighting because it is sensitive to blood and its paramagnetic/diamagnetic changes. Given that most fMRI is currently conducted at or below 3 Tesla, Echo Planar Imaging (EPI) can be used due to its enhanced T_2^* contrast. [7]

Echo Planar Imaging is a particular MRI sequence allowing the scanning of an entire slice in a short time. With this type of sequence, it is indeed possible to fill the entire k-space with only one single magnetic excitation. This is done by applying

the gradients as depicted in Fig. 1.14.

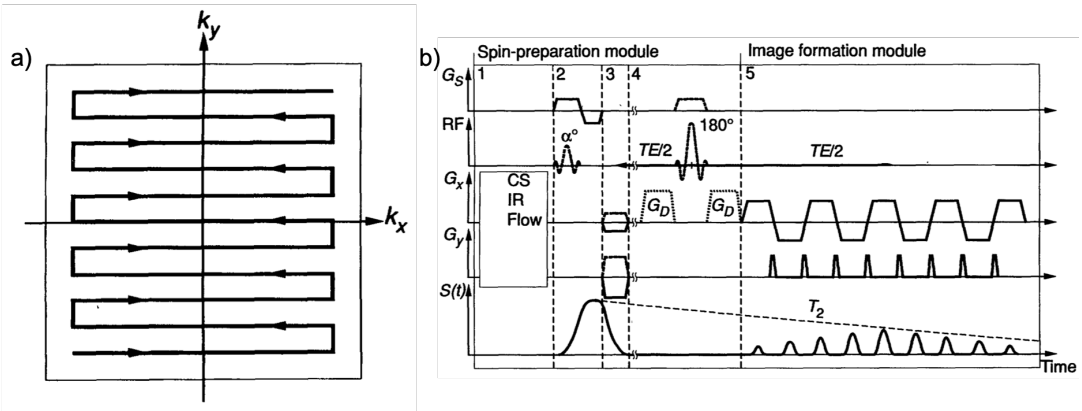

Figure 1.14: Echo Planar Imaging. *On the figure are shown a) a typical k-space filling and b) its associated EPI sequence. On this EPI sequence are plotted the temporal variations of the three orthogonal gradients (G, Gx, Gy), the Radio-frequency pulses (RF), and the resulting signal S(t). Optional pulses for fat or water suppression (CS), T2-weighting with inversion recovery (IR), or flow encoding are contained in Box 1. Slice selection is represented in Box 2. Boxes 3 and 4 illustrate the necessary pulses for EPI. The largest echo occurs at a time TE (in the middle ox box 5) following the initial RF pulse. The dashed line T_2 in S(t) represents the inevitable signal decay during EPI sequences, which imposes limits on the duration of the acquisition window. What is representative of EPI is in the fifth box where Gx oscillates, resulting in left-right motions in k-space. For Gy, the peaks represent the moments when there is a row change in the k-space, allowing to scan the two-dimensional space. This figure has been proposed in [11].*

As fMRI is a functional imaging method, it is necessary to be able to obtain images quickly in order to preserve temporal resolution. Therefore echo planar imaging (EPI) sequences are the most frequently used. These allow indeed whole volume coverage in a brief scan time of 10-100ms, which is important as we want to observe images depicting the brain reaction to our protocol. While the time needed to detect the BOLD response of an activated tissue typically ranges in a few seconds, this echo planar imaging method is thus very useful in fMRI. [12]

1.2.4 Study designs

When preparing an fMRI experiment, the choice of the experimentation design is also very important. First of all, two design categories are distinguishable: resting state and task-based designs. As stated in its name, the first design aims at studying the resting brain and what are called resting state networks, implying thus also the study of their modification by disease conditions such as Alzheimer's, depression and other psychiatric disorders. It is the most straightforward experimental design and

here subjects are only asked to perform very simple tasks. For example, they can maintain their eyes closed, open, or fixed on something, depending on the research question and purpose of the experiment.

The second type of design is related to protocols where the subject is asked to do something or to pay attention to particular stimuli. This category is divided into different strategies: blocks, event-related and mixed designs.

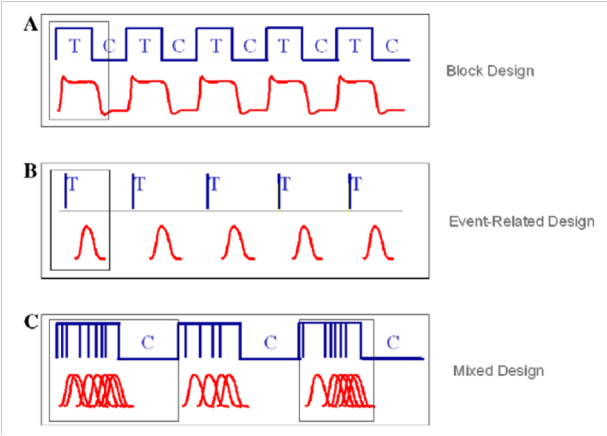

Figure 1.15: The 3 different task-based designs. *In this figure are depicted the 3 types of study designs in fMRI. On A) is the block design, where prolonged stimuli ("T" on the blue curve) allow a plateau in the BOLD signal (in red). B) shows an event-related design where short stimuli induce a classical hemodynamic response. C) is represented as an example of mixed design, showing many brief stimuli during precise periods. Retrieved from [9].*

In a block design, or "two-condition" design, one state is designated as the experimental condition, while the other is referred to as the control condition. The objective is to test the hypothesis according to which the signals vary between the two states. The trials are arranged to alternate between the experimental and control conditions using a block design, as illustrated in Fig. 1.16. Typically, each block is a few tens of seconds long, which allows the block design to be the most effective for detecting brain activation. Indeed, if the stimuli are prolonged, there is the formation of a plateau after the "peak" of the BOLD signal induced by the haemodynamic response. This plateau will thus produce a more significant and stable signal.

However, when characterizing the amplitude or timing of the haemodynamic response is desired, a jittered event-related (ER) design is preferred. In the ER design, task events are brief and occur at non-constant intervals. This implies thus using longer periods of control condition, which enables the haemodynamic response to return more fully to baseline. Having jittering timing allows for higher temporal frequency sampling of the haemodynamic response, but it can also be utilized to induce a desired cognitive strategy, such as avoiding an anticipatory response or

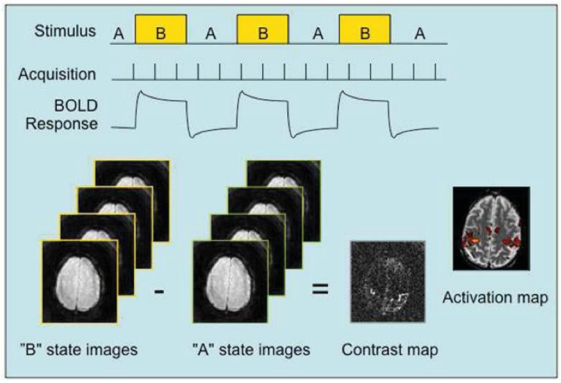

Figure 1.16: Block, or "two-condition" design. *Here "A" state represents the control condition while "B" state is the experimental condition. Like in Fig.1.15, we can see the plateau formation in the BOLD response. Retrieved from [7].*

maintaining attention. [7]

The third design, the mixed design, is a hybrid of block and event-related designs. It can provide information about "sustained" and "transient" neural activity during paradigm performance. This technique combines the repetitive stimulus measurements of the block design with the detection of transient responses found in event-related designs. It enables researchers to identify brain regions which exhibit item-related information processing (transient) or task-related information processing (sustained). [9]

1.3 Alcohol dependence

1.3.1 Alcohol use disorder

Following National Institute on Alcohol Abuse and Alcoholism, Alcohol Use Disorder (AUD) is a medical condition characterized by an impaired ability to stop or control alcohol use despite adverse social, occupational, or health consequences. It encompasses the conditions which some people refer to as alcohol abuse, alcohol dependence, alcohol addiction, and the colloquial term, alcoholism. [13]

Globally, AUD is one of the most common mental disorders. Individuals suffering from such disorders experience symptoms such as lacking control over their alcohol consumption and engaging in heavy and progressively increasing alcohol use. Even though it has severe negative impacts on their overall health, their family and friends' lives, and society in general. This compulsive alcohol use remains undertreated, despite its significant public health consequences. [14]

While alcohol consumption is a major risk factor for multiple diseases, the global production and marketing of alcohol have increased its consumption and associated

harms. According to the Alcohol Group of the Global Burden of Disease study, [15] alcohol ranked seventh in terms of risk factors for deaths and disability-adjusted life years (DALY), with a worldwide significant percentage of male (6.8%) and female (2.2%) deaths attributed to alcohol consumption. In 2016, 2.8 million deaths were globally linked to alcohol consumption, making it the top cause of premature death and disability in individuals between 15 and 49 years old. The study also concluded that minimizing alcohol consumption to zero would reduce overall health risks. [16] Comparable numbers have been stated by the World Health Organization (WHO). They indeed declare worldwide 3 million deaths every year resulting from the harmful use of alcohol, representing 5.3% of all deaths. Concerning the global burden of disease and injury, WHO attribute 5.1% of it to alcohol. [1]

Fig.1.17 shows the alcohol use prevalence in the world in 2016, without distinguishing men and women. It is notable that both men and women have the highest prevalence of alcohol use disorders in high-income countries (8.4%) and upper-middle-income countries (5.4%). [14] This map proves that AUD should not be underestimated or disregarded, due to its significant impact on individuals and society. It also shows that there are socioeconomic inequities regarding this.

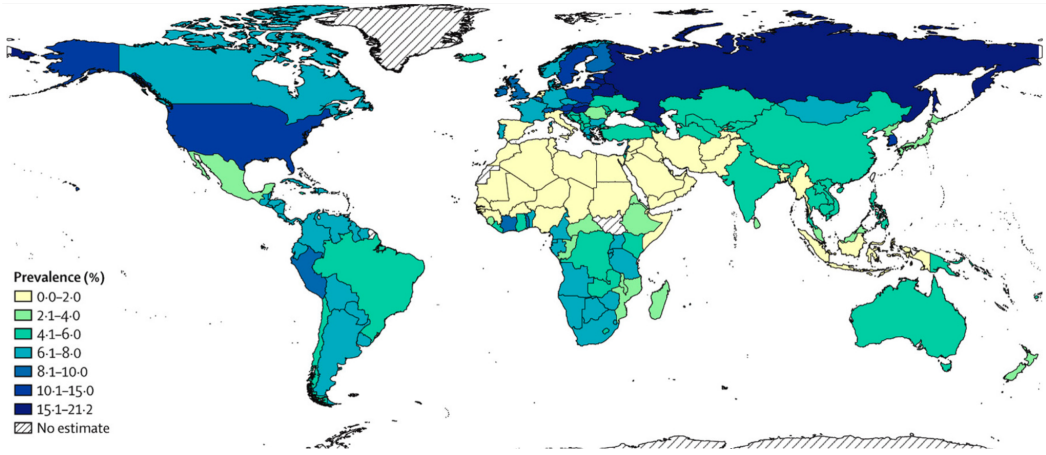

Figure 1.17: *Alcohol use disorders prevalence in 2016. Retrieved from [14].*

1.3.2 Alcoholics and alcohol-associated stimuli

Now that we know a bit more about alcohol use disorder, we can dive into what interests us for this thesis, i.e. the way the brain reacts to alcohol cues depending on the abstinence level of the subjects.

For understanding this, it is important to review all the different areas of the brain implicated in this process according to the literature.

The mesocorticolimbic system

The mesocorticolimbic system, illustrated in Fig. 1.18, is composed of two dopaminergic pathways: the mesolimbic and mesocortical pathways. As our interest is focused on the dopaminergic pathways, we can look at the green-coloured connections in this figure, between prefrontal cortex (PFC), ventral tegmental area (VTA) and ventral striatum (VS).

The mesolimbic pathway connects the VTA in the midbrain to the VS of the basal ganglia in the forebrain, including the nucleus accumbens and olfactory tubercle (see Fig.1.19). This pathway is primarily involved in processing rewards and has an impact on motivation and desire for rewarding stimuli. Studies have shown that abnormalities in this pathway and in the nucleus accumbens play a significant role in the development and maintenance of addictions. [17, 18] While the nucleus accumbens has dopaminergic neurons coming from VTA, it also has glutamatergic neurons of the hippocampus, amygdala, and medial prefrontal cortex.

The mesocortical pathway, on the other hand, is characterized by dopaminergic projections from the VTA to the PFC (see Fig. 1.19). With one extremity (PFC) being thought primarily involved in higher order cognitive functions, [19] the mesocortical pathway is likely to play a role in cognitive control, motivation, and emotional response. [17, 20]

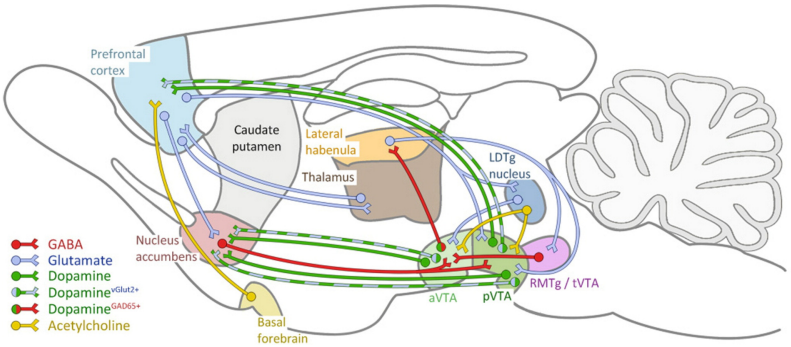

Figure 1.18: Mesocorticolimbic system. *This figure depicts a simplified illustration of the primary connections to and from the mesocorticolimbic system. The view is presented here in a sagittal section of a rodent's brain. The projections of glutamatergic, dopaminergic, cholinergic, and GABAergic pathways are colour-coded in blue, green, yellow, and red, respectively. The abbreviations used in this figure are aVTA for the Anterior Ventral Tegmental Area, LDTg for Laterodorsal Tegmental Nucleus, NAc for Nucleus Accumbens, PFC for Prefrontal Cortex, pVTA for Posterior Ventral Tegmental Area, RMTg for Rostromedial Tegmental Nucleus, and tVTA for the Tail of the Ventral Tegmental Area. Retrieved from [21].*

Globally, this mesocorticolimbic pathway is responsible for assessing and integrating environmental and emotional stimuli, resulting in the appropriate activation of motor patterns supporting various motivated behaviours, determined by our reward system. According to experimental studies, the principal neurotransmitter

of this system, dopamine (DA), plays a crucial role in encoding the motivational value and significance of a particular stimulus. [22] Additionally, it has been well-established that the motivation to self-administer drugs of abuse despite their harmful effects is influenced by both short-term and long-term changes in DA transmission. [21]

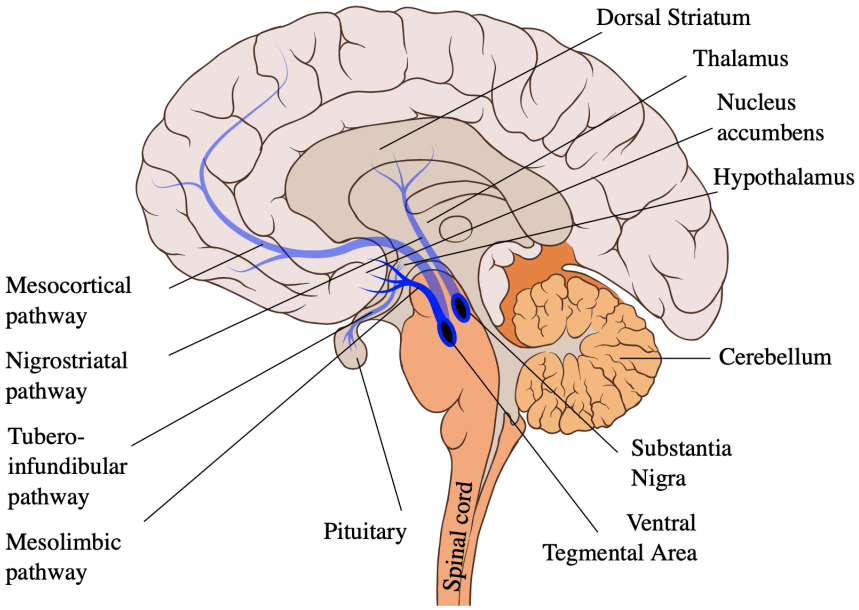

Figure 1.19: Dopaminergic pathways. *In this figure are presented in blue the four main dopaminergic pathways, i.e. mesolimbic, mesocortical, nigrostriatal and tuberoinfundibular pathways. Some anatomical structures are also annotated for facilitating one's understanding. Retrieved from [18].*

Getting back to the main topic of this chapter, let's see what impact alcohol and other drugs have on this system. Drugs of abuse stimulate the mesocorticolimbic system. While this system responds to natural rewards like food, water, and sex, drugs of abuse elicit a larger amplitude and longer duration of dopamine response than normal physiological responses. Repeated drug intake allows drug-related cues to become conditioned stimuli predicting drug response. This leads to an increase in the salience of drug cues and associated contexts. It has been proven that drug-related cues elicit greater brain activation within the mesocorticolimbic circuits, including the VTA, ventral striatum (VS), amygdala, anterior cingulate cortex (ACC), prefrontal cortex (PFC), insula, and hippocampus in drug users. [23, 24] If many of these structures are logically impacted by these drug-related cues because of their place in the mesocorticolimbic system, the amygdala and the hippocampus are activated because they are known to play distinct roles in conditioned learning. [25] This suggests that when these regions are activated in neuroimaging studies, it is due to the processing of learned reward values associated with conditioned cues and contexts.

The anterior cingulate (ACC) and insula are believed to play important roles in drug-cue reactivity and addiction. The ACC is involved in cognitive tasks such as control, conflict, and error monitoring, [26] but it is also activated by salient stimuli, including reward-related and negative affect stimuli. [27] Similarly, the insula is associated with interoception, but it is also engaged during tasks requiring cognitive control and in response to salient external stimuli. These regions are thus part of a larger brain network integrating internal and external signals of salience and initiate interactions between brain networks to meet control demands. [28]

Drugs of abuse can enhance the way the brain senses and processes cues associated with rewards. This enhanced processing can trigger attentional biases in drug users and it increases drug-seeking behaviours. This effect is thought to be mediated by increases in dopamine and other neurotransmitters and may promote learning and plasticity processes. Neuroimaging studies have often shown strong activation in sensory and perceptual cortices in response to drug cues, which may be due to these mechanisms. [28]

Nigrostriatal system

In addition to the mesocorticolimbic system, connecting various brain regions such as aforementioned above, drug-induced increases in dopamine affect another ascending dopaminergic system: the nigrostriatal system. The nigrostriatal DA system consists of dopamine projections from the substantia nigra to the globus pallidus, caudate and putamen (see Fig.1.19), which are involved in habit learning and automaticity. Together, the caudate and putamen form the so-called dorsal striatum (DS). Other evidence suggests that the dorsal striatum is more strongly activated in response to drug cues than to neutral stimuli in drug users.

The DS can be divided anatomically and functionally into the dorsomedial striatum (DMS) and the dorsolateral striatum (DLS), corresponding respectively to the dorsal caudate nucleus and to the dorsal putamen. The DMS is involved in action and outcome learning, and in the acquisition of an instrumental response. While the DLS is involved in the development and expression of habits. Habits are learned behaviours becoming automatic responses to stimuli and are no longer goal-directed. The neural control of behaviour shifts from the ventral to the dorsolateral striatum as habits become more automatic. [28]

Several studies have shown that drug addicts exhibit higher activity in the DS region of the brain in response to drug cues than neutral cues. [29] A recent study showed that heavy drinkers had high cue-induced activation in the DS region when presented with alcohol-related taste cues. [30] This DS activation was added to an expected activation in the VS region (due to the mesocorticolimbic system). Activation in both regions was stable over a short period. Heavy drinkers showed greater cue-induced activation in the DS than light social drinkers, while light drinkers

showed greater activation in the VS and PFC. Activation of the DS to drug cues was positively correlated with drug craving in all participants, in contrast to the VS where activation was negatively correlated with drug craving in heavy drinkers. These results are consistent with the theoretical hypothesis suggesting that drug use begins with haedonic and controlled behaviour (mediated by the VS and PFC) before moving to habit-oriented and ultimately uncontrolled and compulsive behaviour (mediated by the DS). [28]

Other anatomical structures activation

While these two systems are the most studied in the literature when looking into reactivity to alcohol and drug cues, some other anatomical structures are often mentioned. This includes thalamus, [28, 29, 31, 32] fusiform gyrus, [28, 29, 33, 32] and cerebellum. [29, 28]

The thalamus is a pair of grey matter clusters located bilaterally in the forebrain, positioned superior to the brain stem, near the centre of the brain. This structure sends neurons in all directions to the cerebral cortex. The medial surface of the thalamus forms the upper portion of the lateral wall of the third ventricle. It performs multiple functions, including the transmission of sensory and motor signals to the cerebral cortex, as well as the regulation of states of consciousness such as sleep and alertness. It is thus relatively logical to find this type of structure when considering reactivity to specific cues.

In the case of alcohol cues, thalamic activity was found to be positively correlated with differences in skin conductance responses between alcohol and neutral cue blocks. Mediation analyses showed that thalamic activity mediated the correlation between craving and skin conductance response. These findings show thus the physiological and neural connections with the reaction to alcohol cues. [34]

Concerning the fusiform gyrus, it is situated in Brodmann area 37 and is part of both the temporal and occipital lobes. It is positioned between the lingual, parahippocampal and inferior temporal gyri. If some believe it plays a role in recognition (notably face recognition among others), [35] others also attribute it a role in the processing of emotional pictures. [36] Its role in cue reactivity can thus easily be explainable.

The human cerebellum appears as a distinct structure located beneath the cerebral hemispheres and attached to the bottom of the brain. The cerebellum is primarily recognized for its vital role in motor control, although it has also been linked to certain cognitive functions like attention and language, as well as emotional regulation such as the control of fear and pleasure responses. However, its motor-related functions are the most well-established. The cerebellum's role would be to assist in the coordination, precision, and timing of motor information. It receives input from

sensory systems of the spinal cord and other regions of the brain, and integrates these inputs to refine motor activity. It has thus also an important impact on motor learning. [37, 38]

The cerebellum is particularly sensitive to the effects of alcohol, even at low concentrations (typically after consuming 1-2 units of alcohol). As a result, the cerebellum is responsible for the well-known motor and balance impairments associated with alcohol consumption. Furthermore, research has revealed that the cerebellum plays a role in more cognitive and emotional responses to alcohol. [39] Studies have shown that genetic variation in the cerebellum response to alcohol affects susceptibility to AUD. The cerebellum's sensitivity to alcohol also makes it a common target for brain damage in adults with AUD. [40]

Factors influencing alcohol cue reactivity

If the systems and structures previously mentioned always play important roles in the reaction to alcohol (and more generally drugs) cues, it is still important to note that neuronal reactions to specific cues can further be influenced by some factors. Jasinska et al. (2014) proposed a summarizing model of all these factors as depicted in Fig.1.20.

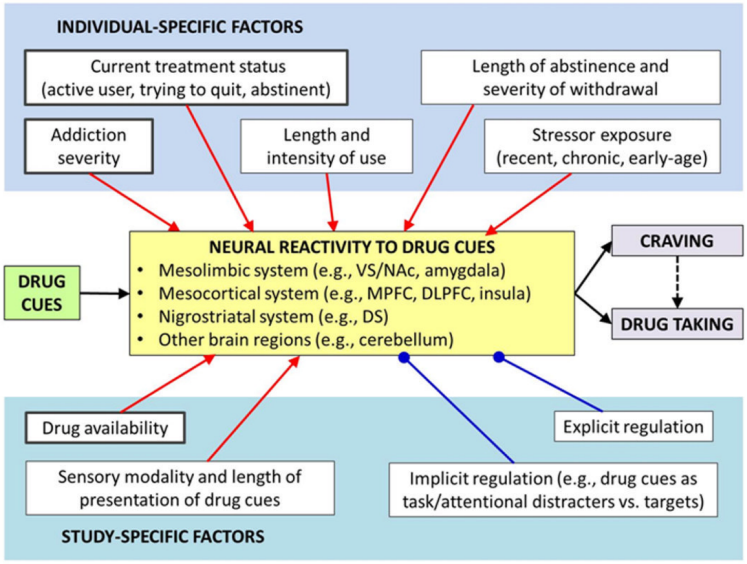

Figure 1.20: Factors influencing reactivity. *The model uses red arrows to indicate that, for most factors, a higher or more active level of the factor is hypothesized to enhance brain responses promoting craving and/or motivation to take the drug. On the other hand, the model uses blue circle-ended lines to indicate that regulation factors are hypothesized to enhance brain responses suppressing craving and/or drug taking, decreasing the brain responses to drug cues. Factors believed to be strong or dominant (relative to other factors) are depicted in thicker boxes, as they may mask or decrease the effects of other factors unless they are appropriately controlled. Retrieved from [28].*

Chapter 2

Materials and methods

The following chapter will cover the topic of the experiment and the different steps needed in the experiment to obtain the results.

2.1 Description of the experiment

The aim of the experiment behind this thesis is to spot and assess the activation of the different regions of the brain reacting to alcohol cues. These activations will then allow further comparisons between alcohol-dependent subjects and control subjects, and among alcohol-dependent subjects for differentiating the steps of their cure.

For measuring the activation of the brain, we will use an MRI scanner in order to produce functional magnetic resonance images during a task. These images will then be used to create activation maps from which we will be able to retrieve the main activation zones.

The participants of this study have all signed consenting documents and they form our "set" of subjects. This set is composed of 73 subjects, among which 53 are alcohol-dependent subjects looking for a detoxification treatment and 20 are control subjects corresponding to some criteria.

The subjects were asked to come for multiple sessions in order to collect data at different times, for the evaluation of their results. Concerning alcohol-dependent subjects, they were asked to come for 3 sessions, the first one taking place on their first day of treatment, the second being made after 18 days and the last one after 90 days (3 months). Unfortunately, if we count 53 first sessions, we only have 48 second sessions (90.5%) and 13 subjects count 3 sessions (24.5%). For the 20 control subjects, they were asked to come for only 2 sessions. These two sessions took place 18 days apart. Their results between the different sessions should indeed be relatively similar as their condition isn't supposed to evolve with time. Out of our 20 controls present for the first session, 19 came back for the second session (95%).

The experiment which interests us for this study consists of a simple task performed by the participants: look at a computer where different images are displayed. These images are visual stimuli and subjects don't have any explicit action to do while witnessing these. These stimuli are divided into 3 categories: alcoholic beverages, non-alcoholic drinks (water, soft drinks, tea, coffee) and food. Having these 3 categories permits the study of one condition compared to another removing general activation zones (e.g. activation linked to random visual stimulation, general stress-induced activation etc.).

The experiment follows a block-design (see 1.2.4) pattern. A typical session is divided into 4 parts which we will call "sequences". Each of these sequences is composed of 3 blocks, each of 10 images. Within a block, there are only pictures belonging to the same category of stimulus (alcohol, soft or food). The order of the 3 blocks within a sequence varies, providing sequences with first food, then alcohol and soft, or with first alcohol, then soft and food, and so on. In one sequence, there is always one block of each category. About the timing, each image within a block lasts for 1.5 seconds, with 0.5 seconds of "washout time" between these. The resting time between two blocks of a sequence is of 12 seconds during which a fixation cross is displayed. Adding these timings, we obtain a total duration of around 7 minutes. A diagram resuming the protocol aforementioned is depicted in Fig. 2.1.

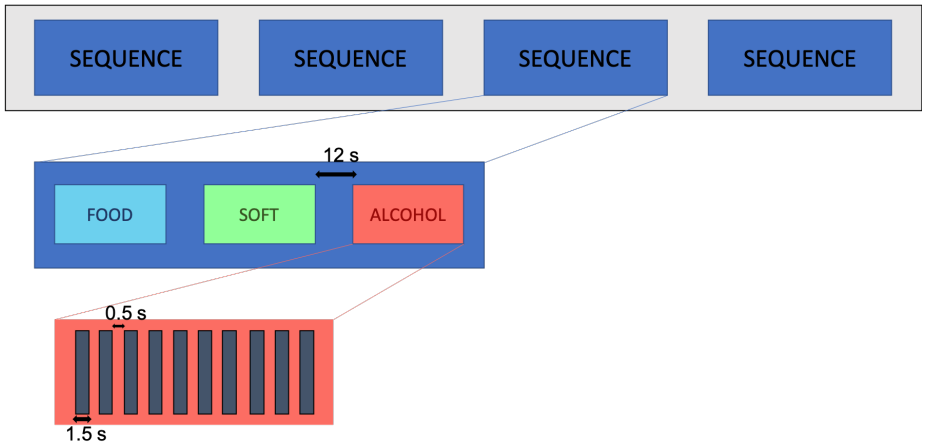

Figure 2.1: Schema of the experimental protocol. *This figure is a summary enabling a better understanding of the experiment protocol. In this figure are presented in blue the 4 "sequences", with each of them containing 3 "blocks" in different colours. These colours represent the categories of stimuli sent to the subjects (red = alcohol, light blue = food and green = non-alcoholic beverage). On the lower part of this figure is a block containing alcohol images. We find in it 10 pictures displayed 1.5s and separated by 0.5s intervals.*

2.2 Raw data treatment

Once the experiment is made, the scanner gives us many data, in the form of DICOM (Digital Imaging and Communications in Medicine) files. As they are, they are not classified in a standardized way. Also, if DICOM files are very practical for storing and transmitting medical images, they contain lots of data and are not directly usable for further operations. Functional Magnetic Resonance (FMR) images need to be extracted from these raw data structures. While extracting this information in order to produce ".fmr" files, a reclassification will also be made in order to standardize our file sorting. This new way of classifying will follow what is called "Brain Imaging Data Structure" standards, or "BIDS". [41]

The objectives of this standardized classification are multiple. First of all, the data will be easily accessible for other researchers to work with. Indeed, if the standardization is clearly stated, one can easily understand the file organization and format by referring to BIDS documentation. [41] This is particularly valuable if multiple individuals are expected to work on the same data over time. Implementing BIDS saves the effort of decrypting and reusing data collected by a previous worker. Furthermore, there is an increasing number of data analysis software supporting BIDS-compliant data.

Finally, if the data were to be published in by journal requiring them, using BIDS to structure and describe the data can significantly reduce the time and effort spent during the publication process and accelerate eventual further work being done on it. [42]

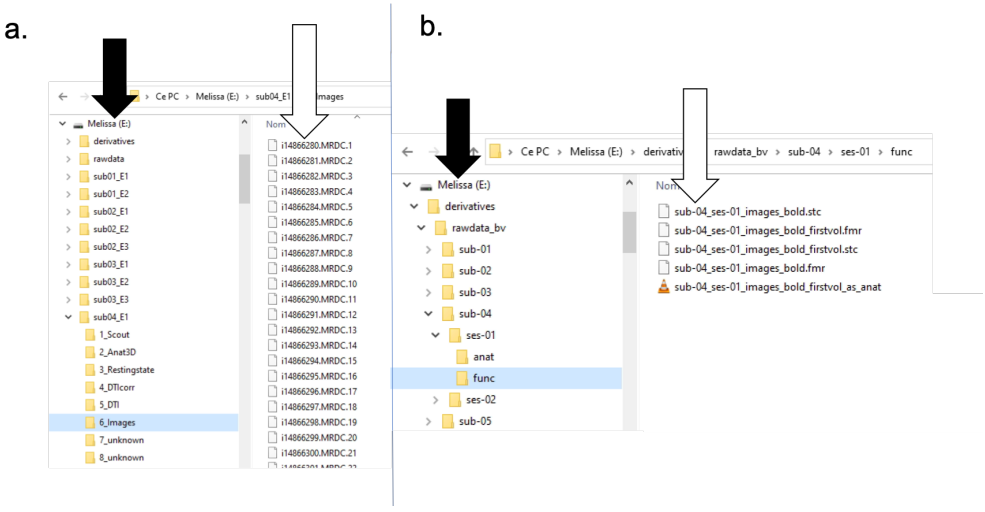

Figure 2.2: Raw data treatment. *This figure shows what has been done in terms of standardized classification and FMR data extraction. On* ***a.*** *is the data as it was received originally and on* ***b.*** *is how it was transformed after this first step. The filled arrows indicate the easier classifying of files and the empty arrows show the creation of FMR files.*

The figure presented here (Fig.2.2) is an example of how the data has been standardized and what is obtained after the extraction of FMR data from the DICOM file.

This step has been entirely automatized thanks to Python scripts which are available at the following address: `https://gitlab.com/maxboyens/neuroimagery-and-alcohol-addiction`. The concerned scripts on this git are the two firsts.

2.3 Preprocessing

Once the data of interest are extracted (our FMR files), and classified following the BIDS standard, we must preprocess it to correct for scanning errors/inaccuracies or physical phenomenons impacting the quality of our measurements.

The following steps, until VTC Creation (cf. section 2.5), have also been automatized by Python scripts available on the aforementioned git. Unlike the first step, the Python scripts used for these steps have to be run through the BrainVoyager (BV) application. BrainVoyager is a powerful neuroimaging software package for data management and data analysis. It will be used to treat and analyze the data of our experiment.

2.3.1 3D motion correction

In fMRI, the experiment is taking several minutes. Therefore, there is always variation in the head positioning during this experiment. Even if motion is very discrete and unseen by the doctor taking the measurements, it is necessary to take it into account afterwards. Moreover, this experiment tested patients suffering from AUD. Hence, they can present tremors while being in the MR scanner. Considering these elements, it is mandatory to process the data regarding the head motion in order to improve the results and the statistical efficiency of the study. In order to do this, BrainVoyager provides a built-in motion correction algorithm.

Motion correction consists first in selecting a reference functional volume from a run, generally the first volume. All other volumes are then aligned to this reference one. Head motion algorithms typically describe head movements using six parameters: three translation parameters and three rotation parameters. These six parameters are used because it is possible to express any spatial displacement following three axis and rotations around these.

The algorithm proposed by BV works as follows. By iterations, the parameters are estimated by analyzing how a volume should be translated and rotated to align with the reference volume. A common measure of adequacy is the difference

in intensity values between corresponding positions in the two volumes. The iterative parameter adjustment process continues until no further improvement can be achieved. This process usually uses a standard optimization algorithm, e.g. a non-linear least squares routine. In our case, BV uses the Levenberg-Marquardt method.

Once the final motion parameters have been determined, they can be applied to the volume to generate a new one in the motion-corrected data set. It is important to note that the creation of the corrected volume involves spatial interpolation, where the signal values are calculated for the positions between the measured data points.

Line plots of the translation and rotation parameters over time are provided for visual inspection. They illustrate how the estimated values change from volume to volume (see Fig. 2.3). [43]

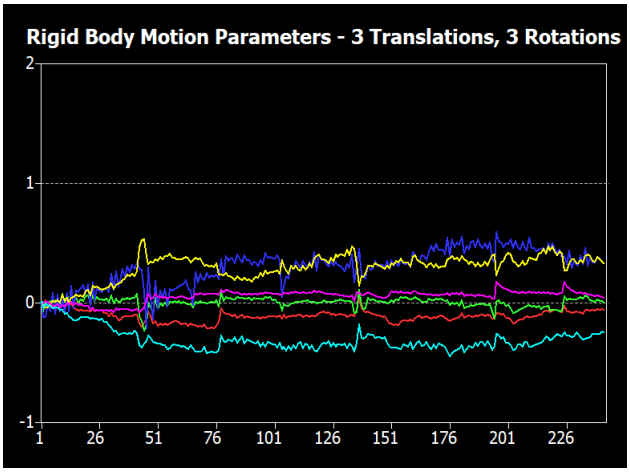

Figure 2.3: 3D motion correction. *This figure depicts the evolution of the motion correction parameters with time. In red, green and blue are the translations following respectively x, y and z axes. In yellow, magenta and indigo are the rotations around the same axes. This plot concerns specifically the parameters obtained when applying 3D motion correction on the third participant's first session (sub03-ses01).*

What is left to choose is the interpolation method to use for detecting the motion and computing the new volume. Three options are available in BV: trilinear interpolation, sinc interpolation and a mix of the two first ones called "trilinear/sinc interpolation". The two first use the named interpolation method for both motion detection and correction. Trilinear interpolation is the fastest one but sinc interpolation offers better results, at the cost of longer computational time. Consequently, the third option proposes an interesting compromise and is often preferred. This method uses trilinear interpolation for motion detection and sinc interpolation for motion correction. It offers thus good motion correction while not losing too much time in the motion detection step. "Trilinear/sinc interpolation" is the method which has been used in this thesis. In the Python script, the corresponding line is `doc_fmr.correct_motion_ext(0, 2, 1, 100, 1, 1)`.

2.3.2 Slice scan time correction

Another essential preprocessing step consists in resolving the differences in the timing of individual slice acquisitions. This issue is due to the process of 3D scanning. A functional volume, such as a brain or a part of it, is typically captured in a sequence of several 2D slices. Hence, the data from the last slice is obtained much later than the data from the first slice. This induces imprecise time specification on the order of a second. While the hemodynamic response is relatively slow, also in the order of a second, this can lead to a loss of statistical power.

To deal with the impact of slice scanning time differences, the method chosen in this thesis consists of "grouping" the slices of an identical volume into the same time point. This approach involves shifting the data of each slice to the reference acquisition's time point. This adjustment transforms thereby the data as if the entire volume had been acquired simultaneously.

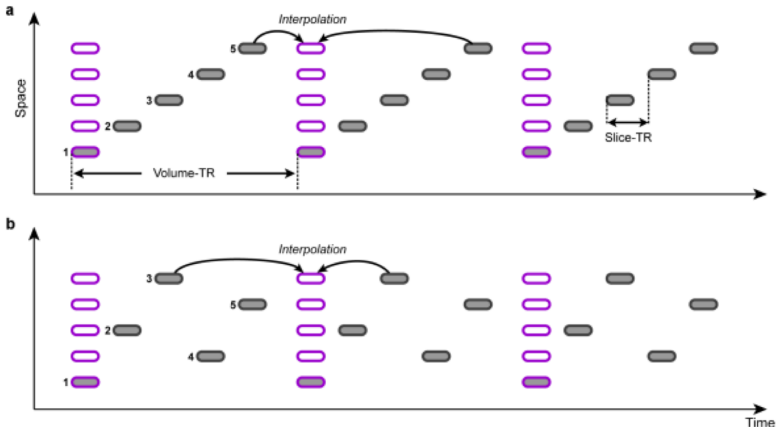

Figure 2.4: Slice scan time correction. *This figure depicts the slice scan time correction discussed in this section. While the pink boxes represent the data shifted to the new time points, the grey rounded rectangles are the original scan times. It also illustrates two examples of scanning orders: ascending scanning (a) and interleaved scanning (b), each consisting of five slices. Retrieved from [43].*

When correcting for slice scan time, it is crucial to consider the scanning method employed during the experiment. Various methods are used, including ascending or descending orders, as well as interleaved scanning. For example, in interleaved scanning, the odd-numbered slices are typically recorded before the even-numbered slices.

In order to estimate values at the non-measured time points, different interpolation methods can be used. In BrainVoyager, three interpolation methods are available: linear, cubic spline, and sinc interpolation.

The first one, the linear interpolation method, computes these values by averaging neighbouring points values. This average is weighted by their relative dis-

tance. While the linear interpolation method is computationally efficient, it tends to smooth the data. In contrast, cubic spline and sinc interpolation methods solve this smoothing issue by incorporating more neighbouring points, resulting in highly accurate resampling. These more advanced interpolation methods are of course demanding more time to process. Considering this, the cubic spline interpolation has been chosen for this thesis. The aim of this choice is to avoid unintentional smoothing lowering the statistical results. In the Python script, the corresponding line is `doc_fmr.correct_slicetiming(1, 1, 1)`.

2.3.3 Temporal high-pass filtering

The temporal signal profile of voxels, or "voxel time courses" in fMRI data often undergo low-frequency drifts. These drifts can be attributed to both physiological and scanner-related noise. These drifts, if not accounted for, significantly lower the statistical power of data analysis. Therefore, the treatment of these low-frequency drifts is a crucial preprocessing step.

To address these slow drifts, a high-pass filter is employed. As its name implies, this filter allows high frequencies to pass through while attenuating low frequencies. High frequencies contain stimulus-related activity and low frequencies correspond to the signal drifts.

BV offers many methods for this temporal filtering. The option chosen in our case is the high-pass filtering using General Linear Model (GLM) approach with a Fourier basis set.

When selecting this approach, the estimation and removal of low frequencies occur using sines and cosines in the time domain. The General Linear Model (GLM) estimates the contributions of low frequencies. The GLM requires a design matrix containing a set of predictors. In this case, the predictors are sines and cosines. For each predictor, the GLM calculates a beta value. These beta values represent weights. In that way, the addition of the predictors, weighted by their betas, generates a predicted time course for each voxel. This temporal evolution corresponds closely to the measured one in the least squares sense.

The effectiveness of the GLM depends upon the predictors. If it is chosen to use sines and cosines as predictors, it remains to decide the number of predictors to use. If only one pair is used, this pair will have a cosine and sine function repeating only once in time. If 2 pairs are selected, functions performing 2 cycles will be added as predictors, and so on. To treat the provided data, 3 pairs of sine and cosine have been used, as it is stated in the code line hereunder. In addition to the sine/cosine predictors, a linear trend and a constant predictor are included in BrainVoyager's GLM. This operation is expressed in Python script by `doc_fmr.filter_temporal_highpass_glm_fourier(3)`.

The predicted time course obtained from the GLM, based on this design matrix, is then subtracted from the original data. This results in a filtered time course only containing frequencies above those specified in the design matrix (see Fig. 2.5).

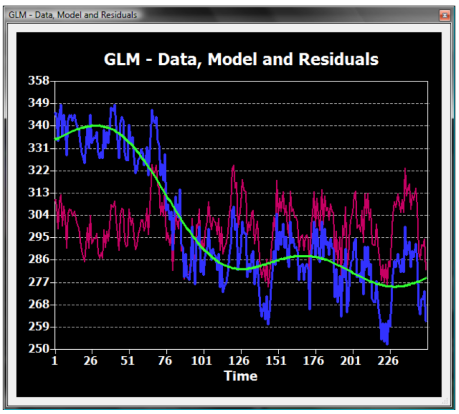

Predictor	Beta
Linear Trend	-27.726
Sine 1	5.613
Cosine 1	12.151
Sine 2	7.112
Cosine 2	-4.823
Constant	299.280

Figure 2.5: Temporal High-Pass Filtering. *This figure depicts an example of how the method combining sines, cosines and GLM works. The left part represents the time course of a voxel in blue, the GLM result in green and the corrected time course in magenta. This magenta curve is obtained by computing the difference between the blue and green curves. In the right part is a table with the predictors and their beta values. Here only two pairs of predictors have been used.*

2.4 Coregistration

Now that the data has been improved by preprocessing, the next step concerns coregistration. In this step, the functional data (FMR file) is aligned with anatomical data (VMR file). This step is mandatory because it provides files necessary for the volume time course (VTC) creation (see section 2.5). Coregistration is proposed by BrainVoyager in a highly accurate and automatized process combining two steps. These steps are called initial alignment (IA) and fine-tuning alignment (FA).

The first one of these, IA, brings functional and anatomical closer together. Before this step, these two data are actually very "far" from each other. There can be many differences between them in terms of orientation or displacement. The initial alignment should therefore align them at least in the same global orientation and spatial location, using large rotations and translations.

As its name suggests, the second step (FA) uses indeed more complicated algorithm to align the data more finely. It takes advantage of the already assured proximity of the data. It would indeed take too long to process without previous IA. This step consists of an iterative minimization of the difference between anatomical and functional data. This results in an accurate alignment.

Regarding the source and target in the coregistration process, the VMR data set (anatomical) remains fixed, while the FMR data (functional) is scaled, translated, and rotated to match the VMR data set. Hence, the FMR file is referred to as the "source" and the VMR file set is referred to as the "target" of the alignment process. In the Python scripts, the line referring to this step is
`doc_vmr.coregister_fmr_to_vmr(fmr_path + fmr_file + '.fmr')`.

2.5 VTC creation

Until now, the data which has been used was stored in STC (slice time course) files. This means that the volumes were divided into 2D slices. However, to perform further analyses, the original FMR data (with an STC format) needs to be transformed into a volume time course (VTC). During this transformation, there will also be a normalization of this volume's space. There exist several normalized spaces but the one chosen for this thesis is the MNI space, which has been defined by Montreal Neurological Institute.

This conversion process from STC to VTC relies on spatial transformation (TRF) files. Three of these are needed to compute the new VTC file. Two of them were obtained from the coregistration step (cf. section 2.4). To get the last one, a former transformation of the VMR from native space to normalized MNI space had been computed. Hence, since the FMR file is aligned with the VMR (cf. section 2.4), the aforementioned anatomical brain normalization transformation can be used. Once the VTC files are created for multiple subjects, they can be used for multi-subject group statistical analyses.

The code lines which were used for creating VTC files are the following.

```
IA_trf = fmr_path + fmr_file + '-TO-' + sub_id + '_' + ses_id + '_IA' + '.trf'
FA_trf = fmr_path + fmr_file + '-TO-' + sub_id + '_' + ses_id + '_FA' + '.trf'
mni_trf = raw_bv_path + '/anat/' + sub_id + '_' + ses_id + '_IIHC' + '_TO_MNI_a12_adjBBX.trf'
vtc = vtc_out + sub_id + '_' + ses_id + '_' + task_name
      + '_bold_3DMCTS_SCCAI_THPGLMF3c' + '_256_sinc3_2x1.0_MNI.vtc'
doc_vmr.create_vtc_in_mni_space(fmr_path + fmr_file + '.fmr', IA_trf, FA_trf, mni_trf, vtc, 2, 2, 100)
```

The MNI normalization computed earlier is obtained thanks to this other line : `doc_vmr.normalize_to_mni_space()`.

It is also worth noting that spatial smoothing with a 5mm kernel has been applied on each VTC. Indeed, VTC smoothing is a processing step commonly employed to enhance the quality of the data. This helps to reduce noise and improve the statistical power of the results. By smoothing the data, small variations caused by random noise are minimized. This results in cleaner and more reliable information. Moreover, it can help to correct for eventual small differences in localization between subjects. These location differences are due to slightly varying functional activation and anatomical dissimilarities across subjects. It makes it thus easier to compare

and analyze data across individuals, allowing for more consistent and meaningful group-level analyses.

2.6 Multi-subject study

2.6.1 Multi-subject design matrix

Now that VTCs are available for each session of each subject, it is time to analyze these by combining subjects in the same study. This is what is called a multi-subject study. For making such a study, the creation of a Multi-subject design matrix (MDM) is needed. The MDM allows researchers to combine and organize data from multiple subjects within a single matrix. This provides a comprehensive overview of the entire study group. This process consists in regrouping all available VTC files for a given session, for a given group of subjects. An example of the MDM file is provided in Fig. 2.6.

```
FileVersion:          3
TypeOfFunctionalData: VTC

RFX-GLM:              1

PSCTransformation:    1
zTransformation:      0
SeparatePredictors:   2

NrOfStudies:          35
"I:/Maxime/derivatives/vtc/sub-04/ses-01/func/sub-04_ses-01_images_bold_3DMCTS_SCCAI_THPGLMF3c_256_sinc3_2x1.0_MNI_SD3DVSS5.00mm.vtc" "I:/Maxime/prt_MNI.sdm"
"I:/Maxime/derivatives/vtc/sub-05/ses-01/func/sub-05_ses-01_images_bold_3DMCTS_SCCAI_THPGLMF3c_256_sinc3_2x1.0_MNI_SD3DVSS5.00mm.vtc" "I:/Maxime/prt_MNI.sdm"
"I:/Maxime/derivatives/vtc/sub-07/ses-01/func/sub-07_ses-01_images_bold_3DMCTS_SCCAI_THPGLMF3c_256_sinc3_2x1.0_MNI_SD3DVSS5.00mm.vtc" "I:/Maxime/prt_MNI.sdm"
"I:/Maxime/derivatives/vtc/sub-11/ses-01/func/sub-11_ses-01_images_bold_3DMCTS_SCCAI_THPGLMF3c_256_sinc3_2x1.0_MNI_SD3DVSS5.00mm.vtc" "I:/Maxime/prt_MNI.sdm"
"I:/Maxime/derivatives/vtc/sub-13/ses-01/func/sub-13_ses-01_images_bold_3DMCTS_SCCAI_THPGLMF3c_256_sinc3_2x1.0_MNI_SD3DVSS5.00mm.vtc" "I:/Maxime/prt_MNI.sdm"
"I:/Maxime/derivatives/vtc/sub-15/ses-01/func/sub-15_ses-01_images_bold_3DMCTS_SCCAI_THPGLMF3c_256_sinc3_2x1.0_MNI_SD3DVSS5.00mm.vtc" "I:/Maxime/prt_MNI.sdm"
"I:/Maxime/derivatives/vtc/sub-16/ses-01/func/sub-16_ses-01_images_bold_3DMCTS_SCCAI_THPGLMF3c_256_sinc3_2x1.0_MNI_SD3DVSS5.00mm.vtc" "I:/Maxime/prt_MNI.sdm"
"I:/Maxime/derivatives/vtc/sub-17/ses-01/func/sub-17_ses-01_images_bold_3DMCTS_SCCAI_THPGLMF3c_256_sinc3_2x1.0_MNI_SD3DVSS5.00mm.vtc" "I:/Maxime/prt_MNI.sdm"
"I:/Maxime/derivatives/vtc/sub-18/ses-01/func/sub-18_ses-01_images_bold_3DMCTS_SCCAI_THPGLMF3c_256_sinc3_2x1.0_MNI_SD3DVSS5.00mm.vtc" "I:/Maxime/prt_MNI.sdm"
"I:/Maxime/derivatives/vtc/sub-19/ses-01/func/sub-19_ses-01_images_bold_3DMCTS_SCCAI_THPGLMF3c_256_sinc3_2x1.0_MNI_SD3DVSS5.00mm.vtc" "I:/Maxime/prt_MNI.sdm"
"I:/Maxime/derivatives/vtc/sub-20/ses-01/func/sub-20_ses-01_images_bold_3DMCTS_SCCAI_THPGLMF3c_256_sinc3_2x1.0_MNI_SD3DVSS5.00mm.vtc" "I:/Maxime/prt_MNI.sdm"
"I:/Maxime/derivatives/vtc/sub-21/ses-01/func/sub-21_ses-01_images_bold_3DMCTS_SCCAI_THPGLMF3c_256_sinc3_2x1.0_MNI_SD3DVSS5.00mm.vtc" "I:/Maxime/prt_MNI.sdm"
"I:/Maxime/derivatives/vtc/sub-22/ses-01/func/sub-22_ses-01_images_bold_3DMCTS_SCCAI_THPGLMF3c_256_sinc3_2x1.0_MNI_SD3DVSS5.00mm.vtc" "I:/Maxime/prt_MNI.sdm"
"I:/Maxime/derivatives/vtc/sub-24/ses-01/func/sub-24_ses-01_images_bold_3DMCTS_SCCAI_THPGLMF3c_256_sinc3_2x1.0_MNI_SD3DVSS5.00mm.vtc" "I:/Maxime/prt_MNI.sdm"
"I:/Maxime/derivatives/vtc/sub-28/ses-01/func/sub-28_ses-01_images_bold_3DMCTS_SCCAI_THPGLMF3c_256_sinc3_2x1.0_MNI_SD3DVSS5.00mm.vtc" "I:/Maxime/prt_MNI.sdm"
"I:/Maxime/derivatives/vtc/sub-29/ses-01/func/sub-29_ses-01_images_bold_3DMCTS_SCCAI_THPGLMF3c_256_sinc3_2x1.0_MNI_SD3DVSS5.00mm.vtc" "I:/Maxime/prt_MNI.sdm"
"I:/Maxime/derivatives/vtc/sub-30/ses-01/func/sub-30_ses-01_images_bold_3DMCTS_SCCAI_THPGLMF3c_256_sinc3_2x1.0_MNI_SD3DVSS5.00mm.vtc" "I:/Maxime/prt_MNI.sdm"
"I:/Maxime/derivatives/vtc/sub-31/ses-01/func/sub-31_ses-01_images_bold_3DMCTS_SCCAI_THPGLMF3c_256_sinc3_2x1.0_MNI_SD3DVSS5.00mm.vtc" "I:/Maxime/prt_MNI.sdm"
"I:/Maxime/derivatives/vtc/sub-32/ses-01/func/sub-32_ses-01_images_bold_3DMCTS_SCCAI_THPGLMF3c_256_sinc3_2x1.0_MNI_SD3DVSS5.00mm.vtc" "I:/Maxime/prt_MNI.sdm"
"I:/Maxime/derivatives/vtc/sub-33/ses-01/func/sub-33_ses-01_images_bold_3DMCTS_SCCAI_THPGLMF3c_256_sinc3_2x1.0_MNI_SD3DVSS5.00mm.vtc" "I:/Maxime/prt_MNI.sdm"
"I:/Maxime/derivatives/vtc/sub-34/ses-01/func/sub-34_ses-01_images_bold_3DMCTS_SCCAI_THPGLMF3c_256_sinc3_2x1.0_MNI_SD3DVSS5.00mm.vtc" "I:/Maxime/prt_MNI.sdm"
"I:/Maxime/derivatives/vtc/sub-35/ses-01/func/sub-35_ses-01_images_bold_3DMCTS_SCCAI_THPGLMF3c_256_sinc3_2x1.0_MNI_SD3DVSS5.00mm.vtc" "I:/Maxime/prt_MNI.sdm"
"I:/Maxime/derivatives/vtc/sub-37/ses-01/func/sub-37_ses-01_images_bold_3DMCTS_SCCAI_THPGLMF3c_256_sinc3_2x1.0_MNI_SD3DVSS5.00mm.vtc" "I:/Maxime/prt_MNI.sdm"
"I:/Maxime/derivatives/vtc/sub-38/ses-01/func/sub-38_ses-01_images_bold_3DMCTS_SCCAI_THPGLMF3c_256_sinc3_2x1.0_MNI_SD3DVSS5.00mm.vtc" "I:/Maxime/prt_MNI.sdm"
"I:/Maxime/derivatives/vtc/sub-39/ses-01/func/sub-39_ses-01_images_bold_3DMCTS_SCCAI_THPGLMF3c_256_sinc3_2x1.0_MNI_SD3DVSS5.00mm.vtc" "I:/Maxime/prt_MNI.sdm"
"I:/Maxime/derivatives/vtc/sub-41/ses-01/func/sub-41_ses-01_images_bold_3DMCTS_SCCAI_THPGLMF3c_256_sinc3_2x1.0_MNI_SD3DVSS5.00mm.vtc" "I:/Maxime/prt_MNI.sdm"
"I:/Maxime/derivatives/vtc/sub-42/ses-01/func/sub-42_ses-01_images_bold_3DMCTS_SCCAI_THPGLMF3c_256_sinc3_2x1.0_MNI_SD3DVSS5.00mm.vtc" "I:/Maxime/prt_MNI.sdm"
"I:/Maxime/derivatives/vtc/sub-43/ses-01/func/sub-43_ses-01_images_bold_3DMCTS_SCCAI_THPGLMF3c_256_sinc3_2x1.0_MNI_SD3DVSS5.00mm.vtc" "I:/Maxime/prt_MNI.sdm"
"I:/Maxime/derivatives/vtc/sub-45/ses-01/func/sub-45_ses-01_images_bold_3DMCTS_SCCAI_THPGLMF3c_256_sinc3_2x1.0_MNI_SD3DVSS5.00mm.vtc" "I:/Maxime/prt_MNI.sdm"
```

Figure 2.6: Multi-subject design matrix (MDM). *In this figure is shown what a MDM file looks like. In the beginning, is some information about the study such as the number of subjects and activation of RFX (this will be discussed in the next subsection). Then for each row is written the path to a VTC and a path to the associated protocol.*

In Fig. 2.6 is presented an example of what will be thereafter referred to as a "single-session" analysis, presenting thus an analysis of a unique session. However, other MDM files were also created allowing the comparison between two sessions.

Moreover, during the creation of the MDM, the list of VTCs is linked to a study design matrix. This one is referring to a protocol (PRT) file. In this thesis, this PRT file is called "ALCOOL.prt" and was provided by Professor Laurence Dricot. Its structure can be observed in Fig. 2.7. This protocol will enable the study of

different stimuli and the differences between these. In this case, the protocol of the experiment was the same for every session so it was easy because all VTCs could be linked to the same protocol. In the comparative studies, study design matrices were modified to adapt to the sessions of interest.

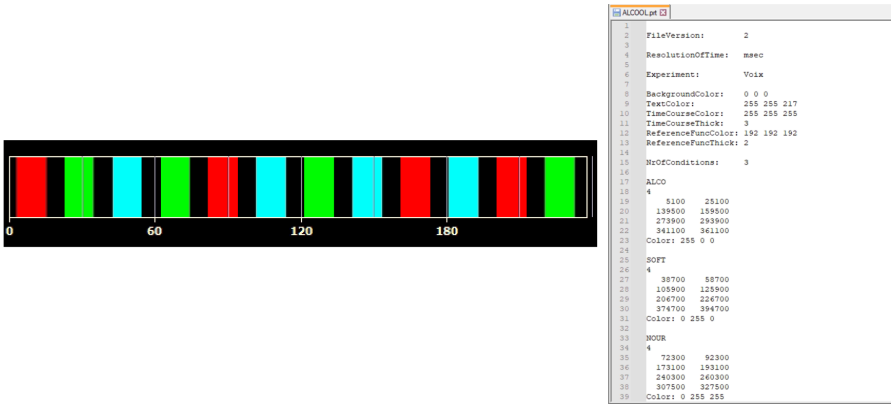

Figure 2.7: Protocol file. *In the left part is represented the protocol of the experiment, following what has been explained in the description of the experiment (see 2.1). Colours are the same as earlier with food stimulus in blue, soft in green and alcohol in red. On the right part is the PRT file itself, with above the colour definitions and below, the timings of each stimulus.*

2.6.2 Random-effects analysis

A random-effects (RFX) analysis is a statistical analysis used for data involving multiple subjects. It is an approach taking into account the variability between and within subjects in the analysis. It enables us to view the subjects of the study as samples of a larger population. If group effects are found to be significant at the random effects level, the conclusions drawn from the sample can be extended to the population from which the subjects were selected.

In contrast, in fixed effects (FFX) analysis, the data from all subjects are combined and treated as if it comes from a single subject. This is thus not possible to account for inter-subject variability. The obtained group results cannot therefore be generalized to the population level. In the FFX case, the error variance is only based on the variability across individual measurement time points. Meanwhile, in an RFX analysis, it is estimated by considering the variability of subject-specific effects across subjects.

To explicitly compute the variability of effects across subjects, a typical RFX analysis is split into multiple levels. In the first level, data for each subject are merged, resulting in mean effect estimates per condition. These mean effects are then used in the second level. They represent the new dependent variable and are examined across subjects (group analysis). This group analysis allows us to model

the variability of estimated effects across subjects at the second level. Therefore, the obtained results can be generalized to the population from which the subjects were drawn.

In this project, RFX was used to evaluate all the individual sessions, producing thus an analysis for each of the 3 sessions of alcohol-dependent participants and for each of the two control sessions. It was also used to assess differences between the sessions, providing 3 analyses of this type which will be detailed in section 3.

2.6.3 Analysis of variance (ANOVA)

Another type of analysis was introduced in this thesis, in addition to the RFX analysis. This new scope allows us to take into account other characteristics of the patients in our study. This method is called the analysis of variance (ANOVA).

ANOVA is a statistical method used to analyze differences between means of multiple groups. It determines whether the observed differences between groups are statistically significant or simply due to chance. If the analysis reveals a significant difference, it suggests that at least one of the groups differs from the others in terms of the mean.

ANOVA compares the observed variations between groups with the expected random variation within groups. If the variations between groups are much larger than the variations within groups, it suggests that there are significant differences between the populations. ANOVA generates a p-value representing the probability that the observed differences between groups are due to chance.

In this thesis, a "one-way" ANOVA was used. It means that only one factor was taken into account for the ANOVA study. The factor which has been studied is the relapsing of the subjects. While some subjects remained sober until the end of the experiment, some unfortunately relapsed during this 3-month period. This information is available in the Appendix B.

Concretely, new MDM files were realized to adapt to the available data. We indeed didn't have the information about the relapsing of all the subjects. Moreover, new files called ATD (ANOVA table data) files were created. In these files are written data concerning the relapsing factor of each available subject (see Fig. 2.8). When combining these files and the beta maps obtained earlier for each subject, the one-way ANOVA can be computed.

Two of these ANOVA analyses were made. The first one was relating the alcohol-related activation during the first session of alcohol-dependent subjects. The second analysis concerned the comparison between the two first sessions of alcohol-dependent subjects. Logically, no ANOVA method was used for the control group as they don't have a "relapsing" factor.

```
FileVersion:          2

NrOfSubjectRows:      20
NrOfDataColumns:      1
NrOfGroupingColumns:  1
NrOfCovariateColumns: 0

"Subjects"        "[ALCO_ses01 +1] + [SOFT_ses02 +1] ? [SOFT_ses01 -1] + [ALCO_ses02 -1]" "Between Factor 1"
"Subject sub-03"            0    1
"Subject sub-07"            0    2
"Subject sub-09"            0    1
"Subject sub-11"            0    1
"Subject sub-17"            0    2
"Subject sub-18"            0    1
"Subject sub-20"            0    1
"Subject sub-22"            0    2
"Subject sub-26"            0    2
"Subject sub-28"            0    1
"Subject sub-30"            0    1
"Subject sub-31"            0    1
"Subject sub-33"            0    2
"Subject sub-34"            0    1
"Subject sub-35"            0    2
"Subject sub-37"            0    2
"Subject sub-43"            0    2
"Subject sub-45"            0    1
"Subject sub-48"            0    2
"Subject sub-53"            0    2
```

Figure 2.8: ATD file. *In the left part are listed the subjects concerned by this analysis. The other column which interests us is the third one, composed of 1's and 2's. This column divides the participants into two classes: abstainers (1) and relapsing (2).*

2.7 Analysis

2.7.1 Activation maps

With the MDM files completed, it is possible to produce results. These first results are called activation maps. An example of this is shown in Fig. 2.9. They depict the brain location and associated level of expression for a particular type of stimulus, e.g. alcohol, soft or food. The choice of the stimulus type to be chosen will be called a contrast in the following. Note that this contrast has nothing to do with the contrast explained earlier with T1 and T2 relaxations. They will be mentioned as ALCOHOL, SOFT and FOOD thereafter. If showing the expression of a single stimulus type is a good first result, another type of contrast is even better. This type of contrast is obtained when adding or subtracting two or more effects. They enable us to see differences in activation for two conditions, removing parasitic activation. They will be referred to as ALCOHOL-SOFT, ALCOHOL-FOOD and SOFT-FOOD. All possible contrasts have been stored in a file called "contrasts_all.crt".

To produce activation maps, according to RFX model explained above, GLM will be used in order to compute the first level of this model. BrainVoyager provides a function for doing that, called RFX-GLM, which needs to be specified when analyzing an MDM file. The GLM computation produces beta values, representing the impact of different predictors in each voxel. The predictors refer to the conditions: alcohol, soft and food.

Figure 2.9: Activation map. *In the figure is shown an example of an activation map. In this case, it is the contrast* ALCOHOL-SOFT *which is represented.*

2.7.2 Cluster analysis

If activation maps are helpful visual tools, the final aim of this thesis is to clearly spot the anatomical structures impacted by alcohol addiction. In order to do this, it is possible via BrainVoyager to retrieve information about the different activation clusters. The information of interest which will be obtained is composed of the size of the cluster and its coordinates. To obtain interesting clusters, and not one big cluster containing all brain regions, it is needed to keep only the most valuable information. For this purpose, a threshold has to be set. This threshold is the p-value and it allows us to show only the most relevant data. The p-value represents the level of significance or the probability of observing a particular result by chance. In the context of coloured voxels with a p-value of 0.05, it indicates that if 100 experiments were conducted on the same population, we would expect to see this voxel in more than 95% of the experiments. In addition, as the brain maps contain many voxels, a Bonferroni correction has been used. This Bonferroni correction is a solution to the multiple comparisons problem (MCP). MPC is due to the fact that having many voxels would lead to incorrectly certifying certain voxels as relevant when they are not.

Having this statistically speaking highly restrictive map, accurate clusters can be observed. Their location and importance (size-speaking) are saved into an external text file. To state the anatomical brain regions where these clusters are, many atlases exist. In a brain atlas, one can link spatial coordinates to the associated region. A common atlas used in neuroscience is the Talairach atlas, which works as its name suggests in the Talairach standardized space. In this thesis, the analysis was made in MNI space since the VTCs were created that way. The cluster coordinates were thus obtained in this MNI standard and a transformation had to be

done before looking into the Talairach atlas.

To that end, a software called Ginger Ale was advised by Dr Laurence Dricot. This software enables to transform an entire text file from MNI to Talairach space. As Ginger Ale only accepts rounded values, the cluster's coordinates were beforehand adapted in an Excel file.

Now working with Talairach coordinates, the final step was to use the Talairach client to find out which region corresponds to each cluster. All this information was saved to a new Excel file. This final file contains thus the volume (in number of voxels) and location (in Talairach coordinates and the associated brain region). To visualize these anatomical regions of the brain more explicitly, another software developed by BrainVoyager called Brain Tutor was downloaded, as seen in Fig. 2.10.

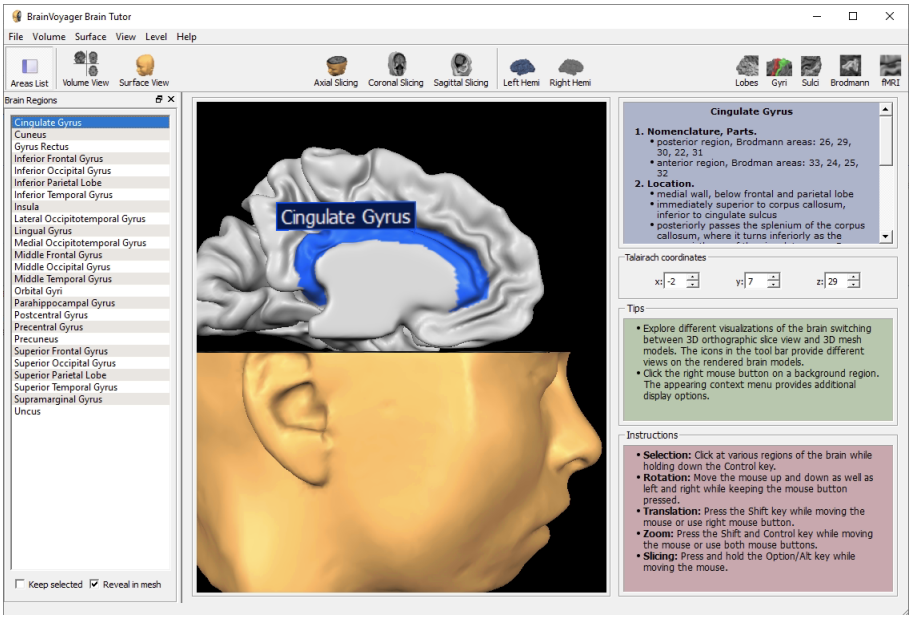

Figure 2.10: Brain Tutor. *In the figure is shown an example of what Brain Tutor looks like. Here is for example shown in blue the anatomical region corresponding to Cingulate Gyrus*

2.8 Tracking the data through the steps

In addition to the aforementioned steps of the data from their raw form to the analysis, tracking has been established. By tracking, it is meant that the amount of information available after each step has been saved in an Excel file. It is indeed possible that after a certain step, a problem occurs. If an issue with a file is detected at a given step, it is not possible to continue with this file for further steps, as these steps are performed consecutively and not in parallel. The complete Excel file is

available in the Appendix A. A summary is proposed hereunder. It regroups the number of subjects remaining at every stage.

	Session	Presence	"Anat_3D" Folder (or equivalent)	"Images" Folder	Preprocessing	Coregistration	VTC	Analysis
Subjects	First	53	50	46	46	40	40	37
	Second	48	47	40	40	34	34	34
	Third	13	12	10	10	10	10	10
Controls	First	20	20	17	17	16	16	14
	Second	19	19	19	19	15	15	15
	Third	0	0	0	0	0	0	0
Total	First	73	70	63	63	56	56	51
	Second	67	66	59	59	49	49	49
	Third	13	12	10	10	10	10	10

Figure 2.11: Data Tracking. *In the figure is shown a table summarizing the available data at each step. Each number represents the number of files which made it to this step.*

It is observable in Fig.2.11 that the number of files available for analysis is lower than at the beginning. During the first step, the loss is due to unusual formatting of the data or missing data. During preprocessing, no data has been lost, implying that everything went well. Concerning coregistration, the decrease in data is either due to a lack of anatomical data associated with the functional data being studied or to an error in the iterative step of the fine-tuning alignment (FA). In the last step, where the analysis is made, some files have been voluntarily removed. This was done because sometimes the VTCs were shorter than normal, resulting in an error while trying to run the analysis on BV. Otherwise, some other files have been removed because the VTC was very strange and could disturb the computation.

For noticing these strange VTCs, the beta maps (maps representing beta values) of each VTC were displayed individually. Examples of that are shown in Fig. 2.12.

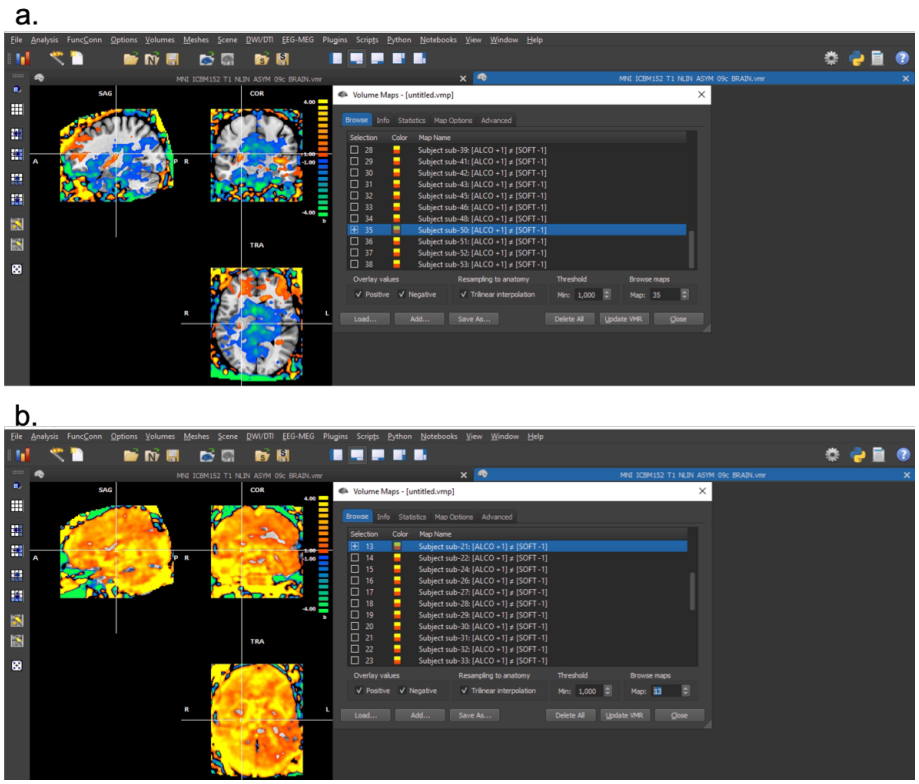

Figure 2.12: Removed VTCs. *In the figure are shown two examples of VTCs which were removed manually from the analysis. The beta map of the first session of the subject n°50 is depicted on* ***a.****. What is wrong with this map is that there is way more negative activation compared to other subjects. The beta map of subject n°21 is shown in* ***b.****, also in his first session. Here, the problem is that the entire brain shows a high level of activation, which isn't normal. For information, the beta maps here above were obtained using* ALCOHOL-SOFT *contrast.*

2.9 Python scripting

As already mentioned, many of these stages were automatized with the help of Python scripts. These were all grouped in a git on the platform Gitlab. Creating this git allows for more clarity. It also facilitates further work being made on the scripts if needed. This repository is available at the following URL: `https://gitlab.com/maxboyens/neuroimagery-and-alcohol-addiction`.

This repository contains all the Python scripts used for this master thesis. The steps covered by the scripts spread from the treating and classifying of the raw data to the VTC creation and processing. The scripts use the BrainVoyager scripting API (Application Programming Interface) for some specific functions. The documentation of this API is available at the following URL: `https://download.brainvoyager.com/bv/doc/PythonGuide/PythonDeveloperGuide.html`.

The different steps of the data processing are referred to as stages. The first stage (DICOM to NIftI) can be interpreted by Python as it stands. In contrast, the following stages (2 to 6) have to be run through BrainVoyager itself. The Python Development tool is available in the upper right corner of BrainVoyager.

Chapter 3

Results

This chapter will present all the results obtained thanks to the methods explained in the previous chapter.

3.1 Single-session studies

The first type of result which seemed interesting was to spot the anatomical structures impacted by alcohol-related stimuli in each session. In order to do this, multiple MDM files were realized. In each of these MDM files are regrouped all the subjects taking part in the session being studied. Of course, alcoholic and control subjects were separated in order to see the results of a given population.

As mentioned in 2.6.1, a single design matrix (SDM) file must be specified for each VTC included in this multi-subject study. For these "single session" studies, SDMs are basic and composed of 3 predictors, referring to the 3 types of stimuli (ALCOHOL, SOFT and FOOD). All the SDMs are identical for each subject because the objective here is to use this design to differentiate the 3 conditions. A simplification of this MDM file is provided in Fig. 3.1.

As the MDM file is ready, an RFX-GLM can be run through BrainVoyager. This computation provides a beta map, a map showing the beta values (of the General Linear Model) for each predictor, and for each voxel.

The first beta map shown by BV is the one depicting the activation of the three predictors together. This is thus a representation of the general activation of the brain when presented with a stimulus, regardless of its type. An example is provided in Fig. 3.2.

General informations of the study
(including the number of subjetcs and the
use of RFX)

"path/to/vtc/of/sub-01/ses-01/vtcfile_sub01_ses01.vtc"	"path/to/sdm/basic_sdm.sdm"
"path/to/vtc/of/sub-02/ses-01/vtcfile_sub02_ses01.vtc"	"path/to/sdm/basic_sdm.sdm"
"path/to/vtc/of/sub-03/ses-01/vtcfile_sub03_ses01.vtc"	"path/to/sdm/basic_sdm.sdm"
"path/to/vtc/of/sub-04/ses-01/vtcfile_sub04_ses01.vtc"	"path/to/sdm/basic_sdm.sdm"
.	.
.	.
.	.
"path/to/vtc/of/sub-53/ses-01/vtcfile_sub53_ses01.vtc"	"path/to/sdm/basic_sdm.sdm"

Figure 3.1: MDM of the first session study on alcoholic patients. *Above is represented an ideal MDM file for studying the first session of alcoholic patients. It is observable that the SDM files designated on the right are the same for each subject. The session investigated here is the first one because all VTCs (on the left) refer to this session. The last observation to make is that here only alcohol-dependent subjects are studied since the subject numbers are between 01 and 53. Of course, the file names are here simplified compared to the ones really used, for facilitating comprehension. The number of subjects truly used for this study is also idealized. As it is said in Fig.2.11, only 37 VTCs were used for this first session analysis.*

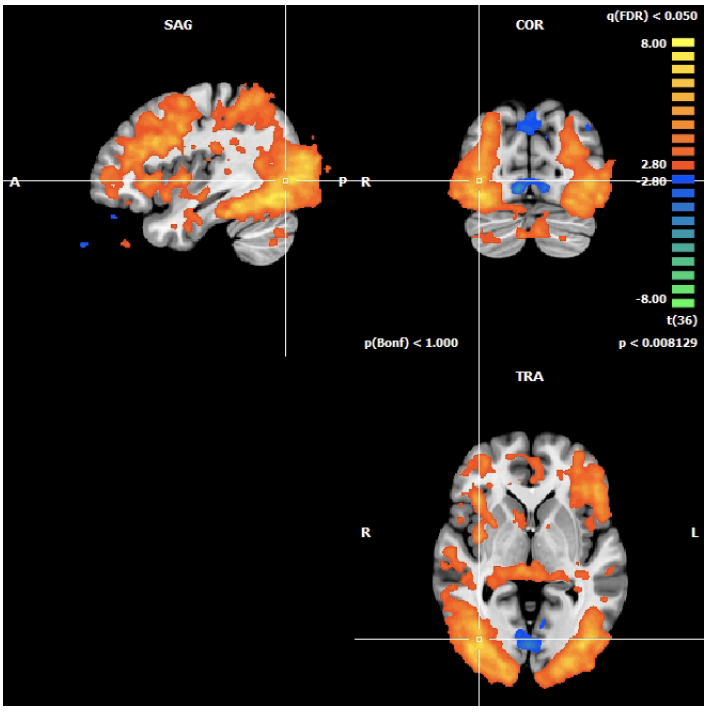

Figure 3.2: Beta map with the three contrasts. *This figure shows the map obtained by adding the three contrasts together. Numerous activations can be observed throughout the brain. Strong activation is particularly noticeable in the occipital lobe. This corresponds to the visual processing of stimuli in general*

If this map is interesting, it doesn't enable the understanding of brain reaction to alcohol-related cues. Therefore, a contrast, in the sense as it was presented in section 2.7.1, needs to be chosen. The most interesting contrast here was the one combining two stimuli: the ALCOHOL-SOFT contrast. In this contrast, the activation due to soft-related stimuli serves as a "baseline". It allows us to spot the activation really related to alcohol especially, and not drinking in general.

Once this contrast is specified, a new beta map is plotted. This map is adjustable by modifying the p-value, as presented in 2.7.2. The smaller the p-value, the most significant the results are. The selected value will differ between the different maps because the aim was to be the most significant possible while keeping enough data for discussion. The resulting beta maps are presented in the following sections.

3.1.1 Alcohol-addicted participants: first session

For the first session, a very low and corrected p-value could be used. The results shown here below were indeed obtained with a Bonferroni-corrected p-value of 5e−20. First, there are figures depicting the visual representation of the beta map, in 3D and 2D. Then is presented a summarizing table regrouping the most activated anatomical regions, ordered by decreasing cluster size. If more than one cluster is recorded for a given anatomical region, the numbers of voxels for each cluster have been summed.

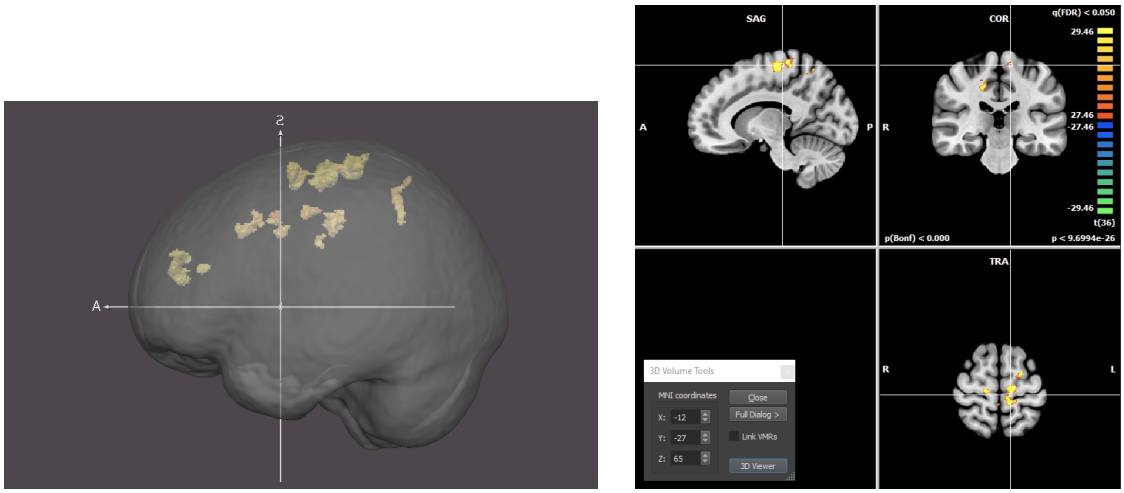

(a) *3D view* ***(b)*** *2D view*

Figure 3.3: 3D and 2D views of alcohol-related activation during the first session for alcohol-dependent subjects. *Above is a representation of the activation of the brains of alcohol-dependent subjects, using* ALCOHOL-SOFT *contrast. On* ***(a)*** *is presented a 3D scope and on* ***(b)*** *is presented a 2D scope, showing the biggest cluster.*

Voxels	Structure	Hemisphere		Coordinates (MNI)			Brodmann area	Voxels in cluster
		Left	Right	X	Y	Z		
1753	Postcentral Gyrus	x		-11,66	-27,27	65,29	4	1640
			x	46,54	-20,35	35,35	2	113
984	Cingulate Gyrus		x	16,5	-26,41	42,95	31	400
			x	15,87	15,15	42,66	24	283
			x	15,13	-14,24	48,27	24	160
		x		-20,58	17,02	36,01	32	141
780	Superior Frontal Gyrus		x	20,5	51,95	21,24	9	780
587	Middle Frontal Gyrus	x		-19,47	-6,4	61,87	6	417
			x	44,49	3,94	46,98	6	170
			x	43,16	41,28	21,02	9	101
			x	28,58	2,86	46,81	6	100
363	Precuneus	x		-19,09	-55,05	50,44	7	363
253	Precentral Gyrus		x	39,55	0,02	40,11	6	253
234	Medial Frontal Gyrus		x	13,67	-22,97	63,3	6	234

Table 3.1: Results of the first session. *Here is shown a summary of the activation clusters found in the first session. This corresponds to activation related to the contrast* ALCOHOL-SOFT *for alcohol-dependent subjects. The results here above are very statistically significant with a very low corrected p-value threshold of* 5e−20.

3.1.2 Alcohol-addicted participants: second session

For the second session, as fewer subjects are available, a bit higher (but still corrected) p-value could be used. The results shown here below were indeed obtained with a Bonferroni-corrected p-value of 5e−14. The results will be discussed in the section 4.

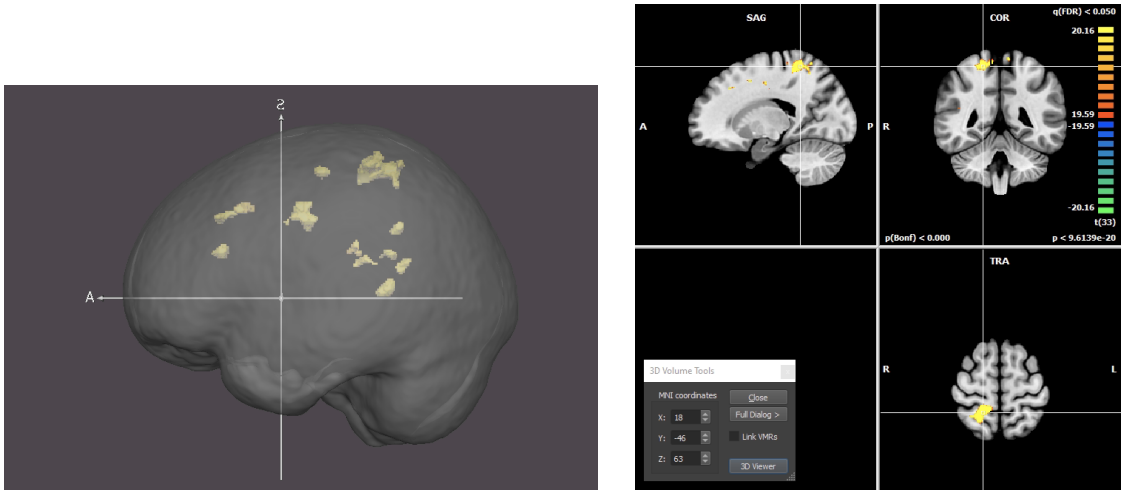

(a) *3D view* ***(b)*** *2D view*

Figure 3.4: 3D and 2D views of alcohol-related activation during the second session for alcohol-dependent subjects. *Above is a representation of the activation of the brains of alcohol-dependent subjects, using* ALCOHOL-SOFT *contrast. On* ***(a)*** *is presented a 3D scope and on* ***(b)*** *is presented a 2D scope, showing the biggest cluster.*

Voxels	Structure	Hemisphere		Coordinates (MNI)			Brodmann area	Voxels in cluster
		Left	Right	X	Y	Z		
1866	Superior Parietal Lobule		x	18,33	-46,34	63,35	7	1866
777	Cingulate Gyrus		x	21,89	-10,69	40,78	24	570
			x	14,53	27,47	40,01	32	207
231	Insula		x	52,83	-37,96	25,6	13	121
			x	46,08	-41,26	19,51	13	110
221	Middle Frontal Gyrus		x	32,76	30,28	23,66	9	221
127	Middle Temporal Gyrus		x	34,53	-57,79	35,35	39	127
126	Superior Temporal Gyrus		x	52,47	-55,72	23,1	39	126
122	Medial Frontal Gyrus	x		-20,55	16,9	40,86	32	122
112	Posterior Cingulate		x	35,43	-60,85	17,13	31	112
100	Precentral Gyrus	x		-17,47	-18,09	57,49	4	100

Table 3.2: Results of the second session. *Here is shown a summary of the activation clusters found in the second session. This corresponds to activation related to the contrast* ALCOHOL-SOFT *for alcohol-dependent subjects. The results here above are very statistically significant with a very low corrected p-value threshold.*

3.1.3 Alcohol-addicted participants: third session

For the third session, only 10 subjects were used for this analysis. Moreover, at this stage (which is 90 days after the first session), it is hoped that the subjects do not show any significant alcohol-related activation anymore. Consequently, the assumption for this session is that the results will not (or at least much less) be statistically significant. Therefore, the p-value is even higher, with a Bonferroni-corrected p-value of 0.05.

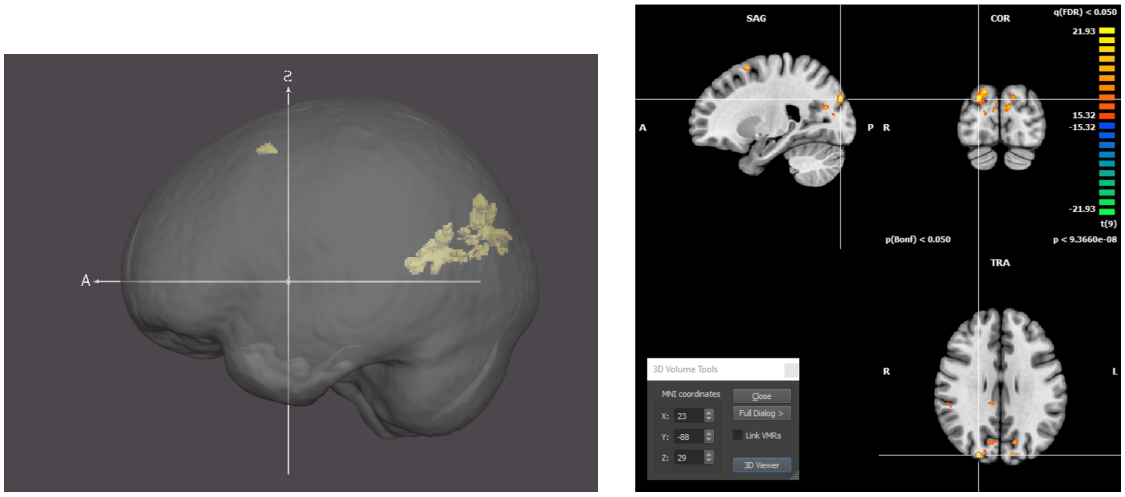

(a) *3D view* ***(b)*** *2D view*

Figure 3.5: 3D and 2D views of alcohol-related activation during the third session for alcohol-dependent subjects. *Above is a representation of the activation of the brains of alcohol-dependent subjects, using* ALCOHOL-SOFT *contrast. On* ***(a)*** *is presented a 3D scope and on* ***(b)*** *is presented a 2D scope, showing the biggest cluster.*

Voxels	**Structure**	**Hemisphere**		**Coordinates (MNI)**			**Brodmann area**	**Voxels in cluster**
		Left	Right	X	Y	Z		
1743	Cuneus	x		18,61	-87,92	25,94	18	1113
				-10,65	-85,65	22,05	18	630
			x	3,46	-83,87	20,66	18	97
957	Posterior Cingulate		x	30,56	-69,95	15,84	30	957
590	Middle Temporal Gyrus	x		-44,84	-56,8	8,79	39	590
151	Superior Frontal Gyrus		x	23,15	10,48	61,54	6	151

Table 3.3: Results of the third session. *Here is shown a summary of the activation clusters found in the third session. This corresponds to activation related to the contrast* ALCOHOL-SOFT *for alcohol-dependent subjects. The results here above are obtained with a high corrected p-value threshold.*

3.1.4 Control participants: first session

Concerning the control subjects, they are not thought to show highly significant activation when considering the ALCOHOL-SOFT contrast. However, still high activation has been noticed. Therefore, the p-value (also Bonferroni corrected) used here

is 5e−6. The following figures and table represent the results for the first session of the control group.

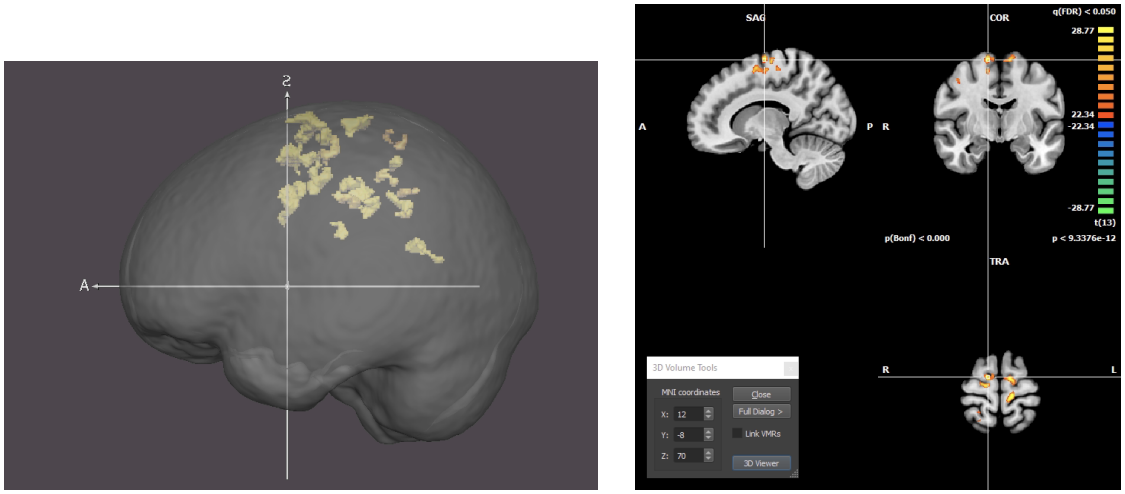

(a) *3D view* ***(b)*** *2D view*

Figure 3.6: 3D and 2D views of alcohol-related activation during the first session for control subjects. *Above is a representation of the activation of the brains of control subjects, using* ALCOHOL-SOFT *contrast. On* ***(a)*** *is presented a 3D scope and on* ***(b)*** *is presented a 2D scope, showing the biggest cluster.*

Voxels	Structure	Hemisphere		Coordinates (MNI)			Brodmann area	Voxels in cluster
		Left	Right	X	Y	Z		
1853	Medial Frontal Gyrus		x	15,73	-6,77	59,2	6	1592
			x	14,99	-16,34	68,95	6	261
1824	Precentral Gyrus		x	49,42	-1,28	41,91	6	1181
		x		-11,94	-9	70,95	6	400
		x		-22,64	-18,07	58,32	4	243
1013	Inferior Parietal Lobule		x	40	-34,18	45,67	40	359
			x	52,95	-40,44	39,99	40	353
			x	58,12	-25,42	28,38	40	172
			x	43,27	-56,32	45,64	40	129
366	Posterior Cingulate		x	35,75	-63,07	18,16	31	366
361	Cingulate Gyrus	x		-8,32	-26,56	38,03	31	199
		x		-20,96	-25,73	43,86	31	162
318	Postcentral Gyrus	x		-11,79	-29,16	70,43	3	318
271	Precuneus		x	22,08	-49,12	57,32	7	154
			x	21,98	-44,79	51	7	117
128	Superior Parietal Lobule		x	22,21	-50,11	67,44	7	128
123	Superior Temporal Gyrus		x	47,02	-56,8	35,93	39	123

Table 3.4: Results of the first session for the control group*. Here is shown a summary of the activation clusters found in the first session. This corresponds to activation related to the contrast* ALCOHOL-SOFT *for control subjects. The results here above are very statistically significant with a corrected p-value threshold of* 5e−6.

3.1.5 Control participants: second session

Thereafter are the results obtained for the second session of the control group. This session is *a priori* not supposed to show many differences in activation compared to the first session of the control group. Consequently, the same threshold has been used for this session as for the first session. The results depicted here were thus obtained with a Bonferroni corrected p-value of 5e−6.

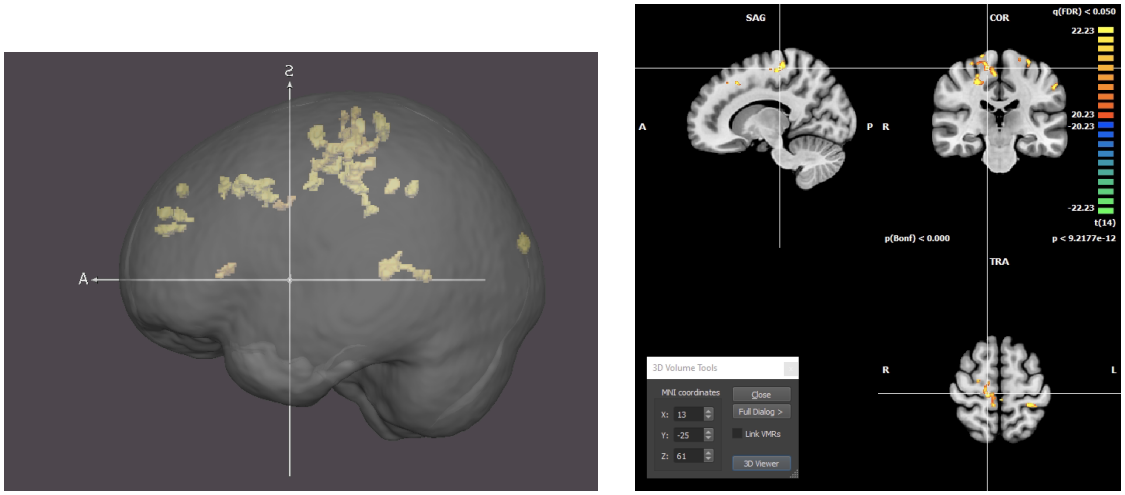

(a) *3D view* ***(b)*** *2D view*

Figure 3.7: 3D and 2D views of alcohol-related activation during the second session for control subjects. *Above is a representation of the activation of the brains of control subjects, using* ALCOHOL-SOFT *contrast. On* ***(a)*** *is presented a 3D scope and on* ***(b)*** *is presented a 2D scope, showing the biggest cluster.*

Voxels	Structure	Hemisphere		Coordinates (MNI)			Brodmann area	Voxels in cluster
		Left	Right	X	Y	Z		
1790	Paracentral Lobule		x	13,36	-24,68	60,71	6	1679
		x		-4,46	-31,05	57,78	5	111
1072	Postcentral Gyrus		x	36,83	-15,63	51,34	3	624
		x		-31,52	-36,66	62,93	5	351
		x		-29,52	-26,23	67,9	3	97
972	Cingulate Gyrus		x	23,28	-28,39	45,88	31	814
			x	16,75	29,54	42,81	32	158
758	Middle Frontal Gyrus		x	35,25	16,45	42,46	6	758
497	Superior Frontal Gyrus		x	17,59	50,17	29,38	9	203
		x		-20,32	51,37	21,43	10	187
		x		-14,11	53,14	28,63	9	107
391	Middle Temporal Gyrus	x		-60,13	-42,07	4,23	22	391
364	Precentral Gyrus		x	22,61	-11,66	65,83	6	237
			x	46,31	3,35	36,44	6	127
349	Medial Frontal Gyrus		x	16,91	19,2	43,91	32	220
		x		-9,57	45,98	38,52	8	129
309	Precuneus		x	20,45	-54,75	41,22	31	183
			x	24,37	-46,06	43,33	31	126
189	Inferior Parietal Lobule	x		-57,96	-26,63	42,62	40	189
139	Middle Occipital Gyrus	x		-17,83	-97,3	15,69	18	139
117	Inferior Frontal Gyrus		x	41,2	30,03	5,03	13	117
115	Supramarginal Gyrus		x	58,17	-38,37	34,05	40	115

Table 3.5: Results of the second session for the control group*. Here is shown a summary of the activation clusters found in the second session. This corresponds to activation related to the contrast* ALCOHOL-SOFT *for control subjects. The results here above are very statistically significant with a corrected p-value threshold of* 5e−6*.*

3.2 Sessions comparison

While evaluating the reaction of the subjects to alcohol-related stimuli at each session is interesting, studying the differences between these sessions can also bring a lot of value. Analyzing the differences between the sessions enables indeed to view the impact of a treatment or of time itself. Three different comparisons were evaluated here. Two of them concern alcohol-dependent subjects, where the differences between the first and second sessions, and between the first and last sessions were studied. The third comparison was made between the two sessions of control

subjects.

By "comparison", it is meant that what has been evaluated are the differences between the alcohol-related activation of two sessions. As with the single session, the ALCOHOL-SOFT contrast was used for each session to identify alcohol-related activation. As it is a difference between two sessions, the resulting final contrast will thus also be a difference of two ALCOHOL-SOFT contrasts. It can be summarized as this: ALCOHOL1-SOFT1-(ALCOHOL2-SOFT2) = ALCOHOL1-SOFT1-ALCOHOL2+SOFT2, where the numbers refer to the studied sessions.

To obtain such a contrast, some modifications must be made in the MDM and SDM files. De facto, as stated in the above paragraph, the contrast is made with 4 predictors. Adding the two predictors relating to FOOD (FOOD1 an FOOD2) which are not used here, it makes a total of 6 predictors, i.e. twice the number of predictors used for single session analyses (3 predictors). Therefore, the SDM has to be modified to create a 6-predictors design. The solution will consist of "splitting" the previous SDM into two SDMs. The first SDM will be used for the first session. The predictors relating to this session (ALCOHOL1, SOFT1 and FOOD1) will therefore be used to calculate the GLM, while the values of the other predictors will be set to zero. In a similar way, another SDM will be created using the predictors related to the second session, while the first session predictors will be set to zero. In the MDM file, the VTCs have been linked to their associated SDM (see Fig. 3.8). Running the GLM with this MDM results in having a beta map where 6 contrasts are available, allowing the combination of ALCOHOL1-SOFT1-ALCOHOL2+SOFT2.

3.2.1 First comparison: between first and second sessions of alcohol-addicted participants

As previously mentioned, two comparisons were studied for alcohol-dependent subjects. Here below are the results of the first comparison, between the first and second sessions. Unfortunately, the results shown here are much less statistically significant than those presented for single-session. The threshold used for obtaining the clusters is 0.01, and it was not Bonferroni-corrected. This threshold and the other uncorrected threshold thereafter were not corrected because it would have been too demanding. Therefore we would not have enough clusters for enabling an interesting discussion. This threshold will be discussed in detail in section 4.

General informations of the study (including
the number of subjetcs and the use of RFX)

”path/to/vtc/of/sub-01/ses-01/vtcfile_sub01_ses01.vtc”	”path/to/sdm/modified_sdm_ses01.sdm”
”path/to/vtc/of/sub-02/ses-01/vtcfile_sub02_ses01.vtc”	”path/to/sdm/modified_sdm_ses01.sdm”
”path/to/vtc/of/sub-03/ses-01/vtcfile_sub03_ses01.vtc”	”path/to/sdm/modified_sdm_ses01.sdm”
.	.
.	.
”path/to/vtc/of/sub-53/ses-01/vtcfile_sub53_ses01.vtc”	”path/to/sdm/modified_sdm_ses01.sdm”
”path/to/vtc/of/sub-01/ses-02/vtcfile_sub01_ses02.vtc”	”path/to/sdm/modified_sdm_ses02.sdm”
”path/to/vtc/of/sub-02/ses-02/vtcfile_sub02_ses02.vtc”	”path/to/sdm/modified_sdm_ses02.sdm”
.	.
.	.
.	.
”path/to/vtc/of/sub-53/ses-02/vtcfile_sub53_ses02.vtc”	”path/to/sdm/modified_sdm_ses02.sdm”

Figure 3.8: MDM of the comparative study between the first two sessions on alcoholic patients. *Above is an ideal MDM file for studying the comparison between the two first sessions of alcohol-dependent patients. The SDM files designated on the right are not the same for each subject. For the first lines, regarding the first session, an adapted SDM for the first session is used. The same principle has also been used for the last lines. Sessions investigated here are the first two because VTCs (on the left) refer to these sessions. The last observation to make is that here, only alcoholic subjects are studied since the subject numbers are between 01 and 53 (for both sessions). Of course, the file names are here simplified compared to the ones really used, for facilitating comprehension. The number of subjects truly used for this study is also idealized. In reality, only 27 subjects had workable data for both sessions.*

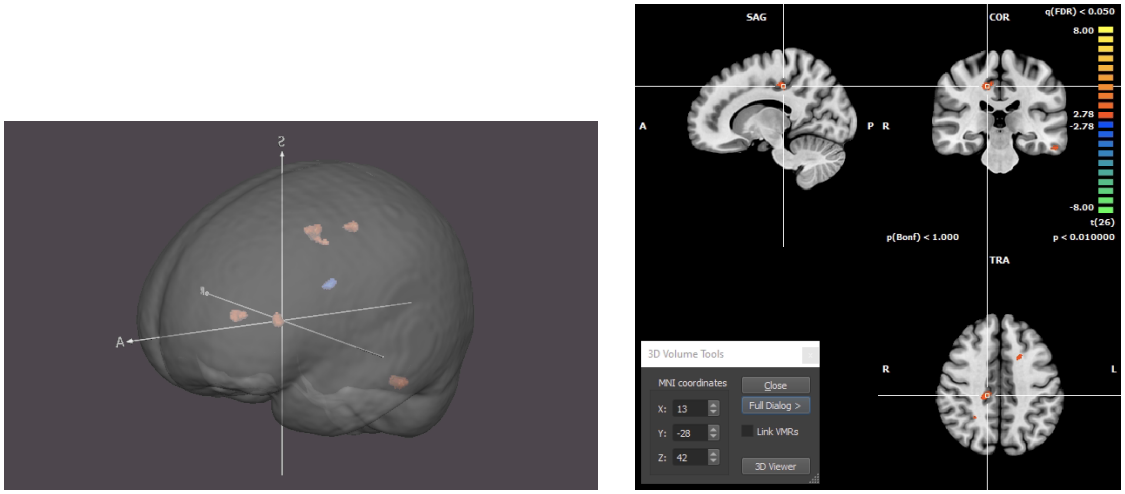

(a) 3D view *(b) 2D view*

Figure 3.9: 3D and 2D views of the comparison of alcohol-related activation between the first and second sessions for alcohol-dependent subjects. *Above is a comparison of alcohol-related activation between the first and second sessions of alcohol-dependent subjects, using* ALCOHOL-SOFT *contrast. On* ***(a)*** *is presented a 3D scope and on* ***(b)*** *is presented a 2D scope, showing the biggest cluster.*

Voxels	Structure	Hemisphere		Coordinates (MNI)			Brodmann area	Voxels in cluster
		Left	Right	X	Y	Z		
604	Cingulate Gyrus		x	13,44	-27,7	42,41	31	473
			x	6,16	-46,6	45,25	31	131
168	Inferior Temporal Gyrus	x		-57,69	-30,38	-22,67	20	168
129	Anterior Cingulate	x		-11,48	33,18	9,3	24	129
99	Insula	x		-33,42	23,93	10,02	13	99

Table 3.6: Results of the comparison between the first and second sessions for the control group*. Here is shown a summary of the activation clusters found in the comparison between the first and second sessions. This corresponds to activation related to the contrast* ALCOHOL-SOFT *for alcohol-related subjects. The results here above were obtained with an uncorrected p-value threshold of 0.01.*

3.2.2 Second comparison: between first and third sessions of alcohol-addicted participants

Concerning the second comparison, between the first and last session of alcohol-dependent subjects, the significance of the results was similar to the one obtained earlier. A threshold of an uncorrected p-value of 0.01 was used here.

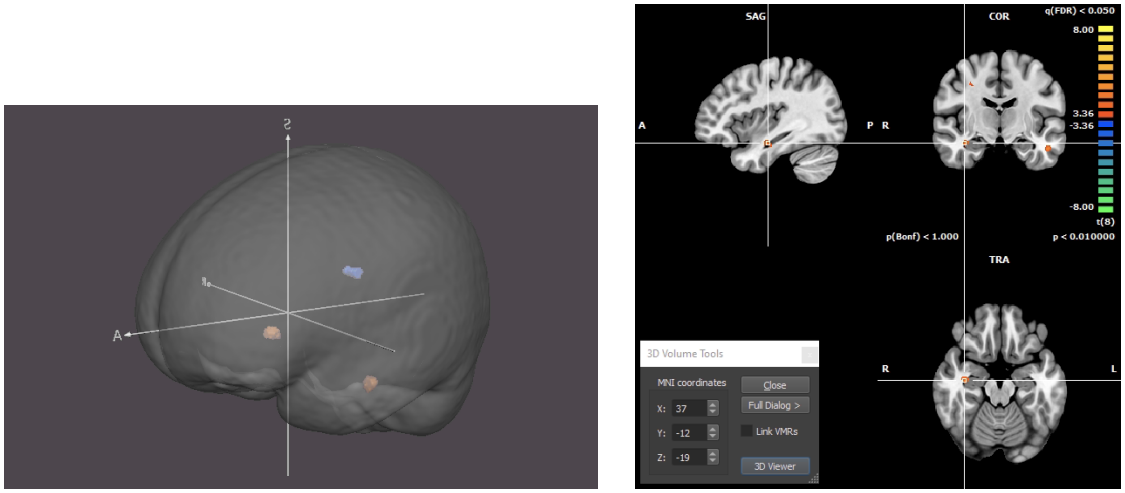

(a) *3D view* ***(b)*** *2D view*

Figure 3.10: 3D and 2D views of the comparison of alcohol-related activation between the first and third sessions for alcohol-dependent subjects.*Above is a comparison of alcohol-related activation between the first and third sessions of alcohol-dependent subjects, using* ALCOHOL-SOFT *contrast. On* ***(a)*** *is presented a 3D scope and on* ***(b)*** *is presented a 2D scope, showing the biggest cluster.*

Voxels	Structure	Hemisphere		Coordinates (MNI)			Brodmann area	Voxels in cluster
		Left	Right	X	Y	Z		
195	Middle Occipital Gyrus		x	52,56	-75,38	4,99	17,18,19	195
189	Parahippocampal Gyrus		x	36,6	-11,85	-19,05	Hippocampus	189
113	Inferior Temporal Gyrus	x		-50,88	-12,16	-24,18	20	113

Table 3.7: Results of the comparison between the first and third sessions for the alcohol-dependent group*. Here is shown a summary of the activation clusters found in the comparison between the first and third sessions. This corresponds to activation related to the contrast* ALCOHOL-SOFT *for alcohol-dependent subjects. The results here above are obtained with an uncorrected p-value threshold of 0.01.*

3.2.3 Third comparison: between first and second sessions of control participants

The last comparison is the one between the two sessions of the control subjects. The results shown here are nearly as significant as they were for comparisons be-

tween alcohol-dependent subjects. The threshold here was 0.005 and was also not corrected, for the same reasons as previously mentioned.

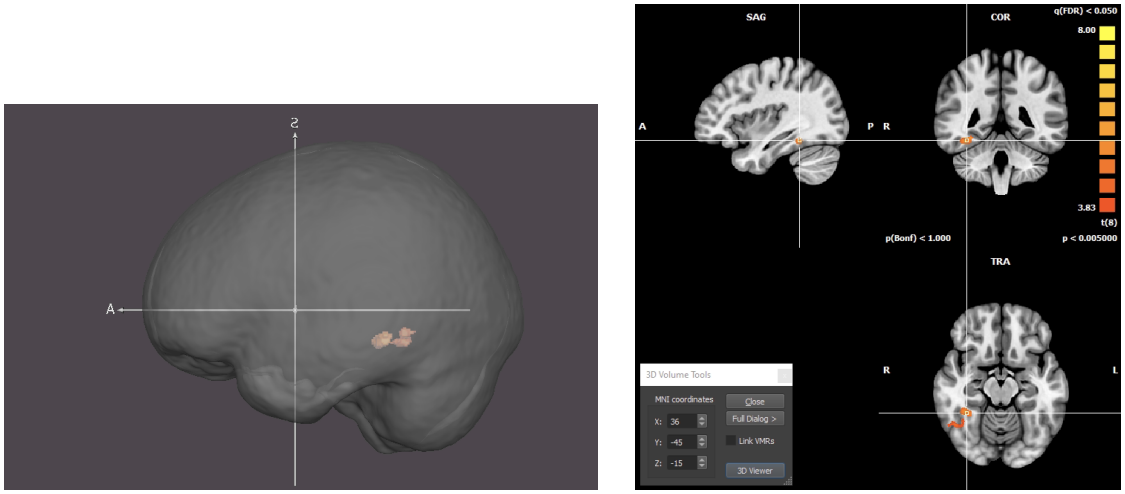

(a) *3D view* ***(b)*** *2D view*

Figure 3.11: 3D and 2D views of the comparison of alcohol-related activation between the first and second sessions for control subjects. *Above is a comparison of alcohol-related activation between the first and second sessions of control subjects, using* ALCOHOL-SOFT *contrast. On* ***(a)*** *is presented a 3D scope and on* ***(b)*** *is presented a 2D scope, showing the biggest cluster.*

Voxels	**Structure**	**Hemisphere**		**Coordinates (MNI)**			**Brodmann area**	**Voxels in cluster**
		Left	Right	X	Y	Z		
800	Fusiform		x	36,12	-44,51	-15,25	37	448
	Gyrus		x	47,64	-56,98	-14,99	37	352

Table 3.8: Results of the comparison between the first and second sessions for the control group*. Here is shown a summary of the activation clusters found in the comparison between the first and third sessions. This corresponds to activation related to the contrast* ALCOHOL-SOFT *for alcohol-related subjects. The results here above are obtained with an uncorrected p-value threshold of 0.005.*

3.3 ANOVA studies

Having established the foundations for discussion through the aforementioned single-session and comparison analyses, this thesis goes further by incorporating the analysis of variance (ANOVA) method. This additional scope offers the opportunity to consider other characteristics of the patients involved in the study. Specifically, the study focuses on examining the relapse factor in alcohol-dependent subjects, drawing comparisons between individuals who successfully maintained sobriety and

those who unfortunately experienced a relapse. The behavioural data of the participants are available in the Appendix B of this thesis.

New files were created to adapt to the available data, including MDM files and ATD files containing relapse data for each subject (see section 2.6). These files, combined with previously obtained beta maps, enabled the computation of one-way ANOVA. Two ANOVA analyses were conducted; one examining alcohol-related activation during the first session of alcohol-dependent subjects, and another comparing the first two sessions of the same group.

No ANOVA method was used for the control group, as they did not have a relapse factor. The application of ANOVA allowed for the identification of significant differences in alcohol-related activation between groups, providing insights into the impact of relapse on brain activity in alcohol-dependent individuals.

The results presented here were obtained using thresholds of 0.005 and 0.01, for respectively the study on the first session and the comparison of the two sessions. As for the comparative studies made earlier, the thresholds here were not corrected. Indeed, the Bonferroni correction being very selective, there was (almost) no cluster available when applying this correction. The choice of using uncorrected thresholds was thus preferred here to obtain enough clusters for discussion.

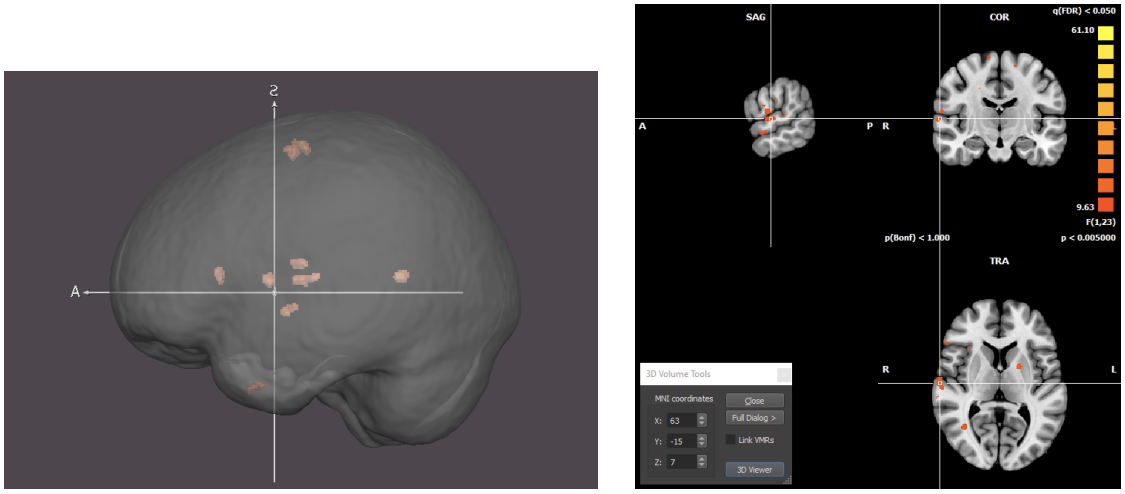

(a) 3D view *(b) 2D view*

Figure 3.12: 3D and 2D views of the alcohol-related activation during the first session for alcohol-dependent subjects, taking into account the relapse factor. *Above is a representation of the impact of the relapse factor on alcohol-related activation during the first session for alcohol-dependent subjects, using* ALCOHOL-SOFT *contrast. On* ***(a)*** *is presented a 3D scope and on* ***(b)*** *is presented a 2D scope, showing the biggest cluster.*

Voxels	**Structure**	**Hemisphere**		**Coordinates (MNI)**			**Brodmann area**	**Voxels in cluster**
		Left	Right	X	Y	Z		
268	Transverse Temporal Gyrus		x	62,99	-14,82	7,16	42	268
245	Superior Temporal Gyrus		x	62,33	-6,42	-8,21	22	141
		x		-34,98	8,01	-38,76	38	104
218	Medial Frontal Gyrus		x	9,72	-8,44	66,03	6	218
188	Postcentral Gyrus		x	63,12	-12,08	15,07	43	188
152	Lingual Gyrus		x	37,21	-60,76	8,28	19	152
138	Inferior Frontal Gyrus		x	56,24	28,09	9,41	45	138
132	Precentral Gyrus	x		-14,77	-12,3	63,77	6	132
120	Lentiform Nucleus	x		-20,49	2,86	6,19	Putamen	120

Table 3.9: Results of the impact of relapse factor when used in an ANOVA analysis for the first session for the alcohol-dependent group. *Here is shown a summary of the activation clusters found when studying the impact of relapse factor with an ANOVA analysis for the first session. This corresponds to activation related to the contrast* ALCOHOL-SOFT *for alcohol-related subjects. The results here above are obtained with an uncorrected p-value threshold of 0.005.*

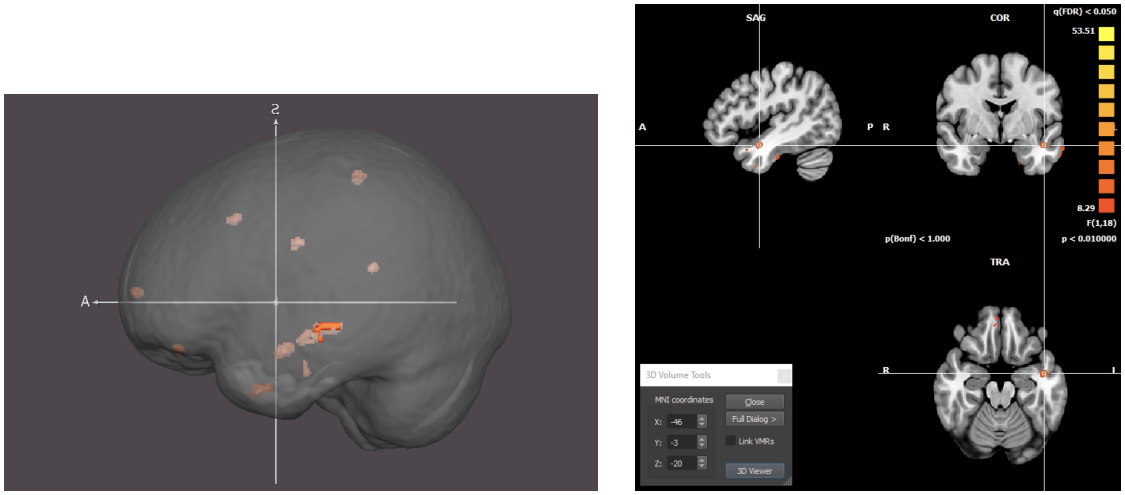

(a) *3D view* ***(b)*** *2D view*

Figure 3.13: 3D and 2D views of the comparison of alcohol-related activation between the first and second sessions for alcohol-dependent subjects, taking into account the relapse factor. *Above is a representation of the impact of the relapse factor on the comparison of alcohol-related activation between the first and second sessions of alcohol-dependent subjects, using* ALCOHOL-SOFT *contrast. On* ***(a)*** *is presented a 3D scope and on* ***(b)*** *is presented a 2D scope, showing the biggest cluster.*

Voxels	Structure	Hemisphere		Coordinates (MNI)			Brodmann area	Voxels in cluster
		Left	Right	X	Y	Z		
594	Superior	x		-33,95	7,53	-37,85	38	262
	Temporal	x		-45,6	-3,38	-19,86	38	207
	Gyrus		x	57,06	-50,37	18,72	22	125
330	Medial	x		-11,17	64,52	5,22	10	117
	Frontal		x	11,08	67,05	4,77	10	112
	Gyrus		x	7,26	46,18	-22,32	11	101
201	Middle Temporal Gyrus	x		-69,26	-19,73	-10,7	21	201
149	Parahippocampal Gyrus	x		-29,66	-12,62	-15,58	Hippocampus	149
140	Caudate	x		-11,16	-8,96	27,31	Caudate Body	140
130	Superior Parietal Lobule	x		-21,84	-36,64	56,85	5,7	130
116	Middle Frontal Gyrus	x		-29,92	19,31	37,09	8	116

Table 3.10: Results of the impact of relapse factor when used in an ANOVA analysis for the comparison of the first and second sessions for the alcohol-dependent group*. Here is a summary of the activation clusters found when studying the impact of relapse factor with an ANOVA analysis for the comparison of the first and second sessions. This corresponds to activation related to the contrast* ALCOHOL-SOFT *for alcohol-related subjects. The results here above are obtained with an uncorrected p-value threshold of 0.01.*

Chapter 4

Discussion

In this section, the results presented above will be discussed in detail. The structure of this discussion is the same as that of the results. First, the single-session analyses will be detailed, then comparisons will be discussed and the last point will concern the ANOVA studies. This discussion aims to adopt a critical viewpoint on the results and methods used. It will also include a comparison to the literature which has been reviewed.

4.1 Single-session studies

4.1.1 Alcohol-dependent subjects: first session

The provided information outlines the analysis results regarding the ALCOHOL-SOFT contrast for each session. Thereby, these results summarise alcohol-related brain activation.

The results were the most significant of all studies in the first session of alcohol-dependent subjects. The cluster presented here are zones where it is very likely that alcohol impacts their activation. The significance threshold was indeed set to a corrected p-value of 5e−20. This high significance is due to two factors. First, it is the study counting the most subjects (37 subjects). This large amount of samples enables it to be well representative of a bigger population. Moreover, as it is the first session of alcohol-dependent subjects, we expect them to have a very high alcohol-related activation. They are indeed at the very beginning of their treatment and are thus very sensitive to alcoholic stimuli.

The regions showing the most significant activation are located in the following lobes:

- Limbic lobe: Cingulate Gyrus
- Parietal lobe: Postcentral Gyrus and Precuneus
- Frontal lobe: Middle, Medial and Superior Frontal Gyri, and Precentral Gyrus

Cingulate gyrus was expected in the results. This structure was indeed already mentioned in the section 1.3.2. The cingulate gyrus is located on the medial surface of the brain and is an integral component of the limbic system. It plays a crucial role in integrating sensory input with emotional processes. It is responsible for generating emotional responses. Additionally, the cingulate gyrus functions as a part of the control network, involved in monitoring conflicts and errors. It is also playing a role in decision-making and attention. [27, 26]

The cingulate gyrus receives input from the anterior nucleus of the thalamus and the neocortex, allowing it to gather information from various sources. It then projects to the entorhinal cortex via the cingulum, establishing a pathway for communication and information transfer between these regions. The presence of significant clusters in this region suggests that alcohol stimuli affect these cognitive and emotional processes. [44]

In the parietal lobe, two areas showed clusters. The first one is the postcentral gyrus, where there were two clusters. The postcentral gyrus is involved in somatosensory processing. It is globally known to play a key role in processing tactile sensations, such as touch, pressure, and proprioception. More precisely, two Brodmann areas present in this gyrus had clusters in them: BA2 and BA4. If BA2 is clearly a part of the postcentral gyrus, it is not the case for BA4. Indeed, Brodmann area 4 is more often presented as within the precentral gyrus. This gyrus is referred to as the primary motor cortex (M1). M1 is generally presented as a control centre for voluntary movements.

Because the centre of this cluster is located at the intersection of precentral and postcentral gyri (x=-11, y=-27, z = 65), we can deduce that both gyri showed significant activation. This assumption is supported by the important amount of voxels (1640) found in this cluster. Therefore, both areas are taken into account in this discussion.

On the one hand, the precentral gyrus, as mentioned above, is known as the primary motor cortex. It is primarily associated with motor control and movement planning. Therefore, when exposed to alcohol-related stimuli, the precentral gyrus may play a role in the motor response and behavioural aspects associated with alcohol consumption. It can be involved in the activation of motor pathways associated with reaching for and consuming alcohol, as well as motor responses to alcohol-related cues.

On the other hand, the postcentral gyrus, or primary somatosensory cortex, is responsible for processing sensory information from the body. In the context of alcohol-related stimuli, the postcentral gyrus may be involved in the sensory processing of alcohol-related cues, such as the tactile and gustatory sensations associated with alcohol consumption. It receives and processes sensory input related to the perception of alcohol's effects, including taste, temperature, and texture. The stimuli

of this experiment are nevertheless purely visual and visual information shouldn't be processed in this gyrus. However, it is now clear that neural networks are interconnected and the view of these stimuli can induce other sensations in subjects.

Moreover, precentral and postcentral gyri are connected to other brain regions involved in reward processing and emotional regulation, such as the limbic system and prefrontal cortex. Their activation in response to alcohol-related stimuli may contribute to the integration of sensory and motor information, as well as the reinforcement and motivational aspects associated with alcohol consumption.

Regarding precuneus, it was also a structure supposed to show significant activation. [29] Indeed, this structure is known for its involvement in sustaining attention and mental imagery. It may thus play a significant role in the automatic attentional biases towards alcohol-related cues.

Precuneus is assumed to play several roles. First, it evaluates the personal relevance of alcohol-related cues and influences emotional and cognitive responses. It also contributes to detecting salient stimuli and directing attention towards alcohol-related cues. Activation in the precuneus indicates its involvement in craving and desire for alcohol. Additionally, the precuneus is connected to emotion-related brain regions and aids in regulating emotional responses to alcohol cues. Overall, the precuneus is crucial in the processing of alcohol-related stimuli and their impact on self-awareness, attention, craving, and emotional regulation. [29, 32]

Let's now dive into the frontal lobe. During the first session of alcohol-dependent subjects, many gyri of this lobe were activated. In addition to the precentral gyrus which has already been discussed, there was activation in the middle, the medial and the superior frontal gyri. These three gyri are part of the prefrontal cortex (PFC) which was also introduced in the section 1.3.2.

The middle frontal gyrus is involved in several cognitive functions, including working memory, attention, control, and planning. It plays a crucial role in the coordination and integration of these cognitive processes. Additionally, the middle frontal gyrus receives and sends widespread connections as part of a network supporting higher cognitive functions. It serves as a central hub for information processing and facilitates communication between various brain regions involved in complex cognitive tasks.

The medial frontal gyrus is a region which extends from the most anterior border of the superior frontal gyrus to the medial surface of the hemisphere. Evidence suggests that this region is involved in executive mechanisms and is associated with high-level executive functions and decision-related processes. [45]

The superior frontal gyrus is functionally involved in several key aspects of motor control. It encompasses the premotor area, which plays a role in the initiation of

voluntary movements. Additionally, the superior frontal gyrus is associated with the control of eye movements, specifically through its involvement in the frontal eye field (FEF). The FEF contributes to the coordination and regulation of eye movements, allowing for precise control and redirection of visual attention. Thus, the superior frontal gyrus serves as an important region for motor planning, execution, and eye movement control.

Globally, the prefrontal cortex receives processed information from various brain systems and integrates it to form representations of learned task contingencies, concepts, and rules. It is often described as the conductor coordinating thoughts and actions in alignment with internal goals. Therefore, its implication in the response to alcohol-related stimuli seems logical.

4.1.2 Alcohol-dependent subjects: second session

For the second session of this alcohol-dependent group, the significance was a bit lower than for the first session, but still very satisfying (Bonferroni corrected p-value threshold of 5e−14). With this threshold, the following brain regions showed an impact from alcohol stimuli:

- Limbic lobe: Cingulate Gyrus (main and posterior part)
- Frontal lobe: Middle and Medial Frontal Gyri, Precentral Gyrus
- Parietal lobe: Superior Parietal Lobule
- Temporal lobe: Middle and Superior Temporal Gyri
- Insula

The structures from the limbic and frontal lobes cited here above have already been discussed. We will thus focus on the other structures mentioned here.

A new zone is activated in the parietal lobe, the superior parietal lobule. This lobule plays various roles related to spatial processing, including spatial attention, spatial orientation, and motion processing. It is responsible for visuomotor transformations, allowing the integration of visual information with motor actions. The superior parietal lobule receives extensive connections from visual and premotor areas, enabling the integration of visual and sensory input. In addition, it contributes to other functions associated with the parietal lobe in general. [44] In the context of alcohol stimuli, a positive association was observed between alcohol expectancy and the connectivity of the right insular cortex with brain regions involved in motivated responses to alcohol-related stimuli. These regions include the superior parietal lobule, postcentral gyrus, and superior frontal gyrus. [46]

A lobe that was not previously activated is now activated: the temporal lobe. The zones within this lobe which showed activation were the middle and superior temporal gyri. The superior temporal gyrus plays a crucial role in various auditory processes. This includes the processing of auditory information such as identifying auditory "objects" and determining the location of sounds. It encompasses the primary auditory cortex (A1). Additionally, it is involved in the processing of speech, particularly in Wernicke's area. However, Wernicke's area is usually located in the left hemisphere, whereas here the cluster is in the other hemisphere. Moreover, the superior temporal gyrus contributes to cross-modal integration, facilitating the integration of visual and auditory information.

The middle temporal gyrus plays a significant role in various cognitive functions, including language processing, auditory and visual processing, and semantic memory. Its implication in the processing of visual stimuli includes object recognition, face perception, and motion perception. It is also associated with semantic memory, which involves the understanding and retrieval of meaning from words and concepts.

For these gyri, the clusters were found in the Brodmann area 39. This area is known for playing a certain role in semantic processing. Previous studies have shown that this area and these gyri, and their implication with different networks, were impacted by alcoholism. [47]

In a sub-lobar structure, two significant clusters were identified. This structure is the insula and is very important. The insula is a region of the brain (present in both hemispheres) counting portions of the frontal, parietal, and temporal lobes. It is known for its involvement in processing convergent information to generate an emotionally relevant context for sensory experiences. The insula can be divided into two main parts: the anterior insula and the posterior insula. The anterior insula is primarily associated with functions related to olfaction, gustation, visceral-autonomic regulation, and limbic processes. On the other hand, the posterior insula is more involved in functions related to audition, and somatosensory and motor control. Also, functional imaging studies have demonstrated the insula's crucial role in pain perception. It is strategically positioned to integrate information associated with the affective and reactive aspects of pain, contributing to the circuitry involved in fear and avoidance responses. Overall, the insula's multidimensional functions make it a significant player in various sensory, emotional, and cognitive processes. [44]

Concerning addictions, it has been presented that individuals who have experienced insula damage exhibit a higher likelihood of successfully quitting smoking without relapse, experiencing minimal withdrawal symptoms, and having reduced cravings to smoke. [48] The insula is recognized as a crucial region responsible for integrating internal bodily states into conscious emotions and decision-making processes. These processes are associated with uncertain outcomes and rewards. In light of this, it has been suggested that the insula plays a role in processing the inte-

roceptive effects of drug use. This processing leads to the development of conscious drug cravings and influences decision-making processes which contribute to relapse. [49]

4.1.3 Alcohol-dependent subjects: third session

Regarding the second session of this alcohol-dependent group, the significance was way lower than for the two first sessions. We indeed put the threshold to a Bonferroni corrected p-value of 0.05. However, this threshold value still enables us to obtain significant results and multiple studies use similar thresholds. [47, 29] This less demanding threshold is a direct consequence of the decreased number of samples for this analysis (10 subjects for this session compared to 37 for the first one). It can also be explained by the lower expected activation when presented with alcohol-related stimuli. After 3 months, it is indeed hoped that the patients will react in a lesser way to alcohol stimuli compared to the first day of their treatment. With this threshold, the following brain regions showed an impact from alcohol stimuli:

- Occipital lobe: Cuneus
- Limbic lobe: Posterior Cingulate
- Frontal lobe: Superior Frontal Gyrus
- Temporal lobe: Middle Temporal Gyrus

As the cingulate, the superior frontal and the middle temporal gyri have already been discussed, the focus will here be set on the cuneus. Moreover, this structure is the most represented in the third session with 3 clusters in it, with a total of 1743 significant voxels, distributed between the two hemispheres.

The cuneus is the first structure belonging to the occipital lobe which has shown significant activation. This structure receives visual input and its primary function is associated with fundamental visual processing. In this case, the clusters were all found inside the BA18. This area is often depicted as a "Visual Association Area" or V2, playing an initial role in processing and extracting features from images. This intermediate-level visual processing can be influenced by external factors such as attention, working memory, and reward expectation. In the scope of alcohol addiction, cuneus was also mentioned in previous studies. Globally, this structure shows altered grey matter volume and functional connectivity in individuals with addiction. However, the functional connectivity of the cuneus isn't the same for relapsers as for abstainers. Relapsers demonstrate increased negative connectivity between cuneus and regions related to executive control and salience. [50]

4.1.4 Control subjects: first session

The control subjects also showed significant results for both sessions. The threshold was set to a corrected p-value of 5e−6 for the two sessions for control subjects.

Considering the moderate number of subjects for the first and second sessions, respectively 14 and 15, this significance is surprising. These subjects being non-dependent social drinkers, their reaction to alcohol stimuli should indeed not be that important.

The several clusters found during the first session are summarized here:

- Frontal lobe: Medial Frontal and Precentral Gyri
- Parietal lobe: Inferior and Superior Parietal Lobules, Postcentral Gyri, and Precuneus
- Limbic lobe: Cingulate Gyrus
- Temporal lobe: Superior Temporal Lobule

All these structures have already been discussed earlier, except for the inferior parietal lobule. Actually, it is a precise zone of this lobule where the 4 clusters were found. This zone is the Brodmann area 40, also corresponding to the supramarginal gyrus. BA40 is the area responsible for secondary somatosensory representation. It is a brain region which becomes active during somatosensory stimulation and tasks involving texture discrimination. It plays a crucial role in processing sensory information related to touch and bodily sensations. In addition, it plays a crucial role in language processing, particularly in tasks related to phonological processing and phonetic awareness. This region is moreover involved in numerical processing, contributing to mathematical calculations and number manipulation. It is furthermore involved in higher-order cognitive processes such as attention, working memory, and decision-making. [51, 44] This region also showed, in a previous study, a decreased activation during inhibitory response for alcohol-dependent subjects. [52] This decreased activation could be an explanation concerning the presence of these clusters in control subjects and not with alcohol-dependent subjects in our study.

Nevertheless, we can note that the order of importance of the clusters has changed between the subjects and the control samples. For alcohol-dependent subjects, activation of the cingulate gyrus was more significant than other gyri. For control subjects, it is located in the middle of the table (see table 3.5). This is probably due to the primordial role of the cingulate cortex in the alcohol-addiction. As a reminder, his roles are coordinator between sensory input and emotion, and conflict/error monitor. It is thus highly important in the control network. This implication of the cingulate cortex justifies its difference of significance between the first session of subject controls and alcohol-dependent ones.

4.1.5 Control subjects: second session

For this session, the threshold is similar to the one chosen for the first session. However, different structures were found to be significant here:

- Frontal lobe: Paracentral Lobule, Middle, Superior, Medial and Inferior Frontal Gyri, and Precentral Gyrus
- Limbic lobe: Cingulate Gyrus
- Parietal lobe: Postcentral Gyrus, Precuneus, Inferior Parietal Lobule, Supramarginal Gyrus
- Temporal: Middle Temporal Gyrus
- Occipital lobe: Middle Occipital Gyrus

While many of these structures have already been discussed earlier, there are some newcomers. Among them are the middle occipital gyrus, paracentral lobule and inferior frontal gyrus. The middle occipital gyrus, like many other structures from the occipital lobe, is responsible for the processing and interpretation of visual information. [44] Alcohol-related cues can trigger a cascade of visual processing, including the recognition and analysis of relevant visual features and the integration of these features into meaningful representations. The middle occipital gyrus contributes to the processing of alcohol-related stimuli by extracting relevant visual information, identifying patterns, and facilitating the recognition and interpretation of these cues.

Concerning the paracentral lobule's implication, we are considering the functions of the implicated Brodmann areas (6 and 5). BA5 is part of the secondary somatosensory cortex and BA6 is part of the premotor cortex. BA6 serves as an intermediate stage between sensory input and motor output, facilitating the translation of sensory signals into appropriate motor commands. [44] The presence of these Brodmann areas can thus be explained by the sensory information of the control subjects, associated with their "mental thoughts" of grabbing what has been presented as a stimulus.

Also located in the frontal lobe, the inferior frontal gyrus is mainly known for hosting Broca's area. This area is implicated in language processing and speech production. However here the cluster was found in the right hemisphere, and Broca's area is usually located in the dominant hemisphere. As the left hemisphere is dominant in right-handed people and the majority of the population is right-handed, it is highly unlikely that this cluster is due to Broca's area. In addition, speaking is not part of the task in our case. This activation is thus not related to this famous area. This activation is probably due to the connections between the gyrus and the other gyri of the frontal lobe. As their roles have already been explained in relation to the first session of alcoholics, we assume that this cluster goes hand in hand with the others.

4.2 Comparative studies

4.2.1 First comparison: between first and second sessions for alcohol-addicted participants

For the comparative studies which were made in this thesis, the significance seems good with this 0.01 p-value threshold. However, this p-value is unfortunately not corrected, unlike the results of previous analyses. Therefore, the results which were presented in section 3 are shown as good indicators of the zones where the activation has decreased during the first 18 days of abstinence, but they are less significant than those obtained before. As a quick reminder, the zones presented were the following:

- Limbic lobe: Cingulate gyrus (main and anterior parts)
- Temporal lobe: Inferior Temporal Gyrus
- Insula

Among these zones, the area of the inferior temporal gyrus which was highlighted was the BA20. As this region is linked to higher-level object representation, we can assume that it was logically more activated in the first session. Subjects are indeed more likely to easily represent the stimulus-related beverage in their head, as they might have consummated it in the days before the experiment.

The most represented structure in this difference is the cingulate gyrus and this is due to multiple reasons. First, as mentioned earlier, cingulate gyrus plays an important role in emotional processing and formation. The presentation of alcohol may trigger emotional responses related to cravings, desire, or anticipation of the pleasurable effects of alcohol. The heightened activity in the cingulate gyrus during the first session could thus reflect the engagement of emotional processes associated with alcohol stimuli.

Secondly, the cingulate gyrus, and especially the anterior cingulate, is involved in reward processing and plays a role in assessing the salience and value of stimuli. [53] For individuals with alcohol dependence, alcohol-related cues hold strong reward value. The increased activity in the cingulate gyrus could thus indicate the high attention and evaluation of alcohol stimuli, reflecting the significance and reward-related properties attributed to alcohol. While this cluster represents the difference between the two first sessions, one can assume that the reward value associated with alcohol stimuli has decreased thanks to abstinence.

Additionally, the cingulate gyrus is implicated in cognitive control processes, such as inhibitory control, conflict management and decision-making. When alcohol-dependent individuals are presented with alcohol-related cues, the higher activation in the cingulate gyrus could reflect the intensive cognitive processing they undergo.

De facto, all the subjects volunteered to follow an abstinence treatment. This activation could thus reflect resistance to the desire to consume alcohol, and decision-making consistent with treatment objectives.

The last structure showing different activation is the insula. First, this region is known to play a critical role in the processing of interoceptive information, including the detection of bodily sensations and signals. Alcohol consumption can elicit specific physiological changes in the body, such as changes in heart rate, blood pressure, and temperature. The heightened activation of the insula during the first experiment may reflect the expected interoceptive signals associated with alcohol intake. The decrease of this activation between the sessions can be seen as the lowering of sensory expectations related to alcohol consumption.

Furthermore, the insula is likely to be implicated in the development of conscious drug cravings. It is also influencing decision-making processes which contribute to relapse. For individuals with alcohol dependence, exposure to alcohol-related stimuli can trigger craving responses. The high insula activation during the first experiment may reflect the emotional and craving-related processing evoked by the presence of alcohol cues, which is, therefore, lowered with abstinence.

4.2.2 Second comparison: between first and third sessions for alcohol-addicted participants

A similar threshold was used for this comparison, corresponding to a 0.01 uncorrected p-value. This thresholded map showed the three following clusters:

- Temporal lobe: Inferior Temporal Gyrus
- Occipital lobe: Middle Occipital Gyrus
- Limbic lobe: Parahippocampal Gyrus

Concerning the temporal zone, it is similar to what has been witnessed in the first comparison, with the more important activation of BA20 during the first session.

The cluster found in the occipital lobe was the only cluster in the study showing a negative difference in activation between the two sessions. This means that it was more activated during the third session than during the first one. The higher activation can be due to different factors. The first idea is that prolonged abstinence allows for neurological changes in the brain. The middle occipital gyrus, as a part of the visual processing network, may undergo modifications in response to the absence of alcohol. These neuroadaptations could result in altered neural responses to alcohol-related visual cues, leading to increased activation in the middle occipital gyrus.

Secondly, it is known that, during abstinence, individuals may experience higher cue reactivity and craving for alcohol. The middle occipital gyrus can thus play a role in this cue reactivity and attentional bias towards alcohol-related cues. This higher activation after 3 months of abstinence may reflect an enhanced sensitivity to these cues and a stronger neural response associated with craving and cue reactivity.

The third structure showing a notable difference in activation between the first and third sessions is the parahippocampal gyrus. This structure hasn't been discussed yet, but it was already mentioned in the introductory work (see section 1.3.2). This gyrus, also known as the hippocampal gyrus, is a cortical region of the brain surrounding the hippocampus and is part of the limbic system. It has been studied a lot and is considered one of the key areas involved in memory processing. Specifically, this structure is implicated in complex aspects of learning and memory, particularly in the encoding and retrieval of memories. Studies have shown that this region exhibits a strong response to stimuli depicting places and scenes, giving it the name "parahippocampal place area" (PPA). Researchers have proposed that the parahippocampal gyrus encodes the geometry of the local environment, contributing to our ability to navigate and recognize places. [44, 54]

The close association between the parahippocampal gyrus and the hippocampus, another critical structure for memory, underscores its importance in memory formation and recall. It is believed to play a significant role in consolidating memories related to spatial navigation and the recognition of places. This suggests that the parahippocampal gyrus is involved in the integration of sensory and spatial information to form coherent memories of our surroundings. It is what process the contextual information. Its involvement in memory encoding and retrieval, particularly in relation to places and scenes, highlights its significance in our ability to navigate, recognize, and recall information about our environment.

When individuals with alcohol dependence are presented with alcohol-related stimuli, such as images or cues associated with alcohol, the parahippocampal cortex (PHC) may be activated due to its role in memory and the emotional significance of alcohol-related experiences.

The activation of the PHC in response to alcohol stimuli could be related to the formation and retrieval of memories associated with alcohol use. These memories may include the rewarding effects of alcohol, the context in which alcohol was consumed, or the emotional responses linked to alcohol-related experiences. The PHC's involvement in encoding and retrieving these memories may contribute to the heightened attention and salience of alcohol-related cues for individuals with alcohol dependence.

Furthermore, the PHC's connection to other brain regions involved in emotion, reward, and decision-making, such as the amygdala and prefrontal cortex, may influence the processing of alcohol-related stimuli. The PHC's interaction with these

regions could contribute to the subjective experience of craving, the evaluation of the motivational significance of alcohol cues, and the subsequent decision-making processes related to alcohol consumption.

4.2.3 Third comparison: between control sessions

The threshold used was similar to the two first comparisons, even a bit more selective (uncorrected p-value of 0.005), but the map with a threshold of 0.01 showed comparable results. The only structure showing differences between the two sessions of the control group was the Fusiform Gyrus, with two clusters.

The fusiform gyrus (FG) is a brain region involved in multi-modal integration and high-order processing of visual information. It plays a crucial role in recognizing and identifying complex objects, including faces. Within the FG, there is a specialized region known as the fusiform face area (FFA), which is dedicated to face recognition. The FFA enables us to discriminate and remember faces, as well as interpret facial expressions and emotional cues. The two clusters in this beta map were precisely found in this specific FFA.

In addition to its role in face recognition, the FG is involved in various other cognitive functions. It contributes to colour processing. The FG also plays a role in the recognition of other visual stimuli, such as words and numbers. This involvement in word and number recognition suggests its contribution to visual language processing and the understanding of symbolic representations.

The FG, being a region involved in high-order object recognition, seems thus to play a role in processing visual cues. However, no special difference should *a priori* be witnessed between alcohol-related and other stimuli. However, many studies have shown its activation when treating alcohol-related stimuli compared to control stimuli. The activation of this region is likely to be linked with the emotional processing of visual cues. [55, 32, 29, 33]

4.3 ANOVA studies

The purpose of these ANOVA analyses is to spot the brain regions which show predominant activation for subjects having relapsed afterwards. The assessment of this relapsing factor was divided into two parts. The first part is the study of the impact of this factor during the first session. The other part was the evaluation of the comparison between the two first sessions, taking into account the relapsing of patients.

4.3.1 First ANOVA study: first session

The threshold used here was similar to the one used for comparisons. It corresponds indeed to a 0.005 uncorrected p-value. This corresponds to an uncorrected p-value of 0.005. As this value is not corrected, the results presented here should be treated with caution and should be considered more as an indication than as a certainty. During the first session, the regions which were more activated in relapsing subjects than in the other subjects are the following:

- Temporal lobe: Transverse and Superior Temporal Gyri
- Frontal lobe: Medial and Inferior Frontal Gyri, and Precentral Gyrus
- Parietal lobe: Postcentral Gyrus
- Occipital lobe: Lingual Gyrus
- Putamen

The structures mentioned here belonging to the Temporal lobe are both likely to be involved in auditory processing. Their roles in this experiment have already been similarly discussed before. The structures of the frontal and parietal lobes have also been mentioned multiple times in the previous parts of the discussion and won't be detailed again here.

The lingual gyrus however hasn't already been mentioned. This structure is close to the aforementioned parahippocampal and fusiform gyri. The Brodmann area where the cluster was found is BA19. This zone is known for playing a role in visual processing. More generally, the lingual gyrus is responsible for different roles associated with this visual processing.

First of all, as mentioned with BA19, this gyrus is involved in early visual processing, particularly in the perception and analysis of shapes, colours, and visual patterns. Secondly, it is involved in object recognition and identification. It helps in categorizing and distinguishing different objects based on their visual features, allowing us to recognize and discriminate between various visual stimuli. Moreover, it plays a role in the encoding, storage, and retrieval of visual information, allowing us to remember and recognize previously encountered visual stimuli. And last, but less important in our case, the lingual gyrus is also involved in the reading processes. It contributes to visual word recognition, processing written words and integrating them with language-related areas of the brain for comprehension and understanding. [44, 56]

The last structure which was highlighted here is the putamen. The presence of putamen in these results is very welcome. This structure was indeed already mentioned in the section 1.3.2. With the caudate, this structure forms the dorsal striatum (DS). The DS receives dopaminergic projections from the substantia nigra and is implicated in the so-called nigrostriatal system. This system is known for

its implication in the creation and consolidation of habits and behaviours leading to automatic response. Moreover, the neural control of behaviour shifts from the ventral to the dorsal striatum as habits become more automatic. This higher activation in relapsing subjects has already been demonstrated in multiple studies. More generally, this region of DS has always shown higher activation in alcohol-dependent subjects, when presenting alcohol-related stimuli. [28, 29, 32, 33]

4.3.2 Second ANOVA study: comparison between first and second sessions

This second use of the ANOVA method concerned the comparison between the first two sessions. It has been decided to compare these two sessions as they offered the highest number of subjects. The results were, to a certain extent, as significant as they were for the other study with the ANOVA method. The threshold used was an uncorrected p-value of 0.01. The significant areas are summarized here below:

- Temporal lobe: Superior and Middle Temporal Gyri
- Frontal lobe: Medial and Medial Frontal Gyrus
- Parietal lobe: Superior Parietal Lobule
- Limbic lobe: Parahippocampal Gyrus
- Caudate

Overall, these results suggest that the way activation varies between sessions has an impact on the subjects' future relapse. The regions showing the greatest difference between relapsers and abstainers are those shown here.

While many areas have been discussed before, it's only now that the caudate comes into play. Caudate is often present in studies in association with putamen. As mentioned in the previous part of the discussion, they form indeed together the dorsal striatum. This structure is implied in the nigrostriatal dopaminergic pathway and has thus a very important role to play in the reward-associated system, the habits and the automatic behaviours. [29, 28] The presence of caudate in this ANOVA analysis suggests that the difference in activation between the two first sessions is higher in the relapsers. This might be due to an initial activation much more pronounced than for abstainers. If this initial activation was higher, then the difference with also be higher as well. Similar observations can be done for the hippocampus-related area presented here.

4.4 Further improvements ideas

This section outlines some ideas for further work on this subject. These possibilities have not been explored by myself because their relevance would still need to

be discussed with subject matter experts. The various suggestions will be presented as they appear in the project timeline.

The first thing which we can work on is the amount of available data for this experiment. The statistical power of the results will indeed increase as the number of data increases as well. There are different ways of obtaining more data. The first idea would be to continue with this experiment on more patients, although this experiment already counts 73 patients in total. The other improvement which could be made would thus be to work on the actual subjects in order to retrieve the maximum data possible. For some subjects, there are indeed one or more sessions with missing (or incomplete) anatomical and/or functional files. What sometimes also happens is that the files are not correctly renamed in the folders, making it impossible to treat. To nuance this last case, it is true that a technique allows one to work with these weirdly renamed files. But this implies checking the size of each folder of the session to compare it with the sizes of files in another "well-renamed" session. According to the "data-tracking" Excel file which has been made (see section 2.8), this initial work would allow us to recover the 21 sessions lost in the first step of data extracting from DICOM files.

Another possibility to improve the statistical power of our analyses is the reduce the file losses due to coregistration. Still, according to the data-tracking Excel file, 17 recorded sessions couldn't operate coregistration between their functional and anatomical files. It is thus again an important loss of data occurring at this stage. The problem with the automated coregistration step is mainly due to the fine alignment (FA) step, which is an iterative step. In the failing sessions, this iterative process cannot find a solution and produce a timeout error, making BV crash. To improve the coregistration, a solution could be to coregister manually the files, with the help of a more qualified person.

The following ideas and suggestions are more analysis-focused. They could serve as a basis for further work on this data set. The first idea would be to evaluate other contrasts. We have indeed here only studied in depth the ALCOHOL-SOFT contrast, which seemed to be the most relevant one. However, three picture types were used in this experiment (ALCOHOL, SOFT and FOOD). We could thus try other contrasts in future studies on this topic.

While here a global point of view was adopted, we could imagine other analyses on this data set but observing only certain regions of interest. There were indeed many papers highlighting the importance of the reward system in the AUD. This system is known to be localized in a very specific part of the brain. We could thus focus on this region in particular, or the diencephalon to analyze the thalamus-related structures, etc.

Then, we could conduct ANOVA studies with different criteria and/or sessions than what has been done here. This can provide a more comprehensive understand-

ing of the alcohol dependence and abstinence phenomenon. By incorporating new sessions and criteria, researchers could observe how the variables of interest may vary over time or in response to different conditions, leading to a richer and more nuanced analysis. An example of a new ANOVA study would be to analyze the impact of craving scores (available in the Annex B).

Another improvement can be achieved by utilizing alternative thresholds to detect more activation. The choice of threshold can significantly impact the identification of significant results. By exploring different thresholds, researchers can potentially uncover additional regions of activation which may have been overlooked in this thesis. This can lead to a more thorough exploration of the data and a broader understanding of the underlying neural processes.

Furthermore, employing peak detection algorithms can aid in identifying the most significant results within a study. These algorithms focus on identifying the highest peak of activation, allowing researchers to prioritize and focus their analysis on the regions which exhibit the most robust and reliable effects. By utilizing this algorithm, researchers can prioritize areas of interest and allocate resources more efficiently. [29]

Lastly, considering alternative correction methods instead of relying solely on Bonferroni correction can be advantageous. Bonferroni correction is a conservative approach which adjusts the significance threshold to reduce the risk of false positives. However, it can also increase the risk of false negatives. Exploring alternative correction methods, such as false discovery rate (FDR) or cluster-size thresholding, can provide a different approach to the actual thresholding. These are both available on BV, either directly or via a plugin.

Conclusion

Quantifying the functional brain changes associated with alcohol dependence and abstinence presents a significant research challenge. However, recent advancements in fMRI techniques and data analysis methods have opened the way for a more comprehensive investigation of these neural processes. This study examined the effects of alcohol abstinence on brain function in 73 participants through a multi-session fMRI approach. The goal was to understand the alterations in brain activity during the early stages of abstinence in individuals with Alcohol Use Disorder (AUD).

The purpose of this thesis is also to contribute to the existing literature by providing insights into the functional changes occurring during alcohol abstinence. Therefore a review of the existing literature was provided as a theoretical background. In addition to this review, an explanation of the principles behind MRI and especially fMRI was also proposed.

Furthermore, the study employed advanced data processing techniques, including motion correction, preprocessing, coregistration, and statistical analysis, to ensure robust and reliable findings. The use of random-effects analysis allowed for a comprehensive examination of the data, considering both inter-subject variability and group-level effects.

The results revealed distinct patterns of brain activation associated with the abstinence period. These changes were observed in regions known to be involved in addiction, emotional and sensory processing, memory, cognitive control, and reward systems.

The brain regions to remember from this study are certainly those presenting higher differences in activation between the first and following sessions. Among them, we can count the cingulate cortex, the parahippocampal gyrus and the insula. These are, among others, known for their important roles in emotion processing, memory consolidating and cognitive processes. The observed alterations in functional activation patterns during abstinence suggest the potential for neuroplasticity and recovery in these regions. In general, however, there was also notable activation in the frontal, parietal and temporal lobes, proving the high general activation in response to alcohol stimuli. An additional study with ANOVA allowed us to better understand the zones implied in the relapsing of the participants. In this scope, we suggest that a high initial activation of putamen, caudate and/or hip-

pocampus in patients suffering from AUD has a tendency to lead to relapse. Work on these zones could be done to find a more efficient treatment to avoid relapsing.

While the results of this study provide valuable insights into the effects of alcohol abstinence on brain function, it is important to acknowledge certain limitations. The sample size of 73 participants, although substantial, may still benefit from further expansion to enhance the generalisability of the findings. In addition, many ideas for improvement were suggested, showing that this area still has a lot of potential and deserves to continue to be explored.

In conclusion, this fMRI study contributes to our understanding of the functional changes in the brain associated with alcohol abstinence in individuals with AUD. The findings highlight the neural plasticity underlying alcohol dependence and recovery, offering potential insights for the development of targeted interventions and treatment strategies. Further research, building upon the present study's methodology and addressing its limitations, will continue to advance our knowledge of the complex interplay between alcohol dependence, abstinence, and brain function.

References

[1] World Health Organization: WHO. "Alcohol". In: *www.who.int* (May 2022). URL: https://www.who.int/news-room/fact-sheets/detail/alcohol.

[2] Robert-Jan Van Geuns et al. "Basic principles of magnetic resonance imaging". In: *Progress in Cardiovascular Diseases* 42.2 (Sept. 1999), pp. 149–156. DOI: 10.1016/s0033-0620(99)70014-9.

[3] Dr. Laurence Dricot Ir. "LGBIO1115: Introduction aux Neurosciences". In: 2021. Chap. Thématique Neuroimagerie PART1 23-03-21.

[4] Frank Peeters. "LGBIO2050: Medical Imaging". In: 2018. Chap. MRI : Magnetic Resonance Imaging.

[5] Donald B. Plewes and Walter Kucharczyk. "Physics of MRI: A primer". In: *Journal of Magnetic Resonance Imaging* 35.5 (May 2012), pp. 1038–1054. DOI: 10.1002/jmri.23642.

[6] John P. Ridgway. "Cardiovascular magnetic resonance physics for clinicians: part I". In: *Journal of Cardiovascular Magnetic Resonance* 12.1 (Nov. 2010). DOI: 10.1186/1532-429x-12-71. URL: https://doi.org/10.1186/1532-429x-12-71.

[7] Gary H. Glover. "Overview of Functional Magnetic Resonance Imaging". In: *Neurosurgery Clinics of North America* 22.2 (Apr. 2011), pp. 133–139. DOI: 10.1016/j.nec.2010.11.001.

[8] Costantino Iadecola. "The Neurovascular Unit Coming of Age: A Journey through Neurovascular Coupling in Health and Disease". In: *Neuron* 96.1 (Sept. 2017), pp. 17–42. DOI: 10.1016/j.neuron.2017.07.030. URL: https://doi.org/10.1016/j.neuron.2017.07.030.

[9] Edson Amaro and Gareth J. Barker. "Study design in fMRI: Basic principles". In: *Brain and Cognition* 60.3 (Apr. 2006), pp. 220–232. DOI: 10.1016/j.bandc.2005.11.009.

[10] Valentina Agostini. "Neuroengineering". In: 2022. Chap. 4NE : Measuring the Brain Function and Metabolism.

[11] Michael K. Stehling, Robert Turner, and Peter Mansfield. "Echo-Planar Imaging: Magnetic Resonance Imaging in a Fraction of a Second". In: *Science* 254.5028 (Oct. 1991), pp. 43–50. DOI: 10.1126/science.1925560. URL: https://doi.org/10.1126/science.1925560.

[12] José Maria Soares Jùnior et al. "A Hitchhiker's Guide to Functional Magnetic Resonance Imaging". In: *Frontiers in Neuroscience* 10 (Nov. 2016). DOI: 10.3389/fnins.2016.00515. URL: https://www.frontiersin.org/articles/10.3389/fnins.2016.00515/pdf.

[13] *Understanding Alcohol Use Disorder — National Institute on Alcohol Abuse and Alcoholism (NIAAA)*. URL: https://www.niaaa.nih.gov/publications/brochures-and-fact-sheets/understanding-alcohol-use-disorder.

[14] André F. Carvalho et al. "Alcohol use disorders". In: *The Lancet* 394.10200 (Aug. 2019), pp. 781–792. DOI: 10.1016/s0140-6736(19)31775-1. URL: https://doi.org/10.1016/s0140-6736(19)31775-1.

[15] Max Griswold et al. "Alcohol use and burden for 195 countries and territories, 1990–2016: a systematic analysis for the Global Burden of Disease Study 2016". In: *The Lancet* 392.10152 (Sept. 2018), pp. 1015–1035. DOI: 10.1016/s0140-6736(18)31310-2. URL: https://doi.org/10.1016/s0140-6736(18)31310-2.

[16] Ed Day and James H.F. Rudd. "Alcohol use disorders and the heart". In: *Addiction* 114.9 (July 2019), pp. 1670–1678. DOI: 10.1111/add.14703. URL: https://doi.org/10.1111/add.14703.

[17] Arnan Mitchell, Matthew D. Selby, and Elinor L. Sullivan. *The influence of maternal high-fat diet consumption on neurobehavioral development*. Jan. 2021, pp. 593–606. DOI: 10.1016/b978-0-12-817986-4.00051-1. URL: https://doi.org/10.1016/b978-0-12-817986-4.00051-1.

[18] *Wikipedia - Mesolimbic pathway*. [Online; accessed 12-05-2023]. Feb. 2023. URL: https://en.wikipedia.org/wiki/Mesolimbic_pathway.

[19] Thomas M. Tzschentke. "Pharmacology and behavioral pharmacology of the mesocortical dopamine system". In: *Progress in Neurobiology* 63.3 (Feb. 2001), pp. 241–320. DOI: 10.1016/s0301-0082(00)00033-2. URL: https://doi.org/10.1016/s0301-0082(00)00033-2.

[20] *Wikipedia - Mesocortical pathway*. [Online; accessed 12-05-2023]. Jan. 2020. URL: https://en.wikipedia.org/wiki/Mesocortical_pathway.

[21] Francesco Pistillo et al. "Nicotinic, glutamatergic and dopaminergic synaptic transmission and plasticity in the mesocorticolimbic system: Focus on nicotine effects". In: *Progress in Neurobiology* 124 (Jan. 2015), pp. 1–27. DOI: 10.1016/j.pneurobio.2014.10.002. URL: https://doi.org/10.1016/j.pneurobio.2014.10.002.

[22] Ethan S. Bromberg-Martin, Masayuki Matsumoto, and Okihide Hikosaka. "Dopamine in Motivational Control: Rewarding, Aversive, and Alerting". In: *Neuron* 68.5 (Dec. 2010), pp. 815–834. DOI: 10.1016/j.neuron.2010.11.022. URL: https://doi.org/10.1016/j.neuron.2010.11.022.

[23] Henry W. Chase et al. “The Neural Basis of Drug Stimulus Processing and Craving: An Activation Likelihood Estimation Meta-Analysis”. In: *Biological Psychiatry* 70.8 (Oct. 2011), pp. 785–793. DOI: 10.1016/j.biopsych.2011.05.025. URL: https://doi.org/10.1016/j.biopsych.2011.05.025.

[24] Maartje Luijten et al. “Neurobiological substrate of smoking-related attentional bias”. In: *NeuroImage* 54.3 (Feb. 2011), pp. 2374–2381. DOI: 10.1016/j.neuroimage.2010.09.064. URL: https://doi.org/10.1016/j.neuroimage.2010.09.064.

[25] Trevor W. Robbins, Karen D. Ersche, and Barry J. Everitt. “Drug Addiction and the Memory Systems of the Brain”. In: *Annals of the New York Academy of Sciences* 1141.1 (Oct. 2008), pp. 1–21. DOI: 10.1196/annals.1441.020. URL: https://doi.org/10.1196/annals.1441.020.

[26] Derek Evan Nee, Tor D. Wager, and John Jonides. “Interference resolution: Insights from a meta-analysis of neuroimaging tasks”. In: *Cognitive, Affective, and Behavioral Neuroscience* 7.1 (Mar. 2007), pp. 1–17. DOI: 10.3758/cabn.7.1.1. URL: https://doi.org/10.3758/cabn.7.1.1.

[27] Alexander J. Shackman et al. “The integration of negative affect, pain and cognitive control in the cingulate cortex”. In: *Nature Reviews Neuroscience* 12.3 (Mar. 2011), pp. 154–167. DOI: 10.1038/nrn2994. URL: https://doi.org/10.1038/nrn2994.

[28] Agnes J. Jasinska et al. “Factors modulating neural reactivity to drug cues in addiction: A survey of human neuroimaging studies”. In: *Neuroscience and Biobehavioral Reviews* 38 (Jan. 2014), pp. 1–16. DOI: 10.1016/j.neubiorev.2013.10.013. URL: https://doi.org/10.1016/j.neubiorev.2013.10.013.

[29] Eric D. Claus et al. “Identifying Neurobiological Phenotypes Associated with Alcohol Use Disorder Severity”. In: *Neuropsychopharmacology* 36.10 (June 2011), pp. 2086–2096. DOI: 10.1038/npp.2011.99. URL: https://doi.org/10.1038/npp.2011.99.

[30] Sabine Vollstädt-Klein et al. “Initial, habitual and compulsive alcohol use is characterized by a shift of cue processing from ventral to dorsal striatum”. In: *Addiction* 105.10 (Oct. 2010), pp. 1741–1749. DOI: 10.1111/j.1360-0443.2010.03022.x. URL: https://doi.org/10.1111/j.1360-0443.2010.03022.x.

[31] Mark S. George et al. “Activation of Prefrontal Cortex and Anterior Thalamus in Alcoholic Subjects on Exposure to Alcohol-Specific Cues”. In: *Archives of General Psychiatry* 58.4 (Apr. 2001), p. 345. DOI: 10.1001/archpsyc.58.4.345. URL: https://doi.org/10.1001/archpsyc.58.4.345.

[32] Francesca M. Filbey et al. “Exposure to the Taste of Alcohol Elicits Activation of the Mesocorticolimbic Neurocircuitry”. In: *Neuropsychopharmacology* 33.6 (May 2008), pp. 1391–1401. DOI: 10.1038/sj.npp.1301513. URL: https://doi.org/10.1038/sj.npp.1301513.

[33] Dieter F. Braus et al. "Alcohol-associated stimuli activate the ventral striatum in abstinent alcoholics". In: *Journal of Neural Transmission* 108.7 (Jan. 2001), pp. 887–894. DOI: 10.1007/s007020170038. URL: https://doi.org/10.1007/s007020170038.

[34] Wuyi Wang et al. "Cue-elicited craving, thalamic activity, and physiological arousal in adult non-dependent drinkers". In: *Journal of Psychiatric Research* 116 (June 2019), pp. 74–82. DOI: 10.1016/j.jpsychires.2019.06.005. URL: https://doi.org/10.1016/j.jpsychires.2019.06.005.

[35] Nancy Kanwisher, Josh H. McDermott, and Marvin M. Chun. "The Fusiform Face Area: A Module in Human Extrastriate Cortex Specialized for Face Perception". In: *The Journal of Neuroscience* 17.11 (June 1997), pp. 4302–4311. DOI: 10.1523/jneurosci.17-11-04302.1997. URL: https://doi.org/10.1523/jneurosci.17-11-04302.1997.

[36] Peter Lang et al. "Emotional arousal and activation of the visual cortex: an fMRI analysis." In: *Psychophysiology* 35.2 (Mar. 1998), pp. 199–210. URL: https://doi.org/10.1111/1469-8986.3520199.

[37] *Wikipedia - Cerebellum*. [Online; accessed 13-05-2023]. Apr. 2023. URL: https://en.wikipedia.org/wiki/Cerebellum.

[38] Amy J. Bastian. "Moving, sensing and learning with cerebellar damage". In: *Current Opinion in Neurobiology* 21.4 (Aug. 2011), pp. 596–601. DOI: 10.1016/j.conb.2011.06.007. URL: https://doi.org/10.1016/j.conb.2011.06.007.

[39] Eric A. Moulton et al. "The cerebellum and addiction: insights gained from neuroimaging research". In: *Addiction Biology* 19.3 (May 2014), pp. 317–331. DOI: 10.1111/adb.12101. URL: https://doi.org/10.1111/adb.12101.

[40] David J. Rossi. *Alcohol and the Cerebellum*. Jan. 2023, pp. 431–439. DOI: 10.1007/978-3-031-15070-8_68. URL: https://doi.org/10.1007/978-3-031-15070-8_68.

[41] Krzysztof J. Gorgolewski et al. "The brain imaging data structure, a format for organizing and describing outputs of neuroimaging experiments". In: *Scientific Data* 3.1 (June 2016). DOI: 10.1038/sdata.2016.44. URL: https://doi.org/10.1038/sdata.2016.44.

[42] *Brain Imaging Data Structure*. [Online; accessed 15-05-2023]. URL: https://bids-specification.readthedocs.io/en/stable/.

[43] *BrainVoyager QX Users Guide*. URL: https://www.brainvoyager.com/bvqx/doc/UsersGuide/BrainVoyagerQXUsersGuide.html.

[44] Brain Innovation. *BrainVoyager Brain Tutor*. Software. Version Version 2.5. URL: http://www.brainvoyager.com/products/braintutor.html.

[45] Ardesheer Talati and Joy Hirsch. "Functional Specialization within the Medial Frontal Gyrus for Perceptual Go/No-Go Decisions Based on "What," "When," and "Where" Related Information: An fMRI Study". In: *Journal of Cognitive Neuroscience* 17.7 (July 2005), pp. 981–993. DOI: 10.1162/0898929054475226. URL: https://doi.org/10.1162/0898929054475226.

[46] Thang M. Le, Tessa Malone, and Chiang-Shan R. Li. "Positive alcohol expectancy and resting-state functional connectivity of the insula in problem drinking". In: *Drug and Alcohol Dependence* 231 (Jan. 2022), p. 109248. DOI: 10.1016/j.drugalcdep.2021.109248. URL: https://doi.org/10.1016/j.drugalcdep.2021.109248.

[47] Eva M. Müller-Oehring et al. "The Resting Brain of Alcoholics". In: *Cerebral Cortex* 25.11 (Nov. 2015), pp. 4155–4168. DOI: 10.1093/cercor/bhu134. URL: https://doi.org/10.1093/cercor/bhu134.

[48] Stanislav R. Vorel et al. "Insula Damage and Quitting Smoking". In: *Science* 317.5836 (July 2007), pp. 318–319. DOI: 10.1126/science.317.5836.318c. URL: https://doi.org/10.1126/science.317.5836.318c.

[49] Nasir H. Naqvi and Antoine Bechara. "The hidden island of addiction: the insula". In: *Trends in Neurosciences* 32.1 (Jan. 2009), pp. 56–67. DOI: 10.1016/j.tins.2008.09.009. URL: https://doi.org/10.1016/j.tins.2008.09.009.

[50] Junkai Wang et al. "Combining gray matter volume in the cuneus and the cuneus-prefrontal connectivity may predict early relapse in abstinent alcohol-dependent patients". In: *PLOS ONE* 13.5 (May 2018), e0196860. DOI: 10.1371/journal.pone.0196860. URL: https://doi.org/10.1371/journal.pone.0196860.

[51] *Brodmann's Interactive Atlas Main Page*. URL: https://www.fmriconsulting.com/brodmann/index.html.

[52] Sien Hu et al. "Association of Drinking Problems and Duration of Alcohol Use to Inhibitory Control in Nondependent Young Adult Social Drinkers". In: *Alcoholism: Clinical and Experimental Research* 40.2 (Feb. 2016), pp. 319–328. DOI: 10.1111/acer.12964. URL: https://doi.org/10.1111/acer.12964.

[53] George W. Bush et al. "Dorsal anterior cingulate cortex: A role in reward-based decision making". In: *Proceedings of the National Academy of Sciences of the United States of America* 99.1 (Jan. 2002), pp. 523–528. DOI: 10.1073/pnas.012470999. URL: https://doi.org/10.1073/pnas.012470999.

[54] Elissa Aminoff, Kestutis Kveraga, and Moshe Bar. "The role of the parahippocampal cortex in cognition". In: *Trends in Cognitive Sciences* 17.8 (Aug. 2013), pp. 379–390. DOI: 10.1016/j.tics.2013.06.009. URL: https://doi.org/10.1016/j.tics.2013.06.009.

[55] Jana Wrase et al. “Development of alcohol-associated cues and cue-induced brain activation in alcoholics”. In: *European Psychiatry* 17.5 (Sept. 2002), pp. 287–291. DOI: 10.1016/s0924-9338(02)00676-4. URL: https://doi.org/10.1016/s0924-9338(02)00676-4.

[56] Ali H. Palejwala et al. “Anatomy and White Matter Connections of the Lingual Gyrus and Cuneus”. In: *World Neurosurgery* 151 (Apr. 2021), e426–e437. DOI: 10.1016/j.wneu.2021.04.050. URL: https://doi.org/10.1016/j.wneu.2021.04.050.

Appendix A

Full data-tracking Excel file

	Sujet	Session	"Anat_3D" Folder (or equivalent)	"Images" Folder (or equivalent)	Preprocessing	Coregistration	VTC	Analysis
Alcooliques	1	1	sub-01 ses-01	x	x	x	x	x
		2	sub-01 ses-02	x	x	x	x	x
	2	1	sub-02 ses-01	x	x	x	x	x
		2	sub-02 ses-02	x	x	x	x	x
		3	sub-02 ses-03	x	x	x	x	x
	3	1	sub-03 ses-01	sub-03 ses-01	sub-03 ses-01	sub-03 ses-01	sub-03 ses-01	sub-03 ses-01
		2	sub-03 ses-02	sub-03 ses-02	sub-03 ses-02	sub-03 ses-02	sub-03 ses-02	sub-03 ses-02
		3	sub-03 ses-03	sub-03 ses-03	sub-03 ses-03	sub-03 ses-03	sub-03 ses-03	sub-03 ses-03
	4	1	sub-04 ses-01	sub-04 ses-01	sub-04 ses-01	sub-04 ses-01	sub-04 ses-01	sub-04 ses-01
		2	sub-04 ses-02	x	x	x	x	x
	5	1	sub-05 ses-01	sub-05 ses-01	sub-05 ses-01	sub-05 ses-01	sub-05 ses-01	sub-05 ses-01
		2	sub-05 ses-02	x	x	x	x	x
	6	1	x	x	x	x	x	x
		2	sub-06 ses-02	sub-06 ses-02	sub-06 ses-02	sub-06 ses-02	sub-06 ses-02	sub-06 ses-02
	7	1	sub-07 ses-01	sub-07 ses-01	sub-07 ses-01	sub-07 ses-01	sub-07 ses-01	sub-07 ses-01
		2	sub-07 ses-02	sub-07 ses-02	sub-07 ses-02	sub-07 ses-02	sub-07 ses-02	sub-07 ses-02
	8	1	x	x	x	x	x	x
		2	sub-08 ses-02	sub-08 ses-02	sub-08 ses-02	sub-08 ses-02	sub-08 ses-02	sub-08 ses-02
	9	1	sub-09 ses-01	sub-09 ses-01	sub-09 ses-01	sub-09 ses-01	sub-09 ses-01	sub-09 ses-01
		2	sub-09 ses-02	sub-09 ses-02	sub-09 ses-02	sub-09 ses-02	sub-09 ses-02	sub-09 ses-02
		3	sub-09 ses-03	sub-09 ses-03	sub-09 ses-03	sub-09 ses-03	sub-09 ses-03	sub-09 ses-03
	10	1	sub-10 ses-01	sub-10 ses-01	sub-10 ses-01	x	x	x
	11	1	sub-11 ses-01	sub-11 ses-01	sub-11 ses-01	sub-11 ses-01	sub-11 ses-01	sub-11 ses-01
		2	sub-11 ses-02	sub-11 ses-02	sub-11 ses-02	sub-11 ses-02	sub-11 ses-02	sub-11 ses-02
	12	1	sub-12 ses-01	x	x	x	x	x
		2	sub-12 ses-02	sub-12 ses-02	sub-12 ses-02	sub-12 ses-02	sub-12 ses-02	sub-12 ses-02
	13	1	sub-13 ses-01	sub-13 ses-01	sub-13 ses-01	sub-13 ses-01	sub-13 ses-01	sub-13 ses-01
		2	sub-13 ses-02	sub-13 ses-02	sub-13 ses-02	sub-13 ses-02	sub-13 ses-02	sub-13 ses-02
	14	1	sub-14 ses-01	sub-14 ses-01	sub-14 ses-01	x	x	x
		2	sub-14 ses-02	sub-14 ses-02	sub-14 ses-02	sub-14 ses-02	sub-14 ses-02	sub-14 ses-02
	15	1	sub-15 ses-01	sub-15 ses-01	sub-15 ses-01	sub-15 ses-01	sub-15 ses-01	sub-15 ses-01
		2	sub-15 ses-02	sub-15 ses-02	sub-15 ses-02	x	x	x
	16	1	sub-16 ses-01	sub-16 ses-01	sub-16 ses-01	sub-16 ses-01	sub-16 ses-01	sub-16 ses-01
	17	1	sub-17 ses-01	sub-17 ses-01	sub-17 ses-01	sub-17 ses-01	sub-17 ses-01	sub-17 ses-01
		2	sub-17 ses-02	sub-17 ses-02	sub-17 ses-02	sub-17 ses-02	sub-17 ses-02	sub-17 ses-02
		3	sub-17 ses-03	sub-17 ses-03	sub-17 ses-03	sub-17 ses-03	sub-17 ses-03	sub-17 ses-03
	18	1	sub-18 ses-01	sub-18 ses-01	sub-18 ses-01	sub-18 ses-01	sub-18 ses-01	sub-18 ses-01
		2	sub-18 ses-02	sub-18 ses-02	sub-18 ses-02	sub-18 ses-02	sub-18 ses-02	sub-18 ses-02
	19	1	sub-19 ses-01	sub-19 ses-01	sub-19 ses-01	sub-19 ses-01	sub-19 ses-01	sub-19 ses-01
		2	sub-19 ses-02	sub-19 ses-02	sub-19 ses-02	sub-19 ses-02	sub-19 ses-02	sub-19 ses-02
	20	1	sub-20 ses-01	sub-20 ses-01	sub-20 ses-01	sub-20 ses-01	sub-20 ses-01	sub-20 ses-01
		2	sub-20 ses-02	sub-20 ses-02	sub-20 ses-02	sub-20 ses-02	sub-20 ses-02	sub-20 ses-02
		3	sub-20 ses-03	sub-20 ses-03	sub-20 ses-03	sub-20 ses-03	sub-20 ses-03	sub-20 ses-03
	21	1	sub-21 ses-01	sub-21 ses-01	sub-21 ses-01	sub-21 ses-01	sub-21 ses-01	x
		2	sub-21 ses-02	sub-21 ses-02	sub-21 ses-02	sub-21 ses-02	sub-21 ses-02	sub-21 ses-02
	22	1	sub-22 ses-01	sub-22 ses-01	sub-22 ses-01	sub-22 ses-01	sub-22 ses-01	sub-22 ses-01
		2	sub-22 ses-02	sub-22 ses-02	sub-22 ses-02	sub-22 ses-02	sub-22 ses-02	sub-22 ses-02
		3	sub-22 ses-03	sub-22 ses-03	sub-22 ses-03	sub-22 ses-03	sub-22 ses-03	sub-22 ses-03
	23	1	sub-23 ses-01	sub-23 ses-01	sub-23 ses-01	x	x	x
		2	sub-23 ses-02	x	x	x	x	x
	24	1	sub-24 ses-01	sub-24 ses-01	sub-24 ses-01	sub-24 ses-01	sub-24 ses-01	sub-24 ses-01
		2	sub-24 ses-02	sub-24 ses-02	sub-24 ses-02	sub-24 ses-02	sub-24 ses-02	sub-24 ses-02
	25	1	sub-25 ses-01	x	x	x	x	x
		2	sub-25 ses-02	x	x	x	x	x
	26	1	sub-26 ses-01	sub-26 ses-01	sub-26 ses-01	sub-26 ses-01	sub-26 ses-01	sub-26 ses-01
		2	sub-26 ses-02	sub-26 ses-02	sub-26 ses-02	sub-26 ses-02	sub-26 ses-02	sub-26 ses-02
	27	1	sub-27 ses-01	sub-27 ses-01	sub-27 ses-01	sub-27 ses-01	sub-27 ses-01	sub-27 ses-01
		2	sub-27 ses-02	sub-27 ses-02	sub-27 ses-02	x	x	x
		3	sub-27 ses-03	sub-27 ses-03	sub-27 ses-03	sub-27 ses-03	sub-27 ses-03	sub-27 ses-03
	28	1	sub-28 ses-01	sub-28 ses-01	sub-28 ses-01	sub-28 ses-01	sub-28 ses-01	sub-28 ses-01
		2	sub-28 ses-02	sub-28 ses-02	sub-28 ses-02	sub-28 ses-02	sub-28 ses-02	sub-28 ses-02
		3	x	x	x	x	x	x
	29	1	sub-29 ses-01	sub-29 ses-01	sub-29 ses-01	sub-29 ses-01	sub-29 ses-01	sub-29 ses-01
		2	sub-29 ses-02	x	x	x	x	x
	30	1	sub-30 ses-01	sub-30 ses-01	sub-30 ses-01	sub-30 ses-01	sub-30 ses-01	sub-30 ses-01
		2	sub-30 ses-02	sub-30 ses-02	sub-30 ses-02	sub-30 ses-02	sub-30 ses-02	sub-30 ses-02
		3	sub-30 ses-03	sub-30 ses-03	sub-30 ses-03	sub-30 ses-03	sub-30 ses-03	sub-30 ses-03
	31	1	sub-31 ses-01	sub-31 ses-01	sub-31 ses-01	sub-31 ses-01	sub-31 ses-01	sub-31 ses-01
		2	sub-31 ses-02	sub-31 ses-02	sub-31 ses-02	sub-31 ses-02	sub-31 ses-02	sub-31 ses-02
	32	1	sub-32 ses-01	sub-32 ses-01	sub-32 ses-01	sub-32 ses-01	sub-32 ses-01	sub-32 ses-01
		2	sub-32 ses-02	sub-32 ses-02	sub-32 ses-02	x	x	x
	33	1	sub-33 ses-01	sub-33 ses-01	sub-33 ses-01	sub-33 ses-01	sub-33 ses-01	sub-33 ses-01
		2	sub-33 ses-02	sub-33 ses-02	sub-33 ses-02	sub-33 ses-02	sub-33 ses-02	sub-33 ses-02
	34	1	sub-34 ses-01	sub-34 ses-01	sub-34 ses-01	sub-34 ses-01	sub-34 ses-01	sub-34 ses-01
		2	sub-34 ses-02	sub-34 ses-02	sub-34 ses-02	sub-34 ses-02	sub-34 ses-02	sub-34 ses-02
		3	sub-34 ses-03	sub-34 ses-03	sub-34 ses-03	sub-34 ses-03	sub-34 ses-03	sub-34 ses-03
	35	1	sub-35 ses-01	sub-35 ses-01	sub-35 ses-01	sub-35 ses-01	sub-35 ses-01	sub-35 ses-01
		2	sub-35 ses-02	sub-35 ses-02	sub-35 ses-02	sub-35 ses-02	sub-35 ses-02	sub-35 ses-02
	36	1	sub-36 ses-01	sub-36 ses-01	sub-36 ses-01	x	x	x
		2	sub-36 ses-02	sub-36 ses-02	sub-36 ses-02	sub-36 ses-02	sub-36 ses-02	sub-36 ses-02
		3	sub-36 ses-03	sub-36 ses-03	sub-36 ses-03	sub-36 ses-03	sub-36 ses-03	sub-36 ses-03
	37	1	sub-37 ses-01	sub-37 ses-01	sub-37 ses-01	sub-37 ses-01	sub-37 ses-01	sub-37 ses-01
		2	sub-37 ses-02	sub-37 ses-02	sub-37 ses-02	sub-37 ses-02	sub-37 ses-02	sub-37 ses-02
	38	1	sub-38 ses-01	sub-38 ses-01	sub-38 ses-01	sub-38 ses-01	sub-38 ses-01	sub-38 ses-01
	39	1	sub-39 ses-01	sub-39 ses-01	sub-39 ses-01	sub-39 ses-01	sub-39 ses-01	sub-39 ses-01
		2	sub-39 ses-02	sub-39 ses-02	sub-39 ses-02	x	x	x
		3	sub-39 ses-03	x	x	x	x	x
	40	1	sub-40 ses-01	sub-40 ses-01	sub-40 ses-01	x	x	x
		2	sub-40 ses-02	sub-40 ses-02	sub-40 ses-02	x	x	x
	41	1	sub-41 ses-01	sub-41 ses-01	sub-41 ses-01	sub-41 ses-01	sub-41 ses-01	sub-41 ses-01
		2	sub-41 ses-02	sub-41 ses-02	sub-41 ses-02	sub-41 ses-02	sub-41 ses-02	sub-41 ses-02
	42	1	sub-42 ses-01	sub-42 ses-01	sub-42 ses-01	sub-42 ses-01	sub-42 ses-01	sub-42 ses-01
		2	sub-42 ses-02	sub-42 ses-02	sub-42 ses-02	sub-42 ses-02	sub-42 ses-02	sub-42 ses-02
	43	1	sub-43 ses-01	sub-43 ses-01	sub-43 ses-01	sub-43 ses-01	sub-43 ses-01	sub-43 ses-01
		2	sub-43 ses-02	sub-43 ses-02	sub-43 ses-02	sub-43 ses-02	sub-43 ses-02	sub-43 ses-02
	44	1	sub-44 ses-01	sub-44 ses-01	sub-44 ses-01	x	x	x
	45	1	sub-45 ses-01	sub-45 ses-01	sub-45 ses-01	sub-45 ses-01	sub-45 ses-01	sub-45 ses-01
		2	sub-45 ses-02	sub-45 ses-02	sub-45 ses-02	sub-45 ses-02	sub-45 ses-02	sub-45 ses-02
		3	sub-45 ses-03	sub-45 ses-03	sub-45 ses-03	sub-45 ses-03	sub-45 ses-03	sub-45 ses-03
	46	1	sub-46 ses-01	sub-46 ses-01	sub-46 ses-01	sub-46 ses-01	sub-46 ses-01	sub-46 ses-01
		2	sub-46 ses-02	sub-46 ses-02	sub-46 ses-02	x	x	x
	47	1	sub-47 ses-01	sub-47 ses-01	sub-47 ses-01	sub-47 ses-01	sub-47 ses-01	x
		2	x	x	x	x	x	x
	48	1	sub-48 ses-01	sub-48 ses-01	sub-48 ses-01	sub-48 ses-01	sub-48 ses-01	sub-48 ses-01
		2	sub-48 ses-02	sub-48 ses-02	sub-48 ses-02	sub-48 ses-02	sub-48 ses-02	sub-48 ses-02
	49	1	x	x	x	x	x	x
	50	1	sub-50 ses-01	sub-50 ses-01	sub-50 ses-01	sub-50 ses-01	sub-50 ses-01	x
		2	sub-50 ses-02	sub-50 ses-02	sub-50 ses-02	sub-50 ses-02	sub-50 ses-02	sub-50 ses-02
	51	1	sub-51 ses-01	sub-51 ses-01	sub-51 ses-01	sub-51 ses-01	sub-51 ses-01	sub-51 ses-01
		2	sub-51 ses-02	sub-51 ses-02	sub-51 ses-02	sub-51 ses-02	sub-51 ses-02	sub-51 ses-02
	52	1	sub-52 ses-01	sub-52 ses-01	sub-52 ses-01	sub-52 ses-01	sub-52 ses-01	sub-52 ses-01
		2	sub-52 ses-02	sub-52 ses-02	sub-52 ses-02	sub-52 ses-02	sub-52 ses-02	sub-52 ses-02
	53	1	sub-53 ses-01	sub-53 ses-01	sub-53 ses-01	sub-53 ses-01	sub-53 ses-01	sub-53 ses-01
		2	sub-53 ses-02	sub-53 ses-02	sub-53 ses-02	sub-53 ses-02	sub-53 ses-02	sub-53 ses-02

Figure A.1: Full Excel file of data tracking: Alcohol-dependent participants

Groupe	Sujet	Session	"Anat_3D" Folder (or equivalent)	"Images" Folder (or equivalent)	Preprocessing	Coregistration	VTC	Analysis
Contrôles	54	1	sub-54 ses-01	sub-54 ses-01	sub-54 ses-01	sub-54 ses-01	sub-54 ses-01	sub-54 ses-01
		2	sub-54 ses-02	sub-54 ses-02	sub-54 ses-02	sub-54 ses-02	sub-54 ses-02	sub-54 ses-02
	55	1	sub-55 ses-01	x	x	x	x	x
		2	sub-55 ses-02	sub-55 ses-02	sub-55 ses-02	sub-55 ses-02	sub-55 ses-02	sub-55 ses-02
	56	1	sub-56 ses-01	sub-56 ses-01	sub-56 ses-01	sub-56 ses-01	sub-56 ses-01	sub-56 ses-01
	57	1	sub-57 ses-01	x	x	x	x	x
		2	sub-57 ses-02	sub-57 ses-02	sub-57 ses-02	sub-57 ses-02	sub-57 ses-02	sub-57 ses-02
	58	1	sub-58 ses-01	sub-58 ses-01	sub-58 ses-01	sub-58 ses-01	sub-58 ses-01	sub-58 ses-01
		2	sub-58 ses-02	sub-58 ses-02	sub-58 ses-02	sub-58 ses-02	sub-58 ses-02	sub-58 ses-02
	59	1	sub-59 ses-01	sub-59 ses-01	sub-59 ses-01	sub-59 ses-01	sub-59 ses-01	sub-59 ses-01
		2	sub-59 ses-02	sub-59 ses-02	sub-59 ses-02	sub-59 ses-02	sub-59 ses-02	sub-59 ses-02
	60	1	sub-60 ses-01	sub-60 ses-01	sub-60 ses-01	sub-60 ses-01	sub-60 ses-01	sub-60 ses-01
		2	sub-60 ses-02	sub-60 ses-02	sub-60 ses-02	sub-60 ses-02	sub-60 ses-02	sub-60 ses-02
	61	1	sub-61 ses-01	sub-61 ses-01	sub-61 ses-01	sub-61 ses-01	sub-61 ses-01	x
		2	sub-61 ses-02	sub-61 ses-02	sub-61 ses-02	sub-61 ses-02	sub-61 ses-02	sub-61 ses-02
	62	1	sub-62 ses-01	sub-62 ses-01	sub-62 ses-01	sub-62 ses-01	sub-62 ses-01	sub-62 ses-01
		2	sub-62 ses-02	sub-62 ses-02	sub-62 ses-02	x	x	x
	63	1	sub-63 ses-01	sub-63 ses-01	sub-63 ses-01	sub-63 ses-01	sub-63 ses-01	sub-63 ses-01
		2	sub-63 ses-02	sub-63 ses-02	sub-63 ses-02	x	x	x
	64	1	sub-64 ses-01	sub-64 ses-01	sub-64 ses-01	sub-64 ses-01	sub-64 ses-01	sub-64 ses-01
		2	sub-64 ses-02	sub-64 ses-02	sub-64 ses-02	sub-64 ses-02	sub-64 ses-02	sub-64 ses-02
	65	1	sub-65 ses-01	sub-65 ses-01	sub-65 ses-01	sub-65 ses-01	sub-65 ses-01	sub-65 ses-01
		2	sub-65 ses-02	sub-65 ses-02	sub-65 ses-02	sub-65 ses-02	sub-65 ses-02	sub-65 ses-02
	66	1	sub-66 ses-01	sub-66 ses-01	sub-66 ses-01	sub-66 ses-01	sub-66 ses-01	sub-66 ses-01
		2	sub-66 ses-02	sub-66 ses-02	sub-66 ses-02	x	x	x
	67	1	sub-67 ses-01	sub-67 ses-01	sub-67 ses-01	x	x	x
		2	sub-67 ses-02	sub-67 ses-02	sub-67 ses-02	sub-67 ses-02	sub-67 ses-02	sub-67 ses-02
	68	1	sub-68 ses-01	sub-68 ses-01	sub-68 ses-01	sub-68 ses-01	sub-68 ses-01	sub-68 ses-01
		2	sub-68 ses-02	sub-68 ses-02	sub-68 ses-02	sub-68 ses-02	sub-68 ses-02	sub-68 ses-02
	69	1	sub-69 ses-01	x	x	x	x	x
		2	sub-69 ses-02	sub-69 ses-02	sub-69 ses-02	sub-69 ses-02	sub-69 ses-02	sub-69 ses-02
	70	1	sub-70 ses-01	sub-70 ses-01	sub-70 ses-01	sub-70 ses-01	sub-70 ses-01	sub-70 ses-01
		2	sub-70 ses-02	sub-70 ses-02	sub-70 ses-02	x	x	x
	71	1	sub-71 ses-01	sub-71 ses-01	sub-71 ses-01	sub-71 ses-01	sub-71 ses-01	sub-71 ses-01
		2	sub-71 ses-02	sub-71 ses-02	sub-71 ses-02	sub-71 ses-02	sub-71 ses-02	sub-71 ses-02
	72	1	sub-72 ses-01	sub-72 ses-01	sub-72 ses-01	sub-72 ses-01	sub-72 ses-01	x
		2	sub-72 ses-02	sub-72 ses-02	sub-72 ses-02	sub-72 ses-02	sub-72 ses-02	sub-72 ses-02
	73	1	sub-73 ses-01	sub-73 ses-01	sub-73 ses-01	sub-73 ses-01	sub-73 ses-01	sub-73 ses-01
		2	sub-73 ses-02	sub-73 ses-02	sub-73 ses-02	sub-73 ses-02	sub-73 ses-02	sub-73 ses-02

Figure A.2: Full Excel file of data tracking: Control participants

Appendix B

Behavioural data

Numéro	T1_OCDS_MODIFIE_Total	T1_OCDS_Obsessions	T1_OCDS_Compulsions	T2_OCDS_MODIFIE_Total	T2_OCDS_Obsessions	T2_OCDS_Compulsions	Abstinent trois mois T2/T3	T3_OCDS_MODIFIE_Total	T3_OCDS_Obsessions	T3_OCDS_Compulsions
1	14	8	6	5	2	3	?	/	/	/
2	20	11	9	11	4	7	oui	3	1	2
3	14	8	6	perdu	perdu	perdu	oui	1	1	0
4	18	12	6	11	9	2	oui			
5	22	12	10	2	1	1	oui			
6	26	16	10	12	10	2	non	1	0	1
7	19	12	7	13	9	4	non			
8	12	9	3	8	7	1	?			
9	19	9	10	4	2	2	oui	9	5	4
10	8	4	4	1	0	1	?			
11	5	3	2	0	0	0	oui	0	0	0
12	19	9	10	4	3	1	non			
13	11	8	3	6	3	3	?			
14	8	5	3	8	4	4	?			
15	7	3	4	/	/	/	?			
16	5	4	1	/	/	/	?			
17	23	13	10	15	9	6	non	11	6	5
18	17	10	7	13	8	5	oui			
19	20	11	9	0	0	0	?			
20	16	11	5	14	9	5	oui	3	1	2
21	26	17	9	0	0	0	?			
22	15	9	6	8	5	3	non	14	8	6
23	18	10	8	18	10	8	oui			
24	4	2	2	12	8	4	?			
25	18	9	9	4	3	1	?			
26	24	15	9	23	15	8	non			
27	18	9	9	17	9	8	non	14	8	6
28	3	1	2	0	0	0	oui	2	1	1
29	21	14	7	17	9	8	?			
30	8	4	4	8	5	3	oui	8	4	4
31	6	3	3	5	4	1	oui			
32	21	13	8	15	9	6	?			
33	16	11	5	8	5	3	non			
34	0	0	0	0	0	0	oui	0	0	0
35	18	9	9	10	7	3	non			
36	13	8	5	11	7	4	oui	2	2	0
37	13	7	6	1	0	1	non			
38	21	11	10	21	13	8	?			
39	14	9	5	0	0	0	oui	0	0	0
40	0	0	0	0	0	0	?			
41	14	9	5	4	2	2	?			
42	15	7	8	13	7	6	?			
43	22	13	9	22	13	9	non			
44										
45	15	8	7	12	7	5	oui	0	0	0
46	17	8	9	8	3	5	oui			
47	6	4	2	9	5	4	?			
48	29	19	10	29	18	11	non			
49										
50	18	9	9	1	0	1	oui			
51	14	9	5	9	4	5	?			
52	9	6	3	5	2	3	?			
53	12	8	5	18	10	8	non			
54	0	0	0							
55	0	0	0							
56	0	0	0							
57										
58	0	0	0							
59	2	0	2							
60	0	0	0							
61	0	0	0							
62	4	1	3							
63	1	0	1							
64	0	0	0							
65	1	0	1							
66	0	0	0							
67	0	0	0							
68	0	0	0							
69	10	5	5							
70	5	0	5							
71	1	0	1							
72	0	0	0							
73	0	0	0							

Figure B.1: Excel file: Behavioural data

UNIVERSITÉ CATHOLIQUE DE LOUVAIN
École polytechnique de Louvain
Rue Archimède, 1 bte L6.11.01, 1348 Louvain-la-Neuve, Belgique | **www.uclouvain.be/epl**